Lauren Porter 620007286

Wnt signalling and peroxisome dynamics in the zebrafish (*Danio rerio*)

Submitted by Lauren Porter to the University of Exeter

As a thesis for the degree of

Masters by Research in Biosciences

On 20th September 2019

I certify that all the material in this thesis which is not my own work has been identified and that no material has been previously submitted and approved for the award of a degree by this or any other University.

Signature ……

Abstract

Cell-cell or paracrine signalling is a form of cellular communication in which a cell produces a signal that influences the behaviour of neighbouring cells, which is important because it allows for the local coordination of the activities of groups of cells. This coordination is indispensable during development; for example, paracrine Wnt signalling is fundamental to body patterning in all metazoans where it helps to determine cell fate in a developing embryo. Wnt can regulate the transcription of target genes including *cyclin* and *peroxisome-proliferator activated receptor-δ.* The importance of Wnt signalling is not temporally limited, and Wnt has roles throughout the life of an organism such as the management of stem cells and the cellular abundance of mitochondria, the 'sister organelle' of the peroxisome. The peroxisome is a single membrane-bound organelle with diverse roles in healthy development and life, inclusive of the breakdown of very long chain fatty acids (VLCFAs) and the production of plasmalogens for efficient nervous conduction. The relationship between the Wnt signalling pathway and peroxisomes is unknown. Here I investigate the influence of Wnt signalling on peroxisome dynamics in zebrafish. To do so, canonical *wnt8a* was knocked out and knocked down using the genomic engineering tool CRISPR and Morpholino oligomers. The number and morphology of peroxisomes was observed in Wnt8a-deficient zebrafish embryos and appeared to be aggregated and less numerate than in wild type zebrafish. Consistently, in zebrafish embryos overexpressing *wnt8a,* peroxisomes were visualised as highly numerate singular puncta. I hypothesise that - in addition to a set of functions in development and tissue homeostasis - Wnt signalling has a novel role in regulating peroxisome proliferation in zebrafish.

Abbreviations

acox1 – acyl-CoA oxidase 1

AGS – gastric adenocarcinoma

AP – antero-posterior

APC - adenomatous polyposis coli protein

apoa1 – apolipoprotein A1

BACs – bacterial artificial chromosomes

Bcl9 – B-cell CLL/lymphoma protein

BIO - 6-bromoindirubin-3'-oxime

BMP – bone morphogenetic protein

βTrCP – β-transducin repeats-containing proteins

CBP – CREB-binding protein

Cdc42 – cell division control protein 42 homolog

CKIa – casein kinase Ia

CLEM – correlative light-electron microscopy

CRISPR – clustered regularly spaced palindromic repeats

CRISPRi - CRISPR interference

crRNA – CRISPR ribonucleic acid

dCas9 – deactivated Cas9 enzyme

Dkk-1 – dickkopf 1

DLP1 – dynamin-like protein 1

DMSO – dimethyl sulfoxide

DSB – double-strand break

Dvl – dishevelled

EGF-CFC – epidermal growth factor-Cripto-FRL1-Cryptic

EGFR – epidermal growth factor receptor

ER – endoplasmic reticulum

ERK1/2 – extracellular signal-regulated kinase 1/2

fgf8 – fibroblast growth factor 8

fis1 – mitochondrial fission 1

gbx1 – gastrulation brain homeobox 1

gDNA – genomic DNA

gRNA – guide ribonucleic acid

GSK-3 – glycogen synthase kinase 3

GFP – green fluorescent protein

GTP – guanosine triphosphate

hpf – hours post fertilisation

hPSC – human pluripotent stem cell

IRD – Infantile Refsum's disease

IWR1 - 4-(1,3,3a,4,7,7a-Hexahydro-1,3-dioxo-4,7-methano-2H-isoindol-2-yl)-N-8-quinolinyl-Benzamide

KRAB - Krüppel-associated box

LDLR – low-density lipoprotein receptor

Lef – lymphoid enhancing factor

Lrp5/6 – low-density lipoprotein receptors 5 and 6

Mff – mitochondrial fission factor

MHB – midbrain hindbrain boundary

MITF - micropthalmia-associated transcription factor

MP – medio-lateral

mRFP – monomeric red fluorescent protein

mRNA – messenger RNA

mtp – microsomal triglyceride transfer protein

NFkB – nuclear factor kappa-light-chain-enhancer of activated B cells

ntl – no tail

ORF – open reading frame

otx2 – orthodenticle homeobox 2

PAC2 – zebrafish embryonic fibroblast cell line

PAM – protospacer adjacent motif

PARL – presenilin-associated rhomboid-like protein

PCP – planar cell polarity

PCR – polymerase chain reaction

PFA – paraformaldehyde

PPAR – peroxisome proliferator-activated receptor

PPRE – peroxisome proliferator response elements

PTS – peroxisome targeting signal

RNAi – RNA interference

ror2 – receptor tyrosine kinase like orphan receptor 2

ROS – reactive oxygen species

SEM – scanning electron microscopy

scRNA-seq – single-cell RNA sequencing

sFRP1 – secreted Frizzled-related protein 1

Shh – Sonic hedgehog

shRNA – short hairpin RNA

SKL-GFP – serine-lysine-leucine fused to green fluorescent protein

SWI/SNF – SWItch/sucrose non-fermentable

TALENS – transcription activator-like nucleases

Tcf-3/4 – transcription factor 3/4

TEM – transmission electron microscopy

TSS – transcription start site

UTR – untranslated region

VLCFA – very long chain fatty acid

wg – wingless

wnt8a – Wnt family member 8a

X.EXT1 – Exostosin-1

YSL – yolk syncytial layer

1.0 Introduction

1.1 The history of Wnt discovery

All cells contain the same genetic information, yet there is intrinsic variation in the way that it is expressed due to properties such as single-molecule kinetics (Sanchez & Goulding, 2013). The impact of this inherent variability is that even in a homogenous environment, a group of cells will respond in a heterogeneous manner. Paracrine signalling is a way of locally controlling this inherent variability and coordinating the behaviour and identity of cells by producing signals which are taken up by neighbouring cells (Handly *et al.,* 2015). A typical example of paracrine or cell-cell signalling is Wnt signalling.

Wnt signalling is fundamental to embryogenesis. Present in all metazoans (Holstein, 2012), Wnt proteins have been closely examined in many model organisms such as the fruit fly (*Drosophila melanogaster*), the African clawed frog (*Xenopus laevis*), and zebrafish (*Danio rerio*). The presence of *Wnt* genes in the earliest branches of the animal kingdom, such as Nematostella (Kusserow *et al.,* 2005), has generated speculation that the early diversification of the Wnt protein family is at the crux of the development of more complex bilaterian animal body plans (Holstein, 2012).

Wnt was discovered in mice by Roel Nusse and Harold Varmus (Nusse & Varmus 1982), in parallel with Christiane Nüsslein-Volhard and Eric Wieshaus in *Drosophila* (Nüsslein-Volhard & Wieschaus, 1980). Wnt made its debut respectively as the putative mouse proto-oncogene *Int-1* and the *Drosophila* segment polarity gene *wingless* (*wg*) - combined as *wnt-1* (Nusse *et al*, 1991). Rijsewijk and colleagues (1987a) isolated *Drosophila int-1* (*Dint-1*) and showed that it was almost identical (54%) to and mapped to the same location as *wg*.

Thus, *wnt* was established as one of the first genes to be implicated in both morphogenesis and oncogenesis.

Wnt signalling was initially associated with breast cancer due to the discovery that the mouse proto-oncogene *Int-1/Wnt1* caused mammary hyperplasia and tumours in mice, either via proviral insertion into the *Wnt1* locus or transgenic overexpression (Tsukamoto *et al.,* 1988). *Wnt* rapidly became interesting to cancer biologists seeking to shed light on human oncogenesis, and yet it was difficult to find the link between the human *WNT* homologue and the breast cancer studied by Nusse and Varmus, until the focus shifted to the downstream components of the *WNT* signalling pathway (Nusse & Varmus, 2012). The research that followed identified components of the now infamous canonical signalling pathway such as adenomatous polyposis coli (APC) (Groden *et al.*, 1991), β-catenin (Peifer & Wieschaus, 1990, Peifer *et al*., 1993) and glycogen synthase kinase 3 (GSK-3) proteins (Siegfried *et al.,* 1992). The pathway stretches from the cell membrane to the nucleus and culminates, via stabilisation of intra-cellular β-catenin, in the expression of *WNT* target genes which include cell cycle-regulators and oncogenes (Huelsken & Behrens, 2000).

APC, a component of the canonical Wnt signalling pathway, downregulates Wnt pathway signalling by binding to β-catenin in the cytosol and thereby assisting its degradation by the multi-module β-catenin degradation complex. Loss of APC results in reduced degradation of β-catenin and enhanced canonical Wnt signalling, thus β-catenin can complex with T-cell factor 4 (Tcf-4) at a steady level and induce transcriptional transactivation. This mechanism, triggered by Wnt pathway component APC, was found to underpin hereditary familial adenomatous polyposis – a form of colon cancer (Korinek *et al.,* 1998).

The canonical Wnt signalling pathway, or the β-Catenin pathway, is one of multiple pathways which construct the Wnt signalling network and underscore the multitude of roles for Wnt in both development and in the maintenance of healthy life. All begin with the reception of the Wnt protein at the cell membrane, and the earliest known receptors were from the Frizzled family of seven-pass transmembrane receptors. For the canonical signalling pathway, Wnt is received by the low-density lipoprotein receptors 5 and 6 (Lrp5/6) in vertebrates, and by the *Drosophila* ortholog arrow. Both Lrp5/6, or arrow, are single-span transmembrane proteins from the low-density lipoprotein receptor (LDLR) family and are absolute requirements for the function of the canonical Wnt pathway; in the absence of arrow, *Drosophila* demonstrate a phenotype similar to *wingless*, and mice mutated in *Lrp6* exhibit a compounded phenotype of several Wnt deficiencies (He *et al.,* 2004).

1.2 The canonical Wnt pathway

On the protein level, the entities within the Wnt signalling network are now well elucidated. It is understood that there are distinguishable pathways within the network with distinct molecular functions, yet the components within these pathways are interrelated (Filipovich *et al.,* 2011). In the endoplasmic reticulum of producing cells, Wnt is lipid modified with palmitoleic acids via the O-acyltransferase porcupine before release into the extracellular matrix (Takada *et al.,* 2006), where its dissemination is still the topic of debate. Wnt diffuses poorly, and is therefore usually taken up by neighbouring cells where it activates the cascade of intracellular interactions which comprise the signalling pathways (Wiese *et al.,* 2018).

There are three main signalling pathways; the canonical or β-catenin pathway, the Ca^{2+} pathway and the planar cell polarity (PCP) pathway. Briefly, the PCP pathway coordinates the polarity of a cell within the epithelium of the *Drosophila*, and in vertebrates such as zebrafish, controls the process of convergent extension, that is the extension of the antero-posterior (AP) axis and contraction of the medio-lateral axis (MP), and the polarity of lamellipodial protrusions involved in cell intercalation (Wang *et al.,* 2006). The Ca^{2+} pathway culminates in target gene expression in a β-catenin-independent manner with non-canonical Wnts (Wnt4, -5a and -11) (Kühl *et al.,* 2000). Non-canonical Wnt signalling has disparate roles in heart induction, neuronal migration and cochlear hair cell morphology, amongst others, but is not as well understood as the canonical pathway (Veeman *et al.,* 2003).

The canonical Wnt pathway outlined in Figure 1 is perhaps the most well-known and it culminates in the activation of Wnt target genes within the nucleus. The core tenet of the pathway is the prevention of the degradation of intracellular β-catenin in the Wnt receiver cell. In the absence of canonical Wnt signal reception (Wnt1, Wnt3, Wnt3A (or Wnt3 like), Wnt8a, Wnt8b) (Filipovich *et al.,* 2011) at the cell membrane, intracellular β-catenin is phosphorylated at serine 45 by casein kinase Ia (CKIa), which permits glycogen synthase kinase 3 β (GSK3β) to phosphorylate serine and threonine residues 33, 37 and 41. The primary two motifs trigger ubiquitination of β-catenin by β-transducin repeats-containing proteins (βTrCP) and finally degradation by proteasomes in the cytosol, preventing β-catenin from entering the nucleus and interacting with transcription factors.

When the Wnt ligand is delivered to the cell membrane of the receiver cell, it binds to the seven-pass frizzled transmembrane receptor and co-receptor Lrp5/6. This binding induces the recruitment of cytosolic proteins such as dishevelled, which in turn inhibits the action of the multi-protein β-catenin degradation complex by displacement of GSK3β from scaffold protein axin, thus preventing further phosphorylation of β-catenin and subsequent creation of the two ubiquitination motifs. Therefore, β-catenin goes unrecognised by proteasomes and persists within the cytosol, where it translocates to the nucleus and interacts with T-cell factor (TCF)/lymphoid enhancing factor (LEF) family transcription factors. This interaction leads to the transcription of Wnt target genes such as, but not limited to, cell-cycle regulator *cyclin D1,* oncogene *MYC,* and peroxisome-proliferator activated receptor delta (*PPARδ)*. Target gene transcription is controlled by the relationship between β-catenin and histone acetyltransferase CREB-binding protein (CBP), B-cell CLL/lymphoma (Bcl9) bound to pygopus and chromatin-remodelling complex SWItch/sucrose non-fermentable (SWI/SNF) (Huelsken & Behrens, 2002).

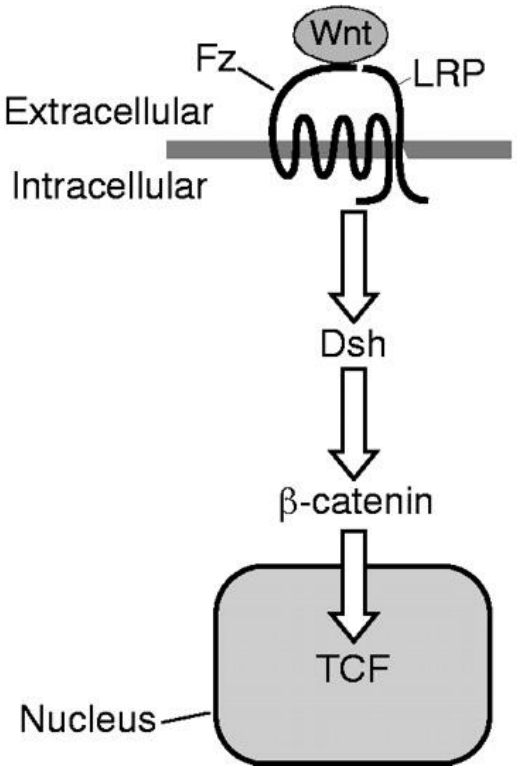

Figure 1: A schema of the β-catenin pathways triggered by the reception of Wnt at the cell membrane, and the genes targeted (Strutt, 2003).

Regulation of the canonical Wnt pathway is required to maintain a healthy state. For example, within the tumours of most breast cancers, the promoter region of negative Wnt pathway regulator secreted Frizzled-related protein 1 (*sFRP1*) is hypermethylated, which downregulates *sFRP1* transcription. This results in dysregulation of the Wnt pathway and increased Wnt transcription, which has been suggested to have a role in tumorigenesis; for example in mice, Wnt trans-activates the transcription of epidermal growth factor receptor (EGFR) which activates the extracellular signal-regulated kinase 1/2 pathway (ERK1/2), thus reducing control over cellular proliferation (Schlange *et al.,* 2007) and opening the door to tumour generation.

Dysregulation of the canonical Wnt signalling pathway is a characteristic of multiple cancer types, a prominent example being colon cancer. The reason for

this involvement in tumorigenesis is due to the role of Wnt in the renewal of tissues and homeostatic turnover of cells. In the mouse intestine, the layer of endodermal cells is entirely renewed every 3-5 days. New cells are produced in the intestinal crypt and travel along intestinal villi in a sheet to the tips where the growth is balanced by apoptosis. Below the crypt lies stem cells which produce the rapidly proliferating progenitor cells housed within the crypt. Dysregulation of Wnt signalling results in loss of the stem cell compartment in mice; both in Tcf-4 neonatal mutants and where dickkopf 1 (*Dkk-1*) is transgenically expressed. Such mice die after birth (Korinek *et al.,* 1998; Reya & Clevers, 2005). In humans, colon cancer is typically derived from mutations in *APC*, resulting in constitutive activation of β-catenin and therefore tumorigenesis. Using a Wnt reporter construct, it is possible to visualise Wnt pathway activity, which is highest in tumour cells. Interestingly, in adenocarcinomas, Wnt signalling was detected at its highest levels in cells proximate to stromal myofibroblasts, which the group took to infer that environmental factors, namely myofibroblast secreted factors, can manipulate Wnt signalling in cancerous cells. Indeed, such secreted factors were found to enhance colon stem cell clonogenicity by activating β-catenin-dependant transcription (Vermeulen *et al.,* 2010).

Wnt signalling has been found to be crucial for stem cell regulation in multiple systems; for example, knockout of β-catenin in the final stage of differentiation of human pluripotent stem cells (hPSCs) prevented progression to the cardiomyocyte end fate. Later, the specification was regained and a high yield of cardiomyocytes produced from the treatment of hPSCs with GSK-3 - a component of the β-catenin degradation complex - inhibitors and inducible expression of β-catenin short hairpin RNA (shRNA) (Lian *et al.,* 2012).

Wnt is essential to life, specifically in relation to homeostatic regulation of cell turnover, as evidenced by its role in the progression and initiation of numerous cancer types, and in the regulation of stem cell differentiation, for example in the mouse intestinal crypt. Wnt signalling is also essential to early life, a statement which harks back to its discovery as the homologue of *Drosophila* segment polarity gene *wingless* (*wg*). When allowed to aggregate, embryonic stem cells derived from the inner cell mass of blastocyst stage embryos form an embryoid body in which cells from all three germ layers can be found. Axis formation is determined by the formation of the primitive streak, and anteroposterior patterning is established, both induced by Wnt ligand or pathway components (Galceran *et al.,* 1999). Cellular differentiation *in vitro* is influenced by manipulation of the Wnt signalling pathway (ten Berge *et al.,* 2008).

1.3 Wnt signalling and its roles in model organisms

In vivo, Wnt signalling and its influence on axis formation can be traced as far back in evolutionary history as diploblastic metazoan *Hydra* (Hobmayer *et al.,* 2000) and has been well-studied in *Xenopus,* where extracellular maternal Wnt11, dependant on glycosyltransferase Exostosin-1 (X.EXT1) and Epidermal growth factor-Cripto-FRL1-Cryptic (EGF-CFC) protein Crypto-1 (FRL1), activates the canonical signalling pathway that initiates axis development (Tao *et al.,* 2005). The dorsal-ventral axis is the second axis that is determined in amphibians and originates at the point of sperm entry. The cortical rotation at this point produces the Nieuwkoop Centre, a progenitor of the Spemann Organiser. The Nieuwkoop Centre is a grouping of dorsal/vegetal blastomeres, which is such a powerful organising centre that when it is transplanted elsewhere in the embryo, it induces additional axis formation (Zeng *et al.,* 1997). It is thought that the Nieuwkoop

Centre is induced by and dependant on components of the Wnt signalling pathway (Fagotto *et al.,* 1997). In mammals, injection of Wnt inhibitor *axin* mRNA into mouse embryos disturbs dorsal axis formation by interfering with Wnt signalling (Zeng *et al.,* 1997).

In zebrafish, the organiser is called the shield, and Wnt signalling induces dorsal axis formation via accumulation of transcriptional effector β-catenin in the nuclei of dorsal margin blastomeres (Schier & Talbot., 2005), beginning at the 128-cell stage (Dougan *et al.,* 2003), which is driven by cortical rotation. Dorsal nucleic accumulation of the Wnt pathway component, where it can interact with Tcf/Lef transcription factors and induce transcription of target genes, and contrasts with ventral cells where β-catenin remains largely cytosolic (Schohl & Fagotto., 2002). Cortical rotation is integral to axis development in zebrafish, as evidenced by Chung and Malacinski (1980) and Scharf and Gerhart (1980), who treated *Xenopus* and zebrafish eggs with microtubule de-polymerising agents which disrupted rotational movement and resulted in ventralised embryos. Disruption of the cytoskeleton prevented the physical rotation and this manifested as embryos absent of axes because cortical rotation results in the translocation of a dorsal signal which locally activates Wnt signalling (Pelegri., 2003).

The importance of Wnt signalling in axis development is underscored by mutants such as *hectate*, where embryos lack accumulation of β-catenin in dorsal nuclei which manifests as malformation of anterior dorsal structures and dysregulation of Ca2+ release during cleavage (Lyman Gingerich *et al.,* 2005). Healthy Wnt signalling and therefore axis development lays the groundwork for all processes later in development such as the specification of tissues, for example the neuroectoderm and dorsal mesoderm. These tissues are induced by the

purported Spemann activity of the organiser, which is consistent between the zebrafish shield, the *Xenopus* dorsal lip of the blastopore and the mouse node (Harland & Gerhart., 1997). As such, axis development presents one in a myriad of important roles for Wnt signalling in development.

Paracrine Wnt signalling is paramount throughout the animal kingdom, from early origins in *Hydra* to inducing axis development in *Xenopus,* mouse and zebrafish embryos. Throughout the life of an organism, it is essential for regulating stem cells and cell turnover; dysregulation can result in cancer, specifically breast and colon cancers. In early development, it sits at the lynchpin of axis formation and therefore the organisation of the body plan and tissue distribution within organisms. Body patterning is determined by specific gene expression which is generated by paracrine Wnt signalling in concentration gradients across responsive tissues.

Despite the body of knowledge accumulated about Wnt and its actions in organisms, there remains a crucial knowledge gap when it comes to how Wnt is trafficked between cells. How does an extracellular signal assemble into a finely-tuned concentration gradient across responsive tissues? How does the source cell retain control over the dissemination of Wnt proteins that it releases into the extracellular matrix?

1.4 Transport of Wnt proteins

The reception of the palmitoylated glycoprotein canonical Wnt ligand at the cell membrane triggers the cascade of reactions introduced in 1.2. It is widely acknowledged that Wnt proteins act as paracrine morphogens, but historically the mode of transport of Wnt proteins from the sender cell to the receiver cell has been debated. Some prominent hypotheses include exosomal transport (Gross

et al., 2012) and chaperone-mediated transport (Kitajewski *et al.,* 1992) to aid diffusion by encompassing the posttranslational hydrophobic modifications to the Wnt protein. The above methods of transport, however, lack the end-to-end control of production and delivery which seems necessary to generate the fine balance of Wnt gradient which produces wild type tissue patterning. In 2015, the Scholpp lab determined that Wnt proteins were in fact delivered on membranous protrusions called cytonemes, previously characterised in *Drosophila* where they delivered signalling proteins such as hedgehog (hh). Stanganello and colleagues (2015) in the Scholpp lab were the first to identify Wnt-positive cytonemes, which delivered Wnt proteins on the tips of the finger-like protrusions from the sender cell to the receiver cell membrane.

Wnt-positive cytonemes are, like filopodia (membranous protrusions without cargo), dependant on small Rho family GTPase Cdc42 for dynamic actin assembly. Perturbations of Cdc42 resulted in reduced length of cytonemes, and in zebrafish embryos, malformation due to aberrant tissue patterning (Mattes *et al.,* 2018). The Scholpp lab investigated the nucleation of cytonemes and found that overexpression of the tyrosine kinase receptor Ror2 increased both the number and length of cytonemes and therefore acted upstream of Cdc42. Further, visualisation of both fluorescently tagged proteins with confocal microscopy determined that Ror2 bound in a membrane-associated complex with Wnt family member *wnt8a*, the association of which induces planar cell polarity (PCP) signalling – another pathway in the Wnt signalling network - and thereby the production of Wnt-positive cytonemes in sender cells (Mattes *et al.,* 2018). In contrast to the diffusion- or exosome-based hypotheses proposed prior to the discovery of cytonemes, the model of Wnt delivery to target cells presented firstly

by Stanganello and colleagues (2015) and developed by Mattes and colleagues (2018) presents a method by which a Wnt-producing cell can have tight, long-range control over the delivery of Wnt glycoproteins to the receiving cell to confer the precise gradient of a protein so integral to developmental processes.

1.5 The *wnt8a* locus

wnt8a is a complex locus, demonstrated by Figure 2. It has two open reading frames (ORF1, ORF2), two untranslated regions (UTR1, UTR2) and three transcription start sites (TSS). Both ORF1 and ORF2 are transcribed into a singular bicistronic transcript, which Lekven and colleagues (2001) demonstrated by designing two primers which span both ORFs, using the zebrafish as a model organism. A singular transcript is produced, which is later spliced to produce the two alternate products. Blocking the translation of ORF1, ORF2 or both splice forms of *wnt8a* using Morpholino inhibition in zebrafish results in fish with indistinct neural structures along the whole dorsal line, including the head, resulting in a crooked tail. The group also investigated the expression pattern of ORF1 and ORF2 using *in situ* hybridisation. The expression of each ORF differs; at 75% epiboly, both ORF1 and ORF2 are expressed in the marginal zone, yet only ORF2 is expressed in the axial mesoderm (Lekven *et al.,* 2001).

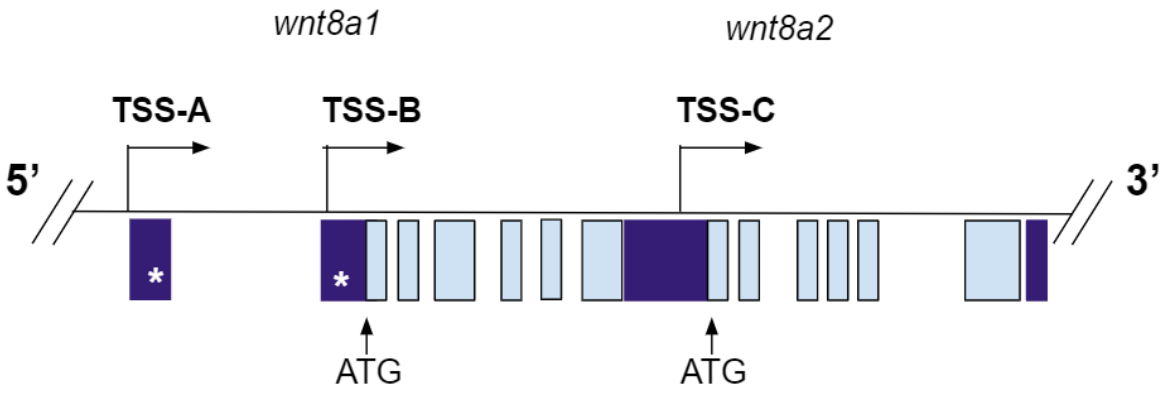

Figure 2: A representation of the *wnt8a* locus, adapted from Wylie and colleagues (2014).
Transcription start sites (TSS) A, B, and C are labelled with arrows. Exons are denoted by boxes; the navy boxes are unexpressed and the light blue boxes are expressed exons. The two boxes with the white star are alternate 5' exons on the bicistronic transcript. Start codons for the first and second open reading frames are marked below the boxes.

1.6 Role of *wnt8a* in zebrafish

Akin to Wnt in other organisms including *Hydra, Xenopus* and the mouse, zebrafish Wnt8a goes on to play a crucial role in axis development (Luz *et al.,* 2014). In particular, Wnt8a has been found to have a posteriorising effect (Erter *et al.,* 2015) along the anteroposterior axis. Axis development in vertebrates is dependent on signals from the dorsal organising centre, a signalling hub first discovered in *Xenopus* by Spemann and Mangold in 1924 which dictates axis formation. The signals emitted by the organiser are such that, when transplanted elsewhere in the *Xenopus* embryo, a second axis is formed. Orthologues of the organiser are found in other animals, such as the avian Henson's Node (Selleck & Stern, 1991), or the teleost embryonic shield. The formation of the *Xenopus* organiser is dependent on maternally encoded β-catenin; reduction in maternal β-catenin RNA results in the loss of axial structures and failure to form the dorsal organising centre (Zhang *et al.,* 1998). Parallels can be drawn to the zebrafish,

where β-catenin also plays a crucial role in axes formation as a transcription factor.

The importance of maternal control over β-catenin nuclear localisation in cells of the dorsal yolk syncytial layer is underscored by the maternal effect recessive *ichabod* mutants which fail to form the zebrafish orthologue of the *Xenopus* dorsal organiser, the embryonic shield. Loss of organisation results in embryos which mostly lack anterior structures, notochord, and have excessive production of ventral tailfin and blood (Kelly *et al.,* 2000). Homozygous *headless* mutant embryos also suffer from an absence of anterior neural structures. In wild type embryos, the Wnt pathway inhibitor Transcription factor 3 (Tcf3) limits the reach of the Wnt gradient along the anterior-posterior axes, which enables Wnt to inhibit anterior fates and promote posterior cell fate on the posterior pole of the axis. The *headless* embryos lack the orthologue of Tcf3, thus removing the anterior border to Wnt signalling. Wnt signalling inhibits anterior fates along the entire antero-posterior axis, resulting in loss of head (Kim *et al.,* 2000).

In wild type embryos, downstream canonical Wnt pathway transcription factor β-catenin induces the formation of the embryonic shield and thereby processes allowing axes formation (Kelly *et al.,* 2000). The Wnt pathway inhibits anterior fates and promotes posterior fates by forming a concentration gradient along the antero-posterior axis which facilitates specific gene induction and in turn the fine-tuned acquisition of cell fate underlying tissue specification. The anterior progression of the Wnt signalling gradient facilitated by cytonemes (Stanganello *et al.,* 2015), is prevented by a wall of Wnt inhibitors, such as Tcf3 (Kim *et al.,* 2000). Wnt8 signalling is required for initiation of formation of the neural crest, the cells of which migrate through the embryo and form parts of the peripheral

nervous system, such as glia. The neural crest is segmented into fore, mid and hindbrain primordia, which are later further specialised by local signalling centres such as the midbrain-hindbrain boundary (MHB). The MHB defines the boundary between orthodenticle homeobox 2 (*otx2),* which induces forebrain and midbrain, and hindbrain gastrulation brain homeobox 1 (*gbx1)* expression. The position of *gbx1* expression determines the posterior border of *otx2* expression and requires *wnt8a* for induction. Thereby, *wnt8a* is responsible for the positioning of the MHB in zebrafish (Rhinn et al., 2005).

1.7 Zebrafish as an experimental model

An advantage of using the zebrafish as an experimental model is that the embryos remain clear until 24 hours post fertilisation (hpf) or prim-5 when the earliest pigmentation begins to form. Structures such as the eye, ear, boundaries of the brain and somites are clearly delineated and visible with a light microscope. The staging system set out by Kimmel and colleagues (1995), is well accepted and sets out the stages of zebrafish development independent of time since fertilisation to account for variables which may cause embryos to develop at different rates, such as temperature. Coupling the well-documented and clearly visible developmental stages of the zebrafish with the ability to induce distinguishable *wnt8a*-deficient phenotype with Morpholino oligomer-based inhibition, the zebrafish provides a promising model for the synthesis and application of a genomic engineering toolkit to manipulate the transcription of *wnt8a* and observe changes to the phenotype of embryos until the prim stage. Zebrafish are commonly used as models to study organelles, for example, the peroxisome (Krysko *et al.,* 2010; Den Broeder *et al.,* 2015).

1.8 Peroxisomes in health and disease

Peroxisomes are dynamic, ubiquitous subcellular organelles with a single membrane, and do not contain any DNA (Walker *et al.,* 2018). Historically, peroxisomes were attributed a similar role to the lysosome, but the last of the major subcellular organelles to be identified have in recent years been recognised for their importance in maintaining a healthy state, a journey which has been termed a 'Cinderella Story' (Schrader & Fahimi, 2008). The functions of peroxisomes are multivariate, and are inclusive of but not limited to homeostatic control of reactive oxygen species (ROS), very long chain fatty acid (VLCFA) β-oxidation, and plasmalogen biosynthesis (Schrader *et al.,* 2012). The proteinaceous content is post-translationally imported from the cytosol (Baker *et al.,* 2016). In addition to proteins, peroxisomes are also reliant on the cytosol for environmental cues. The single membrane-bound organelles can increase or decrease their number dynamically in response to environmental cues, such as the uptake of peroxisome proliferators, a wide array of non-mutagenic chemicals including but not limited to herbicides and the adrenal steroid dehydroepiandrosterone. These chemicals interact with peroxisomal proliferator-activated receptors which induce peroxisome proliferation. In fact, excessive stimulation of the receptors by the proliferator chemicals coupled with cellular proliferation can induce the development of liver tumours in rats and mice (Reddy *et al.,* 1983).

There is a subset of '*PEX*' genes within the genome which are absolutely required for peroxisomes to multiply via membrane building and intake of matrix proteins. The 16 *PEX* genes have multiple functions, the most common of which is in the import of proteins into the peroxisomal matrix or membrane for incorporation.

Some PEX proteins, such as PEX1, are membrane-bound, and facilitate in the transfer of peroxisomal proteins through the single membrane (Geisbrecht *et al.,* 1998), and others are cytosolic, recruiting proteins recognised as peroxisome proteins and guiding them to the peroxisomal membrane for import. A group of PEX proteins recognise cytosolic proteins with a peroxisome targeting signal (PTS), of which there are two types; 1, recognised by PEX 13 and 14 (Maxwell *et al.,* 2003; Shimozawa *et al.,* 2004), and 2, recognised by PEX7 (Braverman *et al.,* 1997). One such targeting signal is SKL, or serine lysine leucine, a major PTS1 signal present at the –COOH terminus found in approximately half of all mammalian peroxisomal proteins (Subramani, 1998).

Mutations in *PEX* genes resulting in loss or impediment of peroxisome function or biogenesis are typically causative factors for the spectrum of diseases associated with peroxisome dysfunction, termed peroxisome biogenesis disorders (Steinberg *et al.,* 2004). Loss of function of peroxisomes leads to a build-up of toxic substrates such as VLCFAs, and insufficiency of peroxisome products such as plasmalogen, a component of the myelin sheath which surrounds axons. These pathologies usually lead to extreme developmental defects or death (Camões *et al.,* 2009). Some well-known examples of genetic diseases attributed to mis-functioning peroxisomes include Zellweger Syndrome, X-linked adrenoleukodystrophy and infantile Refsum's disease (IRD). Zellweger syndrome is the most severe, with patients typically passing away within the first year of life, and symptoms include hypotonia, liver and eye problems (Shimozawa *et al.,* 1999).

Similar to Wnts, peroxisomes have gained an association with cancer which was discovered in rodents. It has been found that the chronic administration of

peroxisome proliferators – any compound which induces the proliferation of peroxisomes – induces liver growth and tumour induction in rats (Reddy *et al.,* 1980). Further, the same result has been found when peroxisome proliferator-activated receptor alpha (*Pparα*) is activated in the liver, and it is thought that the key to resistance to hepatic carcinogenesis in rats fed a non-genotoxic yet potent carcinogen is that these rats are *Pparα* -/- (Gonzalez *et al.,* 1998). The low levels of PPARα in the livers of primates and humans are thought to protect against the carcinogenic properties of peroxisome proliferators (Peters *et al.,* 2005), although as many drugs fall into this group, there remains discussion around their safety (Lai, 2004).

1.9 Peroxisome dynamics

Peroxisomes are dynamic organelles which respond to the cellular environment by reducing or increasing the number as required. The latter is performed either by asymmetrical growth and division from pre-existing peroxisomes or *de novo* biogenesis from the endoplasmic reticulum (ER).

Signals which induce peroxisome biogenesis include an increase in the cytosolic concentration of VLCFAs. This phenomenon was detected early in the history of peroxisome research, soon after their discovery in 1965 (Schrader *et al.,* 2012).

Asymmetrical growth and division from existing peroxisomes is regulated by PPARs, members of the steroid hormone nuclear receptor family. There are three isoforms of PPAR, α, β/δ and γ, with distinct expression domains. PPARs bind cognate ligands such as VLCFA and heterodimerise with retinoid X receptors (RXRs). The heterodimer translocates to the nucleus and acts as a transcription factor which targets Direct Repeat-1 *(DR-1)* peroxisome proliferator response elements *(PPREs). PPREs* mediate the transcription of genes required for the

growth and division of peroxisomes, and the combination of transcriptionally activated genes depends on the isoform of the PPAR – for example, the PPARα has been identified as being central to the pathway which is triggered by the presence of cytosolic VLCFAs, inducing the production of peroxisomes with high levels of matrix β-oxidation enzymes (Ziouzenkova *et al.,* 2002).

PPAR-induced peroxisomal proliferation is essential for response to cellular cues, but their roles extend beyond growth and division of peroxisomes. PPAR expression induced by canonical Wnt signalling has an emerging role in neuronal differentiation, although the mechanism of action is yet to be confirmed. PPARs may be integrated into a number of signalling pathways, including nuclear factor kappa-light-chain-enhancer of activated B cells (NFkB) signalling, and they interplay with sonic hedgehog (SHH) or olig 1 or 2 (Cimini *et al.,* 2005). Another divergent role where PPARs are entwined with Wnt signalling is in the maintenance of cardiovascular rhythms; patients with irregular cardiovascular rhythms were divided into two groups, with either inactivation of the canonical Wnt pathway and increased PPARγ, or activation of the canonical Wnt pathway and decreased PPARγ. Both led to a disease state of cardiovascular arrhythmia, and are unified by changes in Wnt signalling leading to changes in expression of a PPAR (Lecarpentier *et al.,* 2014).

Growth and division of peroxisomes follows a widely-accepted model of membrane tubulation, constriction of the membrane to produce a ‘beads on a string’ effect, and fission of the membrane to separate the ‘beads’ into individual peroxisomes, which is a morphologically distinct mechanism visualised in Figure 3. PEX proteins are also integral to the mechanism of growth and division described above, particularly PEX11β (Schrader *et al.,* 1998), which promotes

the initial tubulation step (Figure 3 b). It facilitates membrane bending by parallel orientation of an amphipathic helix and insertion of hydrophobic residues between fatty acyl chains (Figure. 3 a). At constriction sites, Pex11β interacts with other non-PEX proteins such as the large guanosine triphosphate (GTP)ase dynamin-like protein 1 (DLP1) which assembles in a GTP-dependant manner in a ring around the membrane and constricts via GTP hydrolysis, and DLP1-anchoring proteins mitochondrial fission 1 (Fis1) and mitochondrial fission factor (Mff), which facilitate the final cleavage of the membrane (Schrader *et al.,* 2012).

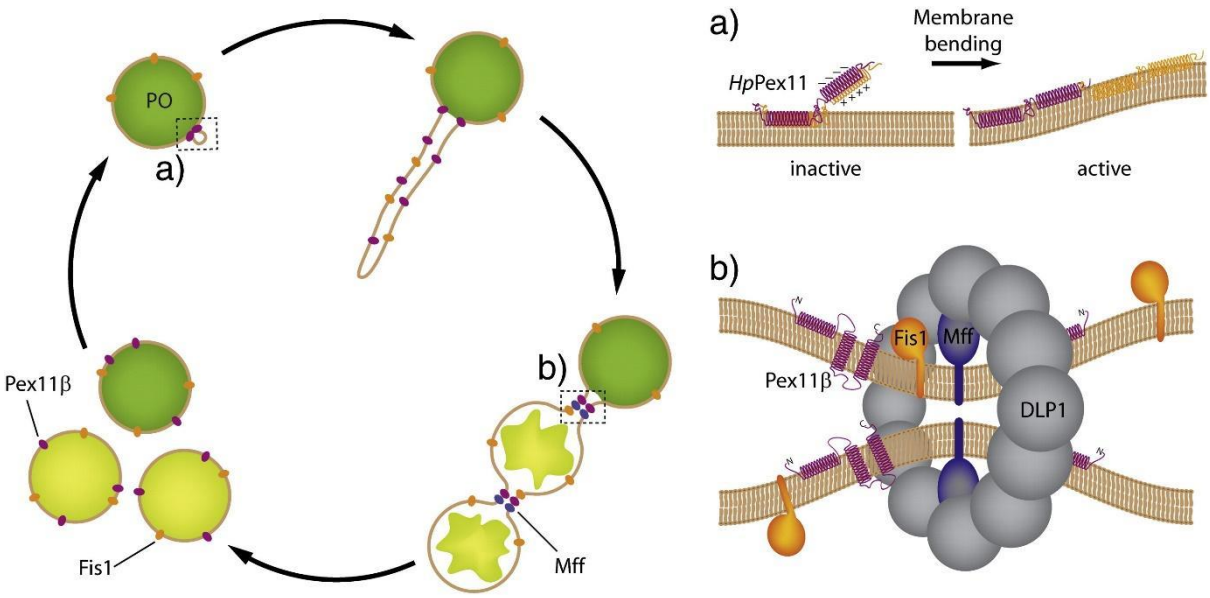

Figure 3: The mechanism of growth and division from pre-existing peroxisomes. A) The facilitation of membrane bending by Pex11β, initiating membrane elongation. B) constriction of the extended membrane by GTPase DLP1 with accessory proteins Fis1 and Mff to form the shape of the future peroxisomes (Schrader *et al.,* 2012).

Interestingly, the components of the division machinery Fis1 and Mff are also shared with mitochondria (Schrader, 2006) across an array of fungi and animals, another cross-link in the 'peroxisome-mitochondria' connection which also includes shared roles in disease prevention and antiviral signalling (Camões *et al.,* 2009). Recently, a link between mitochondrial division and Wnt signalling has

been proposed by Bernkopf and colleagues (2018), whom suggest that mitochondria use Wnt signalling to replenish the pool of mitochondria after a period of stress. During mitochondrial stress, membrane-bound phosphoglycerate mutase Pgam5 is cleaved by presenilin-associated rhomboid-like protein (PARL) and released into the cytosol, where it dephosphorylates Axin-bound phospho-β-catenin. Axin is a component of the β-catenin degradation complex and phosphorylates β-catenin such that it can be later recognised by ubiquitinases to be marked for degradation by a proteasome (Huelsken & Behrens, 2002). By inducing cells to stably express Pgam5, they found that the cells had both greater β-catenin levels and more mitochondria. Conversely, membrane-bound, uncleaved Pgam5 has been found to inactivate the canonical Wnt pathway by dephosphorylating dishevelled, a negative regulator of Wnt signalling (Rauchenberger *et al.,* 2017). Overexpression of Wnt family member Wnt3A has also been found to positively regulate mitochondrial biogenesis through the canonical Wnt pathway (Yoon *et al,* 2010).

Mitochondria and peroxisomes share division machinery (Camões *et al.,* 2009; Schrader, 2006); future investigation may reveal whether they also share Wnt signalling as a positive stimulus for proliferation – Wnt signalling, after all, is linked to expression of PPARs (Cimini *et al.,* 2005; Lecarpentier *et al.,* 2014), master regulators of peroxisome proliferation.

1.10 Following PEX and Wnt through developmental trajectories

Several groups have used large scale single-cell RNA sequencing (scRNA-seq) to analyse the transcriptomes of vertebrates throughout embryonic development. Farrell and colleagues (2018) have implemented scRNA-seq to analyse the transcriptomes of zebrafish embryos from the onset of zygotic transcription until

the 6-somite stage, with a final whole transcriptome data set being produced for some 38,731 cells. Such a high-volume data set is difficult to handle, specifically when coupled with multiple branch sites in the progress from a pluripotent to a fully specified cell type, in addition to complexities induced by developmental asynchrony. Farrell and colleagues tackled the problem using a computational two-pronged approach; a diffusion-based simulation named URD, which mapped out a tree of developmental trajectories beginning at pluripotency and concluding in one of 25 distinct cell fates, and secondly an approach which focussed on modules of co-expressed genes which they connected across developmental time. Combined, they revealed cascades of gene expression leading to each of the 25 cell fates identified. Insights generated from this data include switching of intermediate cell fates at branch points; for example, cell fate switching from notochord to prechordal plate at the axial mesoderm branch point.

Theoretically, this data could be used to identify where *wnt8a* and *pex* genes appear in the developmental trajectory in zebrafish. Given the role of *wnt8a* in segmentation of the neural crest - more specifically in the induction of *gbx1* which antagonises *oxtx2* and therefore dictates the location of the MHB - it may be prudent to focus on trajectories which conclude in neural cell fate. From the 25 cell fates specified by Farrell and colleagues, such trajectories include the neural crest, hindbrain, prechordal plate and notochord. Further, to focus the analysis on when Wnt signalling is at its highest, the data could be further narrowed by examining gene expression at 60-90% epiboly, because this is when Wnt is highly expressed in the marginal zone. Should *wnt8a* and any *pex* genes be co-expressed in the same trajectory at the same developmental stage, it may be a

further indication that there is a relationship between Wnt signalling and peroxisome biogenesis/dynamics.

1.11.0 CRISPR/CRISPRi

To investigate such a relationship between Wnt signalling and peroxisomes, Wnt signalling could be reliably repressed using genomic engineering methods. A novel method of genomic engineering called clustered regularly interspaced short palindromic repeats (CRISPR) has been modified after discovery as part of the microbial immune system (Mojica *et al.,* 2000); the mechanism, advantages and applications of which will be discussed below. CRISPR and its multiple variants have gained traction since their emergence and subsequent development as efficient and precise targeted genome editing tools, and their use is well established in zebrafish. CRISPR can be used to insert (Jung *et al.,* 2016), knock out (Ding *et al.,* 2013), knock down (Gilbert *et al.,* 2013) and enhance the transcription of target sequences (Perez-Pinera *et al.,* 2013). Applications of CRISPR include correcting defective genes in disease, producing disease models and the transfer of advantageous genes in crops and livestock (Sander & Joung, 2014).

The short DNA repeats that constitute the CRISPR system were first recognised in 2005 and were hypothesised to be a prokaryotic adaptive immune system to target foreign nucleic acids (Mojica *et al.*, 2005). Part of this segment of repetitive DNA encodes Cas nucleases, and in isolated *Streptococcus thermophilus* samples resistant to infection by bacteriophages, a large endonuclease now termed Cas9 was found to be encoded (Bolotin *et al.,* 2005) which induces double-strand breaks (DSBs) in DNA at target sites concluding in protospacer adjacent motif (PAM) sites (Deveau *et al.,* 2010). CRISPR Cas9 from the

Streptococcus pyogenes type II system is now widely used, although 40% of bacteria and 90% of archaea possess the machinery (Larson *et al.,* 2013).

Double-strand breaks are repaired by two intracellular repair mechanisms; homology-directed repair and non-homologous end joining. Homology-directed repair is the more precise mechanism but it is much slower than non-homologous end joining, which is more prone to error and commonly results in insertions and deletions (indels). Indels early in the coding sequence can result in frame-shift and non-sense mutations and therefore knockout of the gene of interest. The efficiency of the knockout is variable in zebrafish embryos (Hwang *et al.,* 2013) but can be increased by reducing the distance between the target site and the transcription start codon (Qi *et al.,* 2013). In nature Cas9 endonuclease is guided by a trans-activating CRISPR RNA (crRNA) and targeting crRNA (Jinek *et al.,* 2012), but for genomic engineering, these have been united to form a single chimeric guide RNA (gRNA) consisting of a 3' scaffold region which interacts with Cas9 and a 5' seed sequence directly complementary to the target site concluding in the PAM, NGG (Ablain *et al.,* 2015). The synthetic RNA hybridises to a 20-nucleotide sequence beginning with a G nucleotide and concluding in the PAM (Ding *et al.,* 2013) in a zipper-like fashion. Due to the short size of the gRNA, single base pair mismatches can reduce the efficiency of hybridisation, especially in the 3' end of the seed region where the hybridisation commences (Semenova *et al.,* 2011).

In vivo gene editing to target disease-causing mutations is one of the most exciting applications of CRISPR genome editing technology, yet the potential consequences of unspecific targeting in a live organism are severe. Enhancing the specificity of CRISPR has been addressed recently with the development of

tissue-specific CRISPR, where systemic Cas9 enzyme production is coupled with tissue-specific pol II promoter-driven gRNA synthesis targeted to endogenous genes. Xu and colleagues (2016) have recently shown that it is possible to correct the mutated gene in Duchenne muscular dystrophy model mice by targeting two gRNAs transcribed from muscle-specific promoter MHCK7 to remove the mutant exon. I hypothesise that if a stable CRISPR toolkit is established in zebrafish to target *wnt8a,* this could be made tissue specific to areas of high *wnt* expression such as the marginal zone of the developing embryo, which would be advantageous in increasing the accuracy of knock out in a method which can be limited by mosaicism.

The specificity of CRISPR is not limited to tissues, but also the transcript itself. CRISPR has repeatedly been shown to offer higher levels of target site specificity, and low levels of off-target effects, compared to other genome editing methods currently in widespread use, such as bacterial artificial chromosomes (BACs) and RNA interference (RNAi).

1.11.1 CRISPR in comparison to other knock-out strategies

Mammalian disease models to investigate human pathogenesis have been produced through the insertion of large, stable BACs based on *Escherichia coli* which carry fragments of DNA ranging in size from 150-300 kb. An advantage of this system is that the large DNA insert can include enhancers and other regulatory elements which can reduce undesired effects such as unexpected splicing because of mistargeted insertion into the genome. The stability of such a fragment, coupled with the control rendered by the inclusion of regulatory elements means that it is a widely-used mechanism to produce mammalian models of disease and BACS transgenic mouse models are well-established.

However, the size of the fragment also creates an insertion efficiency problem in addition to an inability to finely tune the insertion site – thus requiring the regulatory elements to mediate the possible effects of insertion in an unintended area of the genome. This has hampered the development of transgenic rat models. In comparison, the precision of the CRISPR method is clearly advantageous and Jung and colleagues (2016) used CRISPR to induce a precise double-stranded break to facilitate insertion of a 4.5 kb BAC using homology-directed repair.

Morpholino oligomer antisense technology has been routinely used to interfere with mRNA translation or splicing. Injection of zebrafish embryos with Morpholino oligomers targeted to splicing regions of fibroblast growth factor 8 (*fgf8)* yielded two aberrantly spliced mRNAs, variant 1 missing exon 3 and variant 2 with a premature stop codon (Draper *et al.,* 2001), which inhibited the ability of the zebrafish to translate wild type *fgf8* transcripts. Morpholino oligomers bind to mRNA due to the affinity of the six-ring heterocycle backbone and non-ionic phosphorodiamidate linkages to ribonucleic acids, the structure of which distinguishes them from other nucleic acid oligonucleotides (Summerton & Weller, 1997). In addition to the affinity for RNA that is given by the modification, Morpholino oligomers also have a high level of stability *in vivo* and are less likely to bind to off-target macromolecules (Summerton, 2007). The sequence of nucleic acids, designed to be complementary to the target region of mRNA, are linked to the morpholine ring backbone.

Yet despite the ease of use of Morpholino oligomers proffered by their stability and strong repressive capability, and the modifications to the oligomer of the morpholine rings which make them less likely to bind to off-target molecules,

there is still a high degree of off-target hybridisation. The resultant off-target phenotypes can be difficult to distinguish from the on-target phenotype, and therefore reduce confidence in the results (Schulte-Merker & Stainier, 2014).

Additionally, due to manipulation of translation as opposed to transcription, PCR methodology cannot be used to screen for target mutations, unlike when using CRISPR and transcription activator-like nucleases (TALENS) (Ding *et al.,* 2013), which would aid in the separation of target and off-target effects. Off-target effects and host toxicity are also a problem that beleaguers RNA interference or RNAi, limiting its development in multiple organisms (Qi *et al.,* 2013).

CRISPR is not only more specific, but also more efficient than other techniques, such as TALENs. TALENs function by pair-wise binding around a target site on the genome, where both strands are broken by a FokI nuclease domain dimer. Construction of TALENs is difficult because cloning is limited by numerous repeat sequences, which are complex and time-consuming to build (Hegazy & Youns, 2016). This contrasts to constructing CRISPR toolkits, which can be done by cloning Cas9 once and designing chimeric gRNAs, which are the only portion of the system that changes. Ding and colleagues (2013) directly compared the efficacy of TALENs and CRISPR in inducing double strand breaks in human pluripotent stem cells (hPSCs) by co-electroporating equal amounts of either plasmid into hPSCs. Electroporated hPSCs were then sorted by fluorescence activated cell sorting (FACS) and then after 24-48 hours, screened for mutation at the target site using PCR. Ding found that while the efficiency of TALENs was 0-34%, CRISPR far exceeded this at 51-79% efficiency. The same was seen in knock-in, and it was hypothesised that this could be partially attributed to greater expression and toleration of Cas9 than TALENs in hPSCs (Ding *et al.,* 2013).

A summary of the attributes of Morpholino oligomers, BACs, TALENs, CRISPR and CRISPRi is provided in Table 1.

Name:	**Morpholino Oligomer**	**TALENs**	**BACs**	**CRISPR**	**CRISPRi**
Interacts with:	mRNA	DNA	DNA	DNA	DNA
Mechanism:	Blocks translation	DSB induction, blocks transcription	Fragment carried on artificial chromosome and inserted	DSB induction, blocks transcription	Physical block to RNA polymerase, blocks transcription
Pros:	*In vivo* stability, strongly repressive	Can use PCR to check DSB position	Stable, can carry high vol. of info.	Specific, can use PCR to check DSB position	Produces a graded phenotype, reversible
Cons:	Volume of off-target effects	Design is highly time consuming	Difficulty finding insertion sites for large fragment	Potential for mosaicism in tissues/whole organisms	Cannot use PCR as a check-point

Table 1: A comparison of Morpholino oligomers, TALENs, BACs, CRISPR and CRISPRi for manipulating gene transcription.

1.11.2 CRISPRi - a flexible method of knocking down genes

In contrast to the aforementioned TALENs, Morpholino oligomers, RNAi and BACs, a variant of the CRISPR system, CRISPR interference or CRISPRi, is also highly specific with low off-target effects. CRISPRi is distinct from CRISPR in that the Cas9 enzyme is rendered catalytically inactive and is termed deactivated

Cas9 (dCas9) by mutations in the two endonuclease domains; RuvC-like, which cleaves the non-complementary strand and HNH, which cleaves the complementary strand (Jinek *et al.,* 2012). Rather than cleaving DNA, dCas9 sits on the strands and forms a steric block to RNA polymerase, blocking either the initiation or elongation of transcription, depending on the location of the target site that the gRNA is engineered to hybridise to. The closer the target site is to the transcription start site, the greater the efficiency of the repression. Additionally, the non-template strand has been found to yield the highest levels of transcriptional repression and targeting the untranslated promoter region also resulted in effective repression. The high targeting specificity made possible by CRISPRi is made tunable by the introduction of nucleotide mismatches in the 5' seed region of the gRNA (Qi *et al.,* 2013).

Aside from high targeting specificity, there are multiple advantages to using CRISPRi to manipulate transcription, including; the ability to target multiple genes, the malleability of inducible and reversible transcriptional repression and variation in capability offered by fusion of effector molecules.

Multiple dCas9-gRNA pairings can be used to target numerous genes simultaneously, or to target different parts of the same gene to enhance repression efficiency (Larson *et al.,* 2013). Recently the problem of limited vector capacity for multiple gRNAs has been investigated by producing multiple gRNAs from a single transcript. CRISPR-associated Csy4 endoribonuclease can be used to cleave the transcript where gRNAs are fused with a Csy4 cleavage site (Nissim *et al.,* 2014), which is advantageous when applying multi-target CRISPRi constructs to cell culture by transfection.

The induction of transcriptional repression by CRISPRi is reversible and inducible. Qi and colleagues (2013) used dCas9 and a gRNA targeting fluorescent signal protein - monomeric red fluorescent protein (mRFP) - with an aTc-inducible promoter in an *E. coli* cell culture. After addition of the inducer, they used time course monitoring to measure the reduction in fluorescence mediated by the action of CRISPRi and found that the fluorescent signal started to decrease 10 minutes after the addition of the inducer, because of transcriptional repression from induced dCas9. Once the inducer was washed away and after a 50-minute delay, the fluorescent signal then began to increase again and it took 300 minutes for single cell fluorescence to equal the positive control. This experiment demonstrated that dCas9-mediated transcriptional repression is simultaneously inducible and reversible. To establish the degree of specificity of transcriptional repression, whole-transcriptome shotgun sequencing, or RNA-seq, was performed on cells transformed with dCas9 and gRNA targeted to mRFP or other loci, and compared to cells transformed with dCas9 alone. Regardless of the locus targeted the only genes with significantly reduced transcription within the whole transcriptome were the gRNA-targeted genes (Qi *et al.,* 2013). This specificity sets CRISPRi apart from other methods such as Morpholino oligomer-mediated inhibition and RNAi, the development of which suffers from off-target effects and toxicity which is hard to trace.

CRISPRi can be further tuned by the addition of effector molecules which can either offer enhanced transcriptional repression or conversely transcriptional activation. Fusion of dCas9 with C-terminal VP64 transactivation domain and pairing this with gRNAs targeted to the promoter region of a target gene has been

shown by RT-qPCR to increase transcriptional activation (Perez-Pinera *et al.,* 2013).

dCas9 can also be fused with effectors that enhance its repressive capacity. HEK293 reporter cells with randomly integrated SV40 promoter-driven green fluorescent protein (GFP) were co-transfected with either GFP dCas9 or dCas9 fused to KRAB, the Krüppel-associated box domain of Kox1, both targeted to GFP. Gilbert and colleagues (2013) found that dCas9-KRAB offered 5 times the repressive capacity compared to dCas9 alone, measured by reduction in GFP fluorescent signal. GFP signal was strongly knocked down for 3 days and silenced for 6 days after transfection, although this can be extended to two weeks by transducing cells stably producing dCas9 with a lentivirus expressing gRNA targeted to GFP. The nucleolytic inactivity of dCas9 was confirmed by sequencing the GFP locus, which retained a wild type sequence without indels. Similar to other studies examining the specificity of CRISPR and its variants, the transcriptome of GFP+ HEK293 cells transfected with dCas9 and gRNA targeting GFP was interrogated using RNA-seq and GFP was the only gene to be significantly down-regulated. Importantly for this project, they also established that CRISPRi could silence endogenous genes, so it can be expected that CRISPRi will be able to repress the transcription of zebrafish *wnt8a* in an efficient, specific and stable manner – which, further, could be made tissue-specific, thus generating mutant zebrafish with *wnt8a* knockout or knockdown at the margin. Subject to successful construction and application of the CRISPR and CRISPRi toolkits, the mutated embryos will be used to observe whether manipulation of *wnt8a* transcription affects peroxisome dynamics.

1.12 Summary of aims and objectives

The aim of this investigation is to interrogate the relationship between Wnt signalling and peroxisome dynamics in the zebrafish. To do this, a multi-faceted approach will be applied. Initially, a CRISPR toolkit will be developed to manipulate *wnt8a* expression. Once established, this genomic engineering will be used in conjunction with methods to visualise peroxisomes in live embryos, to observe any changes in peroxisome dynamics. Peroxisome dynamics may include their subcellular location, morphology and number. Wnt is a family of proteins, and for this investigation, *wnt8a* is selected as the target for CRISPR/CRISPRi. *wnt8a* is known to be highly expressed in the zebrafish embryo in the marginal zone during epiboly, where it is a key structural regulator of nervous tissue (Seiliez *et al.,* 2006).

I hypothesise that there may be a relationship between Wnt signalling and peroxisome dynamics for multiple reasons. Firstly, both Wnt signalling and peroxisome number are high during embryonic development. Additionally, there is a relationship between PPARs, the master regulators of peroxisome biogenesis, and Wnt, in a variety of systems (Huelsken & Behrens, 2002; Cimini *et al.,* 2005; Lecarpentier *et al.,* 2014). Interestingly, a link has also been established recently between Wnt signalling and mitochondrial biogenesis (Bernkopf *et al.,* 2018), with which peroxisomes share components of the division machinery (Schrader, 2006).

2.0 Materials and Methods

2.1 Cas9 and dCas9 retransformation and transcription

Cas9 and dCas9 endonucleases were provided as DNA plasmids (PME-dCas9, P3TSnls-zdCas9-nls, and pCS2-Cas9). Plasmids were retransformed in 5-alpha

competent *E. coli* cells (NEB). Single colonies were selected and incubated in an overnight culture at 37 ˚C. The amplified plasmids were then isolated from the bacteria by mini prep (Qiagen). 5 mL of the overnight culture was spun in a centrifuge at 7000 RPM at 4 ˚C. The supernatant was discarded and the pellet resuspended in 200 µL buffer P1. 400 µL buffer P2 was added and the tubes inverted before incubating at room temperature for 5 minutes. This was then spun at 13,000 RPM for 5 minutes at 4 ˚C. The supernatant was transferred to a new tube and 1 mL of isopropanol added before incubating at room temperature for 20 minutes. The supernatant was spun at 13,000 RPM for 10 minutes at room temperature and the resultant pellet washed with 500 µL 70% ethanol before a final 5-minute spin at 13,000 RPM. The pellet was air-dried and re-suspended in 20 µL H_2O before being stored at -4 °C. The DNA concentration was measured using a Nanodrop (Thermo Scientific). 5 µg of each plasmid was linearized by overnight digest with restriction enzymes (NamH1, Xba, Not1) followed by heat inactivation.

Cas9 and dCas9 mRNAs were transcribed from linear template DNA using the Sp6 (pCS2-Cas9), T3 (P3TSnls-zdCas9-nls) or T7 (PME-dCas9) RNA transcription kits (Invitrogen, Thermofisher). 4 µL of the template was added to 10 µL 2x NTP/CAP, 2 µL 10x reaction buffer, 2 µL enzyme mix and 2 µL nuclease-free water to a total of 20 µL, mixed thoroughly and incubated at 37 ˚C for 2 hours, after which 1 µL TURBO DNase was added and incubated for a further 15 minutes at 37 ˚C. The reaction was stopped by adding 30 µL nuclease-free water and 30 µL lithium chloride precipitation solution and chilled overnight at -20 ˚C. RNA was then pelleted by centrifugation at maximum speed at 4 ˚C for 15 minutes. The RNA pellet was washed with 1 mL 70% ethanol, which was then

removed and the pellet allowed to dry before re-suspending in 20 µL nuclease-free water. A nanodrop (Thermo Scientific) was used to measure the final RNA concentration before storage at -20 ˚C. Efficacy of the amplified Cas9 and dCas9 RNA was tested by coupling with gRNA targeting *tyrosinase* (5' CCCCAGAAGTCCTCCAGTCC 3'), an enzyme required for the conversion of tyrosine to melanin for pigment generation during zebrafish embryogenesis (Camp & Lardelli, 2001).Expression of *tyrosinase* is, therefore, a convenient marker to investigate the functionality of Cas9 and dCas9 by measuring pigment loss.

2.2 Zebrafish maintenance, husbandry and spawning

All zebrafish work has been carried out in accordance with Home Office regulations. Wild type WIK zebrafish (Zfish (WIK), Stock, UoE 26.11.14 GP (PIL:30/6867), 1 (PPL:30/2868)) used are maintained in aerated 28°C ± 1°C water in a flow-through system using mains tap water filtered by reverse osmosis (Environmental Water Systems (UK) Ltd). Water is reconstituted with Analar-grade mineral salts to standardise synthetic freshwater (final concentrations to give a conductivity of 300 mS: 117 mg/L $CaCl_{22}H_2O$, 25.0 mg/L $NaHCO_3$, 50 mg/L $MgSO_{47}H_20$, 2.3 mg/L KCl, 1.25 mg/L Tropic Marine Sea Salt). Fish are housed in a room dedicated to zebrafish maintenance in the custom-built Aquatic Resources Centre (ARC) at the University of Exeter. Fish are fed to satiation thrice daily with *Artemia nauplii* (ZM Premium Grade Artemia, ZM, Hampshire, United Kingdom) and Gemma Micro (300 µm) pelleted food (Trouw France S.A.). The photoperiod program is consistent throughout the lifetime of the fish and consistent through every spawning event: 12 hours light, 12 hours dark with a 30 minute transition period. The zebrafish were sexed by ARC staff and housed in a

2:1 female-male ratio in spawning chambers overnight. At the start of the daily light cycle, the dividers between male and females were removed. Spawning and fertilisation commenced for half an hour before fish were replaced into the mixed population and the embryos collected. Embryos were injected from the one to four cell stages (Kimmel *et al,* 1995) using the Eppendorf FemtoJet 4x with glass microinjection needles. Glass capillaries with filament (1 mm/0.75 mm OD/ID) were prepared on a Flaming/Brown Microcapillary Puller P-97 from Sutter Instrument.

Embryos were maintained in E3 media in a 28 °C incubator until 28 hours post fertilisation (hpf). Embryos were removed from the chorion using pronase and fixed in 4% paraformaldehyde (PFA), henceforth remaining at -4 °C. Images were taken using the Olympus DP71 and analysed using ImageJ software (Schneider *et al.,* 2012). Images were converted to 8-bit and an unsharp mask was added (radius 2). A pigmentation threshold was set which was applied to all images, and the area between the MHB and the first somite was selected for particle analysis.

2.3 Sequencing the *wnt8a* locus

The efficacy of retransformed Cas9 and dCas9 endonucleases thus ascertained, I designed chimeric gRNA to target the gene of interest, *wnt8a.* Both open reading frames of *wnt8a* were sequenced, including both untranslated regions. Primers (*wnt8a1* forward 5’ GGTCTTTTCACAGCGAATTG 3’, reverse 5’ ATGTAGTCTGGTTTTGACCG 3’. *wnt8a2* forward 5’ TGGCATCCTTTGAAGTTCTG 3’, reverse 5’ CCAAACGTCCAGCTTCATT 3’) were designed to span the UTR – exon 3 of both ORFs and the sequences were amplified using polymerase chain reaction (PCR) in the Eppendorf Mastercycler Nexus Gradient GSX1 Thermal Cycler (Hamburg, Germany) with genomic DNA

(gDNA) template (5 minutes at 95 °C to denature the DNA, then 30 cycles of 95 °C for 30 seconds, 50 °C for 30 seconds, 72 °C for 45 seconds, followed by 10 minutes at 72 °C). PCR product was run on 1.5% agar gel electrophoresis at 110V and positive bands selected for insertion into TOPO-TA vector. 2 µL PCR product was combined with 1 µL salt solution, 2 µL water and 1 µL TOPO vector, mixed gently and incubated for 30 minutes at room temperature before pipetting 2 µl into 5-alpha competent *E. coli* cells (NEB) and plating. Plates (one kanamycin, one ampicillin) were treated with X-Gal reporter before incubating at 37 °C overnight. White colonies were selected from each plate for overnight culture in LB medium at 37 °C. Amplified TOPO plasmids with the PCR product insert were purified by MIDIprep using the Qiagen protocol. Purified vectors with *wnt8a1* or *wnt8a2* inserts were sequenced by Eurofins Scientific.

2.4 gRNA design

Sequenced *wnt8a1, wnt8a2* from experimental fish in the ARC facility were compared to sequences available in online databases (NCBI) and were an exact match at all sites where gRNAs would be designed. CRISPR target sites were identified and ranked by off-target quality in the *wnt8a* gene locus using CCTOP, the CRISPR/Cas9 online target site predictor from the Centre for Organismal Studies, Heidelberg (Stemmer *et al.,* 2015). Target sites with low off-target specificity were identified in both untranslated regions, and exons one and three of both open reading frames. 20 (+3) base pair Invitrogen TrueGuide Synthetic guide RNAs (Thermo Fisher Scientific, Synthego, USA) were then designed to be complementary to these target sites as demonstrated in Figure 4, terminating in the PAM site (NGG). Sequences are provided in Table 2. The custom synthetic two-piece gRNAs were diluted to 100 µM stocks, and the RNA concentration

measured using a Nanodrop (Thermofisher). 5 µL stock was incubated with 2 µL tracrRNA, 5 µL annealing buffer and 13 µL of water at 95 ˚C for five minutes, decreasing to 50 ˚C at a rate of 0.1 ˚C/s and remaining there for ten minutes, after which decreasing to 4 ˚C at a rate of 1 ˚C/s.

Target site 5'-3' (PAM)	**Position on locus**	**Strand**
TTGCCAGATTTTTGCGTCGT**TGG**	ORF1 Exon 1	Template
AGTGCAAGCATCAGTTCGCA**TGG**	ORF 1 Exon 3	Template
AGGGAGGATCGAGCAATCAC**TGG**	UTR1 site A	Non-template
GCAAAGCACAAACACTGAGA**TGG**	UTR1 site B	Template
GGCCTTTCTATTCCCTATTT**GGG**	ORF2 Exon 1	Non-template
TATGCAAATAGTGTGCGGGT**TGG**	ORF2 Exon 3	Non-template
AAAGGCAATGTACTGATTCG**AGG**	UTR2 Site A	Template
TTCCTCCAAAGGGGGTCAGA**AGG**	UTR2 Site B	Template
TTGCCTTTGTCTTATCACTT**TGG**	UTR2 Site C	Non-template

Table 2: gRNA target sites in *wnt8a.* PAM sequence is underlined and bolded.

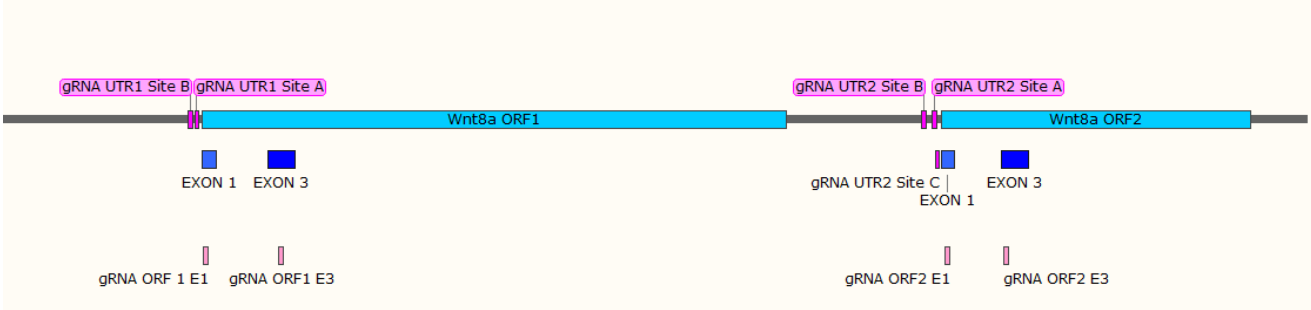

Figure 4: Representation of *wnt8a1* and *wnt8a2*.
Royal blue blocks denote exon 1 and 3, where gRNAs designed to pair with Cas9 endonuclease were targeted, denoted by the light pink sections below (SnapGene® software (from GSL Biotech; available at snapgene.com)).

Cas9 RNA and custom gRNAs were tested by *in vitro* digestion to investigate whether the components would successfully cleave the substrate DNA *in vitro*, using ORF1 of *wnt8a,* amplified previously in TOPO vectors which were digested using restriction enzyme BSA1 (NEB) and CutSmart buffer (NEB) at 37 ˚C for 2 hours followed by a 20 minute heat inactivation at 80 ˚C. 300 nM gRNA was incubated with Cas9 RNA and Cas9 nuclease buffer at 37 ˚C for 10 minutes before adding 2.5 µM of either substrate and incubating for 1 hour. The mixture was then loaded onto a 1.5% agarose gel and ran at 110 V.

2.5 Phenotypic Analyses

Once successful cleavage of target DNA was established *in vitro,* injection mixes were prepared using 50 ng/µL gRNA, 300 ng/µL Cas9/dCas9 enzyme, 0.5 µL each of phenol red (for marking embryos as injected during injection) and mini emerald (as a fluorescent marker for injection so that embryos could later be sorted), and nuclease-free water to a total of 5 µL. Injections were performed using glass microinjection needles pulled as previously (2.2). Care was taken to ensure a consistent droplet size. Embryos were then kept in 1x E3 medium in a 28 ˚C incubator until 28 hpf, where they were fixed in 4% paraformaldehyde

(PFA). Images of the embryos were taken using the Olympus DP71. Embryos in each sample were counted and categorised into three phenotypic classifications; wild type, mild and severe. The three classifications were described as the following: mild embryos showed some disruption to the nervous tissue; loss of clear MHB, misshapen eye, and perturbation of nervous tissue along the dorsal axis resulting in crooked tails. Severe embryos showed disrupted nervous tissue with loss of nearly all or all structure, no visible MHB, misshapen eye and tails crooked to a greater degree. The number of embryos in each phenotypic group was counted and averaged between injection dates and standard error was calculated. Statistical significance was calculated using a Chi-squared test.

Phenotypes generated from CRISPR/CRISPRi targeting of *wnt8a* were compared to Morpholino oligomer targeting of the same gene (Table 3). Injection mixes consisting of 0.5 µL phenol red, 0.5 µL mini emerald, 0.5 µL of Morpholino oligomer targeting ORF1, or ORF2, or a combination of both, diluted to 1:10, plus nuclease-free water to total 5 µL were prepared. Embryos were injected as previously (2.2), categorised and analysed in the same manner as above to provide a comparison.

Morpholino oligomer 5'-3'	**Position on locus**
ACGCAAAAATCTGGCAAGGTTCAT	ORF1
GCCCAACGGAAGAAGTAAGCCATTAA	ORF 2

Table 3: Morpholino oligomer target sites on open reading frames 1 and 2 of *wnt8a.*

2.6 *In situ* hybridisation

Embryos were collected as previously (2.2) and injected with the same combination of Cas9/dCas9 RNA and gRNA as were used to examine the phenotypes generated (2.5). After maintenance in E3 media in a 28 ˚C incubator, embryos were fixed overnight in 4% PFA at ~80% epiboly. Fixed embryos were dechorionated using forceps in PBST and incubated in 100% methanol. The next day, the dechorionated embryos were washed in PBST and re-fixed in 4% PFA. Fixed, dechorionated embryos were incubated at 69 ˚C with hybridisation buffer (Hyb+) for 30 minutes before transferral to a solution of probe diluted 1:20 in Hyb+ overnight.

Probes were transcribed from plasmid stocks (zWnt8a ORF1, zWnt8a ORF2, digested by Cla1/BamH1) using the T7 MegaShort transcription kit (Invitrogen, Thermo Scientific). Both probes were transcribed with 10x digoxigenin (DIG) antigen for 1-2 hours at 37 ˚C before stopping the reaction with EDTA.

The next day, the embryos were washed with Hyb-, SSCT and MABT before blocking for the remainder of the day with 2% Roche blocking buffer. Embryos were then transferred into a solution of pre-absorbed anti-DIG antibodies (Roche Diagnostics) diluted 1:4000 in 2% Roche blocking buffer at room temperature overnight. Embryos were then washed in MABT and immersed in staining solution NCIP-BCP (Roche Diagnostics) diluted 1:200 in freshly made NTMT. Staining was left to develop overnight, and once this was achieved, embryos were stored at 4 ˚C in 70% glycerol.

2.7 RT-qPCR

To quantify changes in gene expression, embryos were collected (2.2) and injected with the same constructs used to observe changes to phenotype (2.5)

and RNA expression pattern (2.6). Additionally, some embryos were injected with 200 ng/µL *wnt8a1* RNA to establish the specificity of the primers designed to amplify either ORF1 or ORF2 of *wnt8a.* Further controls were implemented by injection of 300 ng/µL dCas9 or Cas9 RNA without gRNA.

Injected embryos were maintained at 28 ˚C in an incubator until 75% epiboly. Each sample (50-100 embryos) were homogenised with 250 µL Trizol (Invitrogen, Thermo Scientific) until fully dissolved. 250 µL ice-cold 100% ethanol was added to each sample and after vortexing, transferred to a Direct-zol RNA MiniPrep column (Zymo Research) which was centrifuged (Sorvall ST 8R Centrifuge, Thermo Scientific) at 4 ˚C for 1 minute at 13,000 RPM. 80 µL DNAse solution, consisting of 5 µL DNAse and 75 µL DNAse buffer was added before further centrifugation under the same parameters. 400 µL of pre-washing buffer was added twice, alternating with centrifugation as before, and finally, 700 µL washing buffer was added. The supernatant was discarded and the columns centrifuged dry. When dry, 25 µL of nuclease-free water was added for final centrifugation and the end concentration of extracted RNA was established by a Nanodrop (Thermo Scientific). RNA was stored at -80 ˚C.

Extracted RNA was reverse transcribed to produce cDNA. An initial mix of 1 µg RNA, 1 µL random hexamer primer (Promega) and nuclease water to total 11 µL was incubated for 5 minutes at 70 ˚C. Initially, the samples were doubled to include samples without M-MLV RTase (RT-) (Promega) to ensure that no amplification occurred autonomously. RT+ samples were incubated for 1 hour in a 37 ˚C water bath with 4 µL m-MLV RTase 5x buffer, 1 µL m-MLV Rtase, 2 µL 10 mM dNTP mix, 0.5 µL RNAsin (Promega) and 1.6 µL 25 mM $MgCl_2$

(Fermentas) followed with a 10 minute heat inactivation at 70 ˚C. The final 20 µL of cDNA was diluted to 1:100 for qPCR.

All primers were diluted to 1:100 for qPCR. Primers included: housekeeping gene β-actin 1, Wnt targets axin 2a and lef1, and two primers for each open reading frame of Wnt8a – wnt8a1A, wnt8a1B, wnt8a2A, wnt8a2B. The forward and reverse sequences of the primers are in Table 4. Per well, 4 µL of forward and reverse primer were added to 5 µL SYBR® Green Real-Time PCR Master Mix (Promega) and 1 µL cDNA. Each sample was pipetted in triplicate into a 364 well plate (Thermofisher Scientific) and ran in the Quant Studio 6 Flex Real-Time PCR System (Thermofisher Scientific).

Target Gene	**Forward (5'-3')**	**Reverse (5'-3')**
β-actin 1	CCTTCCTTCCTGGGTATGG	GGTCCTTACGGATGTCCAC
Axin 2	CAATGGACGAAAGGAAAGATCC	AGAAGTACGTGACTACCGTC
Lef 1	CAGACATTCCCAATTTCTATCC	TGTGATGTGAGAACCAACC
Wnt8a 1A	CGGAAAAATGGGTGGTCGTG	GTCGTGACCATTTTCCAGCG
Wnt8a 1B	GAGAGACCGCCTTTGTGCAT	CACGACCACCCATTTTTCCG
Wnt8a 2A	ATTCGTGGATGCGCTTGAGA	TTTACAGCCAAACGTCCAGC
Wnt8a 2B	ACAATTCGTGGATGCGCTTG	TCGCTTTTACAGCCAAACGTC

Table 4: Primer sequences against target genes indicated in the left column.

2.8 Cell culture and peroxisome visualisation

Primary gastric adenocarcinoma cells (AGS) were maintained at 37 ˚C in RPMI 1640 supplemented with 10% fetal bovine serum, 1% L-glutamine and 1% penicillin/streptomycin. Zebrafish PAC2 fibroblasts derived from zebrafish embryos at 24 hours were maintained at 28 ˚C in an incubator without additional CO_2 supply in Leibowitz-15 media, supplemented with the same components as RPMI. Both media and supplementary components sourced from Life Technologies, Gibco.

To visualise possible peroxisomes in cell culture, cells were transfected using FuGENE transfection reagent (Promega) and 1 µg of SKL-GFP DNA. Transfected cells were imaged after 24 hours on the Leica SP8 Hyvolution II confocal microscope (Leica Microsystems, Germany) at 63x magnification. IMARIS x64 9.0.0 imaging software (Bitplane, Switzerland) was used to count the number of SKL-positive spherical structures per cell. A threshold was set in the 'spots' function to capture all 'peroxisomes' whilst eliminating the capture of background fluorescence. The diameter of the spots was 1-1.5 µm, applied to all images. Single cells were selected for each count to eliminate the errors stemming from averaging a group of cells.

After establishing this baseline of an approximate number of peroxisome-like structures in untreated cells, cells were treated with either Wnt inhibitor 4-(1,3,3a,4,7,7a-Hexahydro-1,3-dioxo-4,7-methano-2H-isoindol-2-yl)-N-8-quinolinyl-Benzamide (IWR1, 25 µM) or activator 6-bromoindirubin-3'-oxime (BIO, 2.5 µM) or as a control, dimethyl sulfoxide (DMSO) (equalling the largest volume of effector that was applied) to establish whether a change in count of

'peroxisomes' occurred. Concentrations were selected after several experiments using IWR1 and BIO on both AGS and PAC2 cell cultures at concentrations ranging from 10-50 µM IWR1 and 1-5 µM BIO. The highest concentration which did not induce excessive cell death was selected for each effector. IWR1 binds to Axin and promotes the stabilisation of the β-catenin destruction complex, thus enhancing the degradation of β-catenin and blocking the canonical Wnt signalling pathway (Chen *et al.,* 2009). Conversely, BIO inhibits GSK-3, a component of the β-catenin degradation complex, thereby reducing β-catenin degradation such that cytosolic β-catenin levels increase and the canonical Wnt signalling pathway is maintained (Tseng *et al.,* 2006). Peroxisome-like structures were counted using the same 'dots' function per cell. A student's t-Test, two sample assuming unequal variances, was used to establish statistical significance.

2.9 Visualising peroxisomes in live embryos

Embryos were collected and injected under the same conditions as previously (2.2). SKL-GFP DNA at 50 ng/µL was injected with 50 ng/µL memb-mCherry. Embryos were maintained at 28 ˚C in E3 medium until 50% epiboly when they were dechorionated using forceps and mounted in melted 1.5% agarose. The well was flooded with E3 media and images were taken on the Leica SP8 Hyvolution II confocal microscope (Leica Microsystems, Germany) at a 63x magnification. Images were converted to Easy-3-D.tif files using IMARIS x64 9.0.0 (Bitplane, Switzerland) and analysis was completed in ImageJ. An unsharp mask filter was first applied (radius - 2.0 pixels, mask weight – 0.6) to sharpen the images. This also sharpened any background into distinct, minute dots, which were eliminated by using the de-speckle noise function. A colour threshold was applied to capture the green areas (the peroxisome-like structures) and remained

consistent for all images analysed. A cell was then selected, the area calculated and the area of green puncta within that cell calculated. This allowed both the total area of peroxisome-like structures to be calculated, and the different sizes of the cells within which peroxisomes were analysed were taken into consideration by calculating the percentage of each cell area which was filled by the peroxisome-like structures. Standard error and statistical significance were calculated using a Student's t-Test, two sample assuming unequal variances.

Concurrently, observations were made of the morphology of the peroxisome-like structures and their subcellular locations within the cells at x63 magnification; this included whether the peroxisome-like structures were aggregated or appeared to be presented as separate puncta. Particular note was taken to see if the structures were in formations which resembled the classical asymmetrical membrane extension and fission model of peroxisome biogenesis because it is a morphologically distinct and recognisable process.

As well as the total area of the cell occupied by the peroxisome-like structures, the distribution of sizes of the individual structures were analysed by producing weighted histograms. Bins were initially set wide to establish where the highest frequency sat in each sample then was reduced to 0.000050, 0.000100, 0.000500, 0.001000, 0.005000, 0.010000 and 0.050000 µm. The frequency of measurements which fell into each bin was established and then compared to the total number of measurements for each sample to produce weighted histograms. The weighted frequencies were compared between samples using a student's T-test assuming unequal variances.

Once a baseline number, subcellular distribution and morphology of peroxisome-like structures within cells in the zebrafish embryos was established, zebrafish

embryos were injected as previously (2.2) with mixes all incorporating SKL-GFP (50 ng/µL) and membrane mCherry (50ng/µL). Mixes were designed either to knock out (Cas9 + gRNA), knock down (dCas9 + gRNA), or increase (*wnt8a* RNA) canonical Wnt signalling. Additionally, embryos were injected with Morpholino targeted to *wnt8a* RNA to provide a comparison for CRISPR-mediated silencing. Injection of *wnt8a* RNA artificially increased canonical Wnt signalling and acted as a positive control. Full details of the injections are found in Table 5.

Injection	**Peroxisome Marker (50 ng/µL)**	**Membrane Marker (50 ng/µL)**	***Wnt8a* Targeting System**	**Position targeted on the *wnt8a* locus**
Control	SKL-GFP	Memb-mCherry	-	-
CRISPR	SKL-GFP	Memb-mCherry	Cas9 + gRNA	ORF1 + ORF2
CRISPRi	SKL-GFP	Memb-mCherry	dCas9 + gRNA	UTR1 + UTR2
Morpholino oligomer	SKL-GFP	Memb-mCherry	Oligomer	Wnt8a RNA
Overexpression	SKL-GFP	Memb-mCherry	*Wnt8a* RNA	-

Table 5: Composition of injection mixes injected into zebrafish embryos.

3.0 Results

3.1 Testing dCas9 and Cas9 RNA with *tyrosinase* gRNA

In order to test the efficacy of the CRISPR system and specifically Cas9 and dCas9 RNA *in vivo,* the endonucleases were paired with gRNA targeting the *tyrosinase* gene, which is involved in the generation of pigmentation during embryogenesis. By 28 hpf, embryos injected with *tyrosinase* gRNA and Cas9 or dCas9 RNA exhibited significantly less ($P<0.0005$) pigmented area (Figure 6) between the MHB and the 1st somite (Figure 5) compared to wild type (WT) embryos, which were uninjected. This inferred that Cas9 and dCas9 retransformed and transcribed from plasmids were functioning to either cleave or block the transcription of dsDNA in partnership with gRNA. There is a significant difference between the amount of pigmented area in CRISPR and CRISPRi embryos (Figure 6), which aligns with the role of Cas9 in knocking out the target gene and therefore providing a greater level of transcriptional repression than dCas9 does in knocking down the target gene; their effects are significant in themselves when compared to the wild type embryos but also when compared to each other. Visually, the difference in the phenotypes induced by Cas9 or dCas9 are apparent in Figure 5, where, focussing on the eye, there are white spots where cells are entirely missing pigmentation. Here, Cas9 has knocked out the *tyrosinase* gene. This reflects the mosaic pattern typical of using Cas9; in some cells, there is knock out of the target gene, but in others, tyrosinase is translated without inhibition and the cells are pigmented as a wild type because the cell is absent of active Cas9, gRNA, or both. In the bottom image, again focussing on the eye for comparison, there is some black, grey and white. This colour gradient

directly relates to the level of *tyrosinase* knockdown induced in the cells and visually demonstrates how dCas9 can be used to generate a gradient of responses.

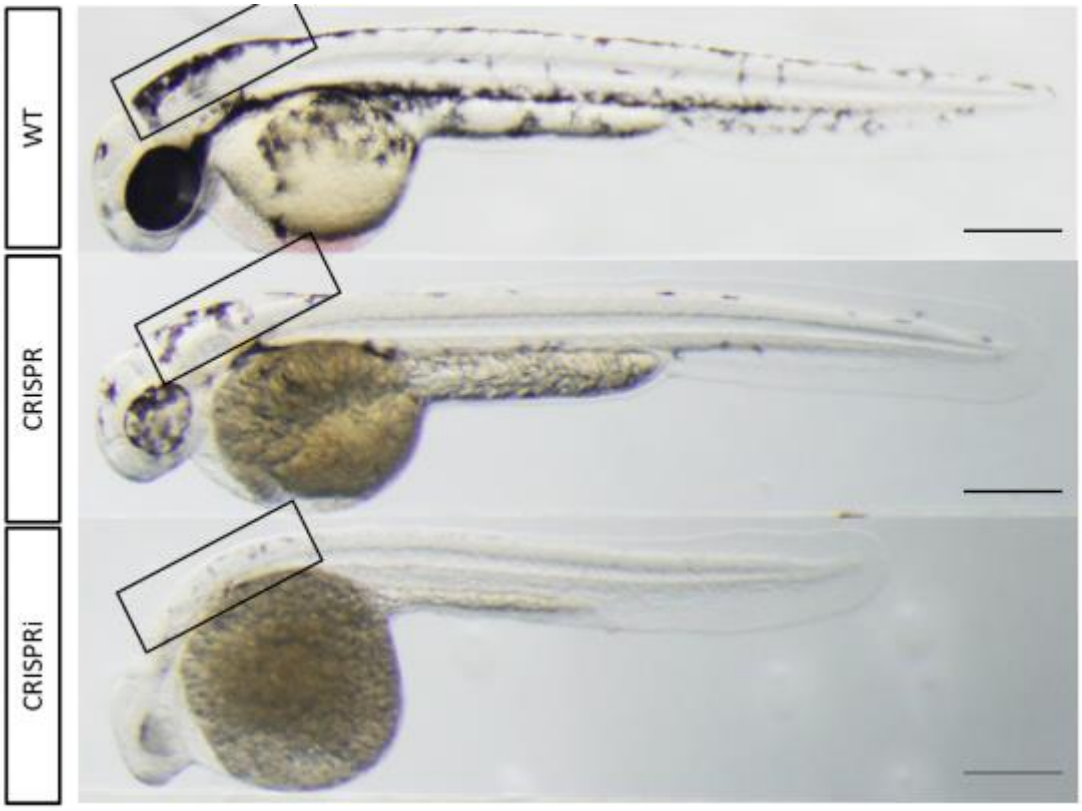

Figure 5: Zebrafish embryos with CRISPR and CRISPRi targeting *tyrosinase.* Images taken of embryos all fixed at 28 hpf. Box represents the area selected for analysis using ImageJ, although the freehand selection tool was used to omit the yolk. The top picture (WT) shows the pigmentation exhibited by a wild type embryo. The central picture shows the pigmentation exhibited by an embryo that was injected at the 2-8 cell stage by Cas9 RNA and *tyrosinase* gRNA. The bottom picture shows pigmentation exhibited by an embryo injected with dCas9 RNA and *tyrosinase* gRNA. Scale bar 500 µm.

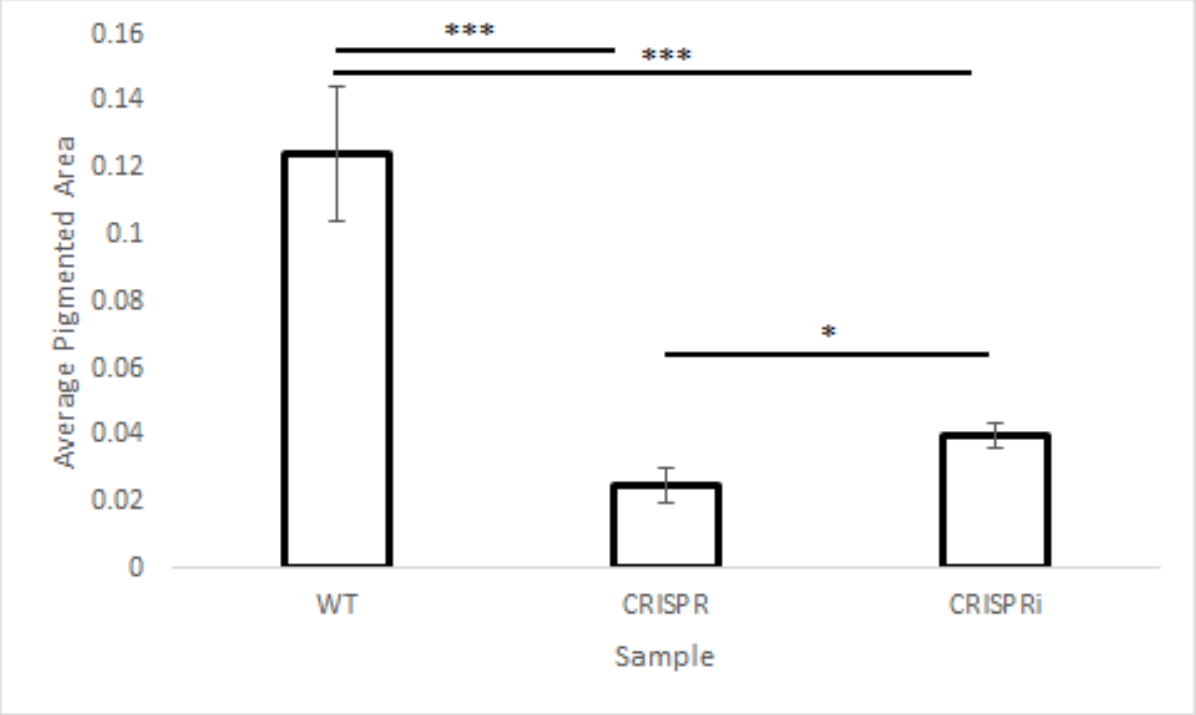

Figure 6: Quantification of pigmented area between the MHB and 1st somite of wild type control embryos.
Embryos injected with Cas9 RNA and *tyrosinase* gRNA and embryos injected with dCas9 RNA and *tyrosinase* gRNA. Error bars show standard error, significance calculated using analysis of variance (ANOVA) (*P<0.05, ***P<0.0005).

3.2 *In vitro* digestion using *wnt8a* gRNAs

gRNA targeting *wnt8a1* and Cas9 RNA cleaved *wnt8a1* DNA *in vitro*, demonstrated by gel electrophoresis of the reaction products. Figure 7 shows in the leftmost lane the DNA ladder, followed by the uncut TOPO plasmid with *wnt8a1* insertion. This band corresponds with the top bands in the remaining 4 lanes, showing that some of the plasmid remained uncut and that the efficiency of the Cas9 enzyme is not 100%. Visualised by the intensity of the band, there is some discrepancy between the cutting efficiency of the gRNA-Cas9 couplings; for example, Cas9 coupled with UTR1B (targeted to the untranslated region of *wnt8a* ORF1, site B) shows a thinner and less intense band than Cas9 coupled

with UTR1A. The two bands below the uncut plasmid in each of the four rightmost lanes corresponds to plasmid cleaved by Cas9 enzyme.

This method does not test whether dCas9 RNA is effective when combined with the *wnt8a* gRNA, but the dCas9 RNA was already tested with *tyrosinase* gRNA *in vivo*. gRNA targeting *wnt8a2* was not tested because of the difficulties in capturing the correct sequence for integration into the TOPO vector. Due to the design process for ORF2 being an exact replica of that for ORF1, and the resultant ORF1 gRNAs successfully guiding Cas9 to the target DNA *in vitro,* both sets of gRNAs were taken forth to the next step of testing the coupling *in vivo.*

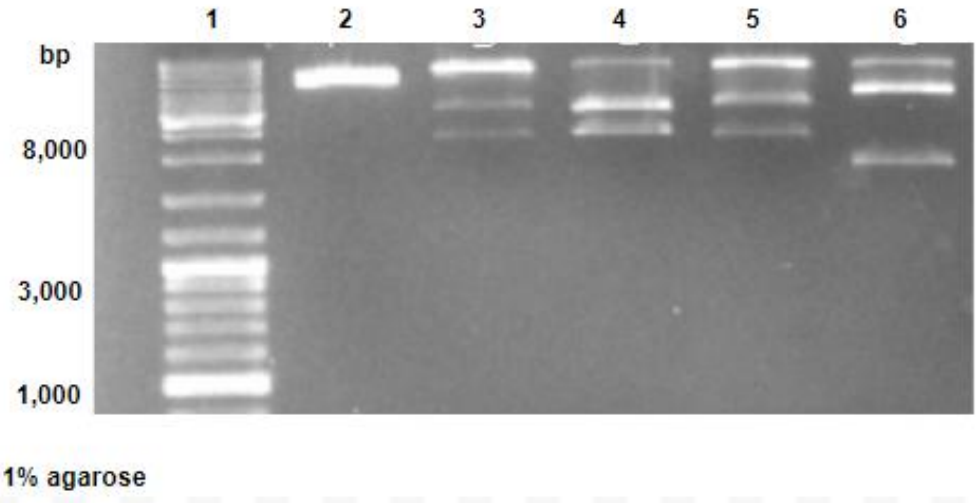

Figure 7: *In vitro* digestion of zebrafish *wnt8a1* DNA after CRISPR.
1: DNA ladder, 2: TOPO-*wnt8a1* plasmid, 3: UTR1A gRNA + Cas9, 4: UTR1B gRNA + Cas9, 5: ORF1,1 gRNA + Cas9, 6: ORF 1,3 gRNA + Cas9. TOPO-*wnt8a1* plasmid is present in all wells, cut by gRNA targeted to *wnt8a1* and Cas9 RNA.

3.3 Phenotypic analysis of injected embryos

The combination of Cas9 RNA and gRNA targeting *wnt8a* cleaved zebrafish genomic DNA *in vitro.* To test the coupling *in vivo,* zebrafish embryos were injected with Cas9/dCas9 RNA and gRNA targeted to either ORF1 or ORF2 of

wnt8a1 or *wnt8a2* to visualise the phenotypes induced *in vivo* by 28 hpf, when neural structure is clearly delineated (Kimmel *et al.,* 1995).

Embryos injected with Cas9 (Figure 8 B) or dCas9 (Figure 8 C) controls, in the absence of a gRNA, appeared phenotypically similar or equivalent to un-injected wild type controls (Figure 8 A), which indicated that injection of the construct did not significantly change the phenotype nor the expression of *wnt8a.* Embryos were not injected with gRNA only, so comparison is not available with this type of control, although should in future studies.

Generally, embryos injected with Cas9 and gRNAs targeting either ORF1 or ORF2 of *wnt8a* showed a stronger phenotype than those injected with dCas9 RNA and gRNAs targeted to the UTRs of *wnt8a*. Regardless of the endonuclease injected, targeting either UTR2 or ORF2 produced stronger phenotypes than those targeting UTR1 or ORF1, in congruence with other studies that used Morpholino oligomers to target the ORFs individually and found that a stronger phenotype was generated when targeting ORF2 (Lekven *et al.,* 2001).

After examination of all samples, I found that the phenotypes could be grouped into three categories to aid quantification. Category 1 contained embryos which retained a wild type appearance, reflecting image Figure 8 A, with a straight tail, clearly visible neural structure including the MHB at 28 hpf. Category 2 contained embryos with a ‘mild’ phenotype; those reflecting Figure 8 E, with some loss of distinction in neural tissue, less distinct MHB, and a curved tail. Category 3 contained embryos with a ‘severe’ phenotype, reflecting Figure 8 D, F, G; loss of distinct neural tissue, which was particularly evident in the head and manifested in loss of visible MHB but was visible down the dorsal line, culminating in crooked tails. Many embryos exhibited what appeared to be developmental delay

compared to wild types from control groups and to the staging set out by Kimmel and colleagues (1995). Embryos which showed a significant developmental delay – being fixed at the 26-somite stage or before – were disregarded because lack of visible MHB, curved tail and aberrant head shape could be attributed to slow development, and I could not say with confidence that such phenotypes were due to injection with endonuclease and gRNA targeted to *wnt8a.*

Importantly, the observed phenotypes in the mild and severe categories reflected those seen in Morpholino oligomer-based inhibition of translation of *wnt8a1* and *wnt8a2,* with the mild and severe categories somewhat reflecting the phenotypes observed when targeting ORF1 or ORF2 (Lekven *et al.,* 2001). The number of embryos within an injected sample that adhered to each category was quantified, and compared to embryos injected with the endonuclease alone as controls (Figure 9). The un-injected wild type samples had small numbers of embryos which fell into the mild or severe categories, reflecting intrinsic variation/mutation rates. There were slightly more mild/severe embryos in the control injections with endonuclease RNA without gRNAs, which could represent mild side effects of the injection itself coupled with the intrinsic variation seen in wild types. Compared to the endonuclease controls, embryos injected with CRISPR or CRISPRi targeting *wnt8a* were significantly ($P<0.0005$) phenotypically distinct. There was a significantly greater induction of the mild or severe phenotypes in embryos injected with CRISPR or CRISPRi constructs than there was in embryos injected with the endonuclease alone.

Collected data has been compared to images of embryos targeted with Morpholino oligomers against *wnt8a* (Lekven *et al.,* 2001), but to ensure that the comparison could be made against embryos injected using the same method as

in the present study, embryos were injected with Morpholino oligomers diluted to 1:10 targeting either *wnt8a* ORF1, ORF2 or both. Control samples were uninjected; no control Morpholino oligomer was used in this experiment. The resultant phenotypes at 28 hpf resembled those generated by Lekven and colleagues and were perhaps even stronger (Figure 10 A). Additionally, the phenotypes generated were similar to those generated by injection of CRISPR/CRISPRi targeting *wnt8a.* Grouping of these embryos into the same categories (wild type, mild and severe) as the CRISPR/CRISPRi embryos showed that there was a significant induction of mild/severe phenotypes compared to un-injected WT embryos.

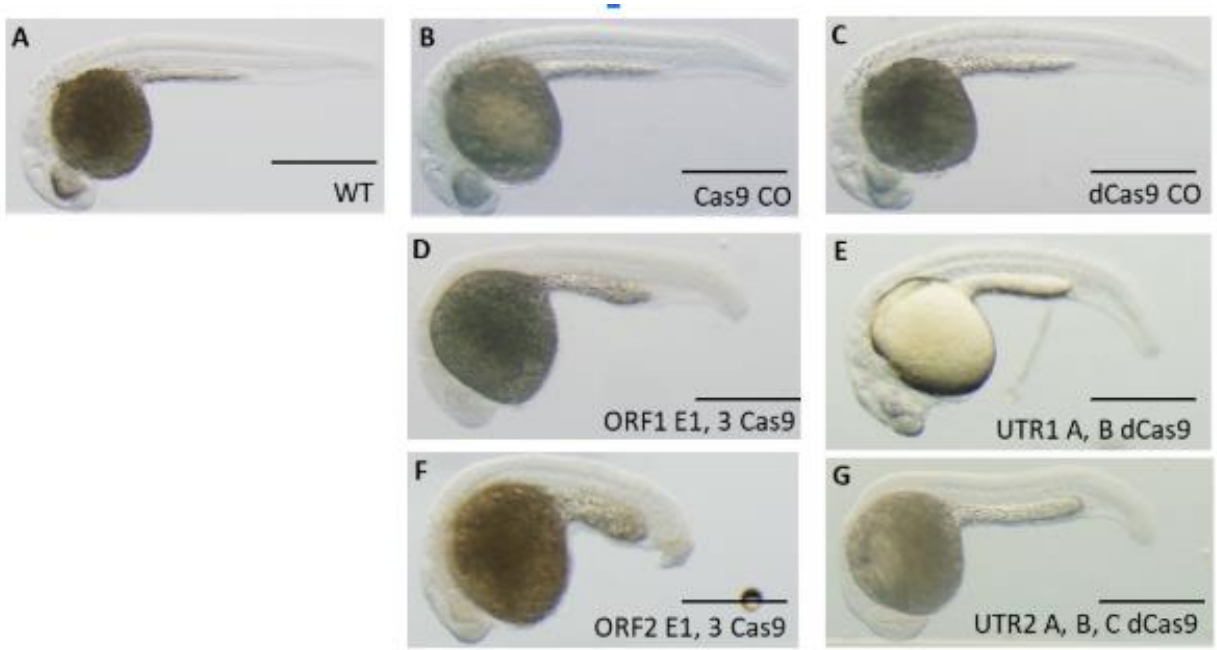

Figure 8: Representation of phenotypes generated by injection.
A Wild type, no injection. **B** Injection with Cas9 RNA, no gRNA. **C** Injection with dCas9 RNA, no gRNA. **D** Injection with Cas9 RNA and gRNA targeted to exons (E) 1 and 3 of ORF1. **E** Injection with dCas9 RNA and gRNA targeted to two sites in UTR1. **F** Injection with Cas9 RNA and gRNA targeted to exons 1 and 3 of ORF2, and an example of one of the embryos categorised as 'severe' for further analysis. **G** Injection of dCas9 RNA and gRNA targeted to three sites in UTR2. All embryos imaged at 28 hpf, fixed in 4% PFA. Scale bar represents 500 µm.

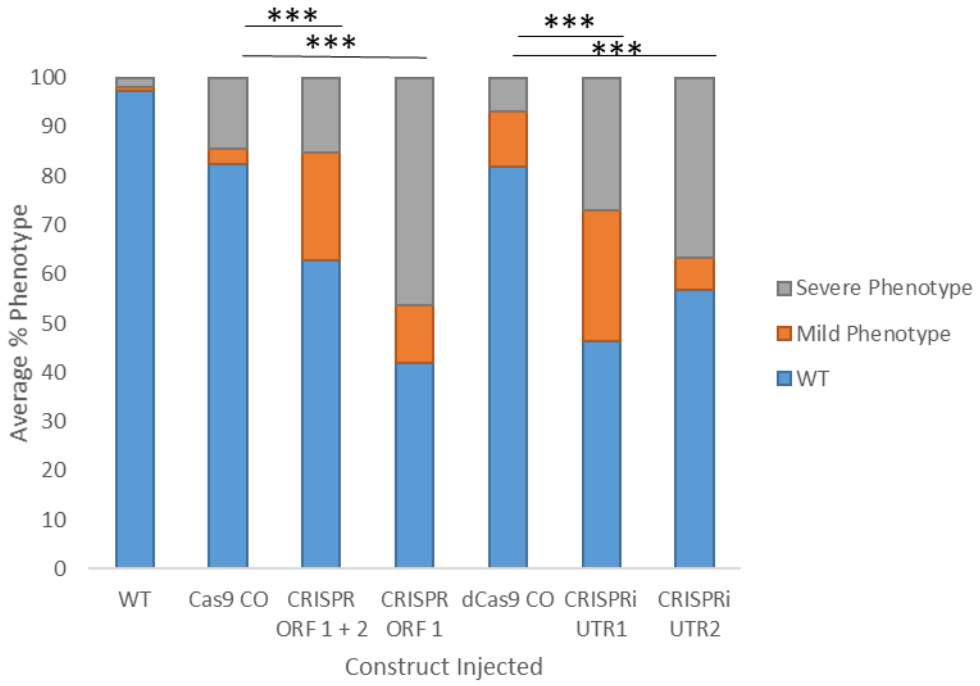

Figure 9: Quantification of embryos grouped into 3 categories; WT, mild and severe.
Embryos injected with gRNA + Cas9 or dCas9 RNA were compared to their respective controls (CO, endonuclease RNA without gRNA) using Chi-squared (***P<0.0005).

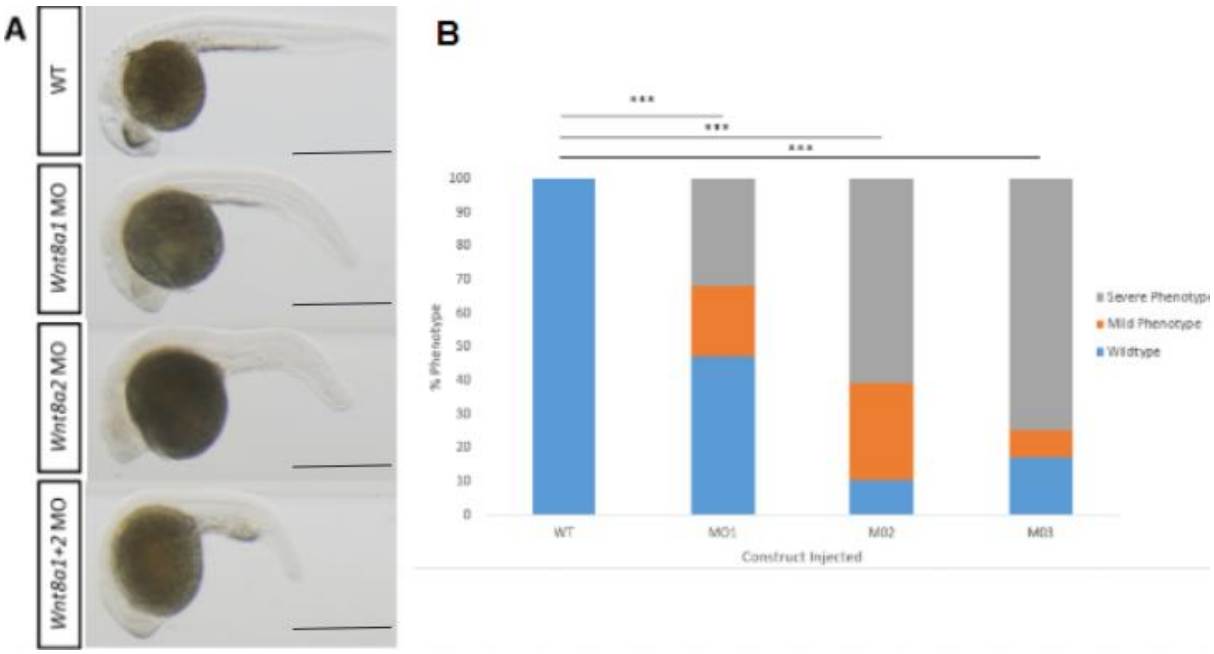

Figure 10: Phenotypes of zebrafish embryos injected with Morpholino oligomer targeted to *wnt8a.*
A Embryos injected with Morpholinos targeting either ORF1 (MO 1) or ORF2 (MO2) of *wnt8a,* or both (MO 1+2). **B** Qualification of embryos injected with Morpholino oligomers (MO1, MO2, MO 1+2, as before) against Wnt8a into wild type (WT), mild or severe categories. All embryos at 28 hpf. Statistical analysis calculated using Chi squared (***P<0.0005). Scale bar represents 300 µM.

3.4 Visualising the expression patterns of *wnt8a1* and *wnt8a2* at 70-80% epiboly

The phenotypic changes in embryos injected with gRNA and Cas9 RNA targeted to *wnt8a1* or *wnt8a2*, which appeared similar to Morpholino oligomer-targeted knock down of the same gene, inferred that the constructs may be successfully changing the expression of *wnt8a.* To visualise changes to expression, *in situ* hybridisation was performed on injected embryos with antisense RNA probes against either *wnt8a* ORF1 (Figure 11) or ORF2 (Figure 12). All injected embryos exhibited patterns of *wnt8a* RNA expression which differed from the wild type un-injected controls, which show a strong band of *wnt8a* signalling around the marginal zone during 70-80% epiboly, with a gap for the dorsal organiser. Injected

embryos displayed a number of changes to wild type patterning; faded staining, mosaic staining where in the wild type it is one strong band, and changes to the width and formation of the organiser. Examples of these can be seen in Figures 11 and 12.

Interestingly, in many cases, the change to the patterning appeared to be asymmetrical (Figure 11 C, D, E, F, Figure 12 C). *wnt8a2* expression is markedly different to *wnt8a1* wild type expression, with a second band forming closer to the animal pole. Congruent with previous research that suggests that perturbation of the expression of *wnt8a2* has more severe effects than reducing the expression of *wnt8a1* (Lekven *et al.,* 2001), visually it appears that injection of the constructs targeting *wnt8a2* produce a phenotype more distant from the wild type, that is, the effect is more severe, than injecting constructs targeting *wnt8a1.* For example, the loss of the second band of staining in Figure 11 images C-F, and the greatly expanded width of the gap in staining where the dorsal organiser is situated (Figure 12 E, F). The difference in patterning may be attributed to the complex structure of the locus, as suggested by Lekven and colleagues (2001) and demonstrated in Figure 2. Coupled with the changes to phenotype observed in later stage embryos, the changes in staining pattern of both *wnt8a1* and *wnt8a2* in early stage embryos infers that the injection of the CRISPR/CRISPRi constructs may be changing the expression of the target gene.

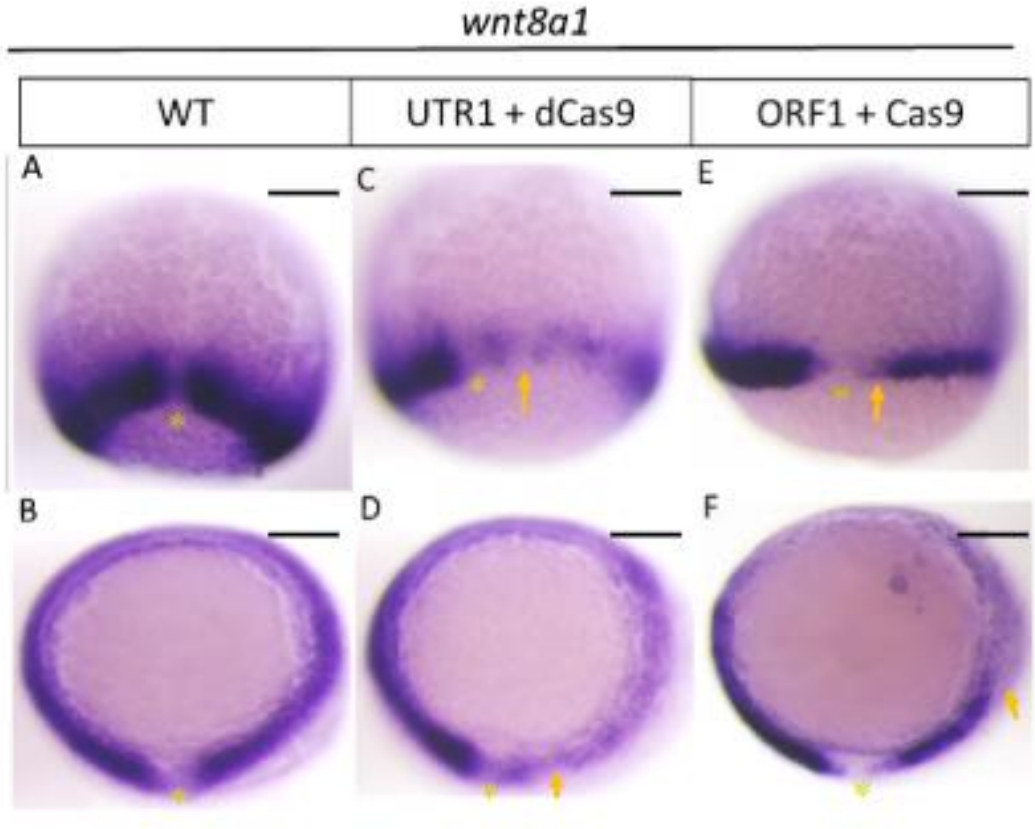

Figure 11: *In situ* hybridisation of zebrafish embryos at 70-80% epiboly using a probe against *wnt8a1.*
The top row of images are all orientated dorsal side up; the organiser is indicated by the yellow asterisk. The bottom row of images are all orientated with the vegetal pole facing upwards. Again the organiser is indicated by the yellow asterisk. *wnt8a1* RNA expression is indicated by the deep purple staining. The orange arrows indicate where the expression pattern particularly deviates from wild type (WT) patterning (left). UTR1 label denotes that the target site for dCas9 was the untranslated region prior to the first open reading frame of *wnt8a* and ORF2 denotes the target site for Cas9 as the second open reading frame of *wnt8a*. Scale bar: 200 µM.

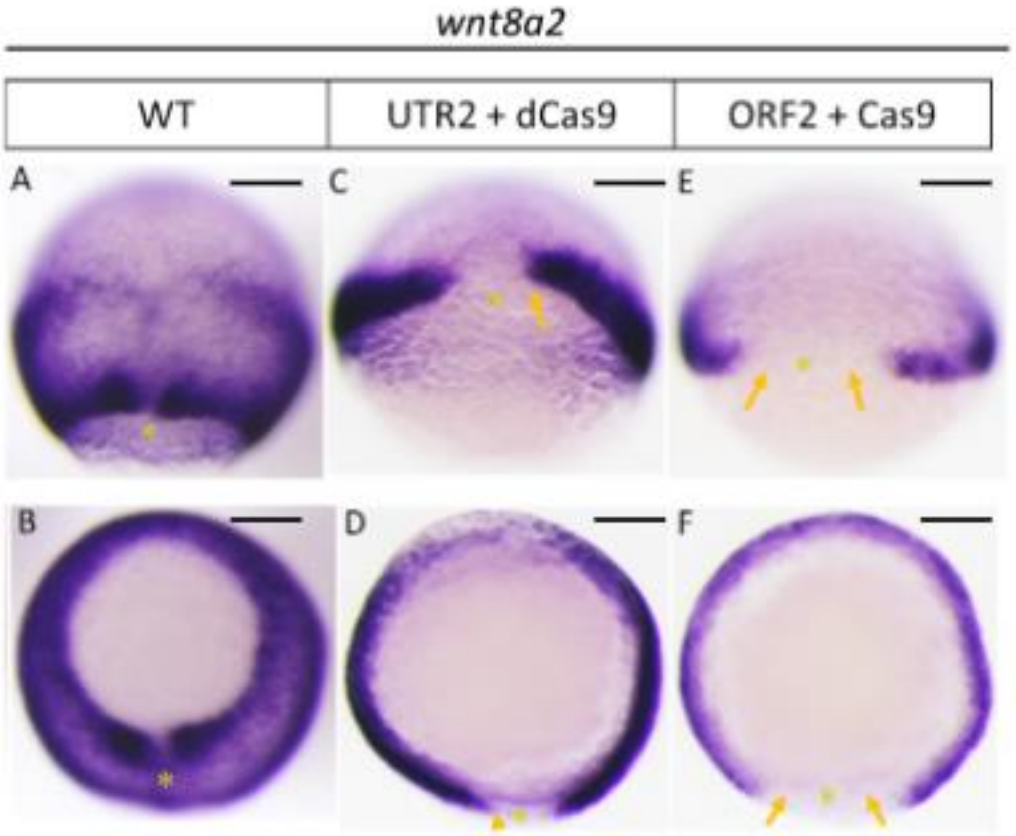

Figure 12: *In situ* hybridisation of zebrafish embryos at 70-80% epiboly using a probe against *wnt8a2.*
The top row of images are all orientated dorsal side up; the organiser is indicated by the yellow asterisk. The bottom row of images are all orientated with the vegetal pole facing upwards. Again the organiser is indicated by the yellow asterisk. *wnt8a2* RNA expression is indicated by the deep purple staining. The orange arrows indicate where the expression pattern particularly deviates from wild type (WT) patterning (left). Scale bar: 200 µM.

3.5 Quantifying *wnt8a1* and *wnt8a2* expression at 70-90% epiboly

To quantify changes in expression of *wnt8a* which appear to occur from analysis of resultant phenotypes and RNA expression patterns, embryos were injected with CRISPR/CRISPRi constructs and total RNA was extracted when embryos were at 70-90% epiboly. Extracted RNA was then reverse transcribed and quantified by RT-qPCR. Normalised to wild type controls, *wnt8a* expression was significantly downregulated in almost all injected samples. For almost all samples,

both ORF1 and ORF2 were downregulated, despite only one ORF or UTR being targeted in each injection (Figure 13).

To ensure that the primers used to amplify each ORF were specific rather than cross-reactive, a *wnt8a1* overexpression experiment was performed which showed that only the primer for *wnt8a1* responded significantly to the overexpression (Figure 14). Thus, it appears that there is in fact a complex relationship between the two ORFs such that when one is targeted, the other is also downregulated. The effect of targeting *wnt8a* on Wnt target genes is less clear, with some fluctuations shown with large standard error (Figure 15), although the absence of a clear-cut relationship between down-regulated expression of *wnt8a* and its downstream signalling components may be expected due to the nature of the web of interrelated pathways and that *wnt8a* is just one of a set of canonical Wnt ligands.

Phenotypically, the injection of dCas9 or Cas9 endonuclease RNA without a gRNA did not appear to have a significant effect (Figure 8). This has been quantified by RT-qPCR (Figure 16), where surprisingly, all injected samples showed an increase in the quantity of RNA assayed, which I hypothesise to be an artefact of injection in mechanical disruption of the cell at the 2-4 cell stage. However, this would be an interesting pattern to investigate further. If an increase in transcription post injection is consistent, it lends more weight to the downregulation of the target genes induced by injection of the CRISPR and CRISPRi constructs.

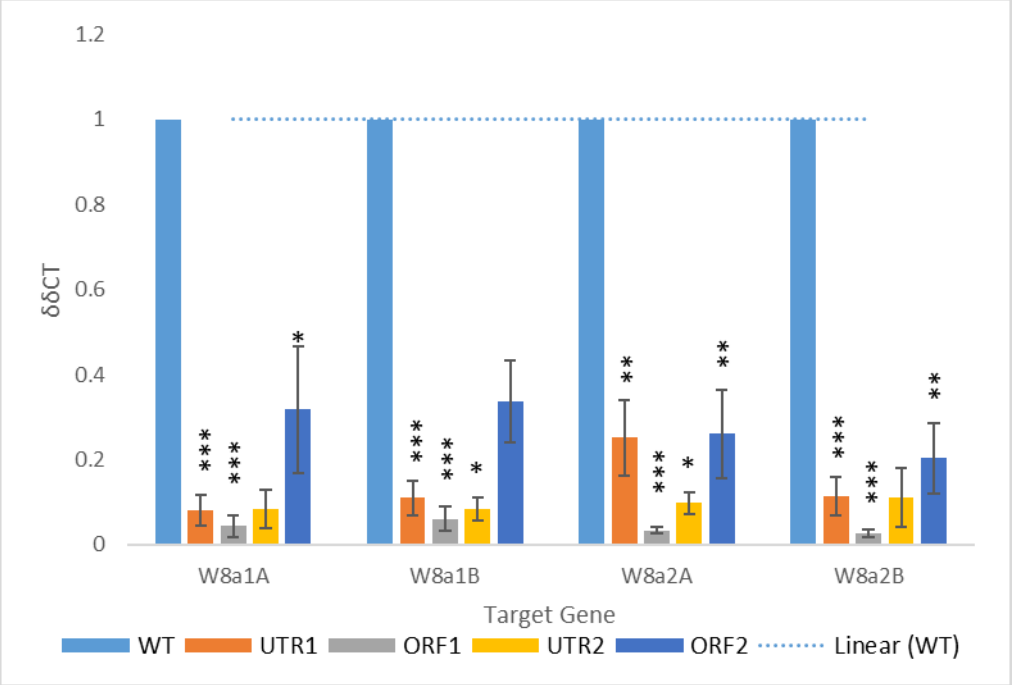

Figure 13: Expression of *wnt8a* after targeting with CRISPR or CRISPRi.
Expression of *wnt8a* ORF1 and ORF2, after injection with dCas9 and gRNA targeting UTR1 or UTR2, or Cas9 and gRNA targeting ORF1 or ORF2. Error bars represent standard error, and asterisks indicate statistical significance. *P<0.05, **P<0.005, ***P<0.0005. Labels along the x axis denote two primers used for each open reading frame (A and B of Wnt8a1 and Wnt8a2).

Figure 14: Primer detection of *wnt8a* overexpression.
Overexpression of *wnt8a1* was detected by both primers for the first open reading frame of *wnt8a* (W8a1A, W8a1B), with the greatest level of detection by the first primer, W8a1A. *wnt8a1* overexpression led to a small increase in Wnt target gene

axin2, but no difference was found in *lef1*. There was also a small increase in detection by W8a2A, which targets the second open reading frame of *wnt8a.*

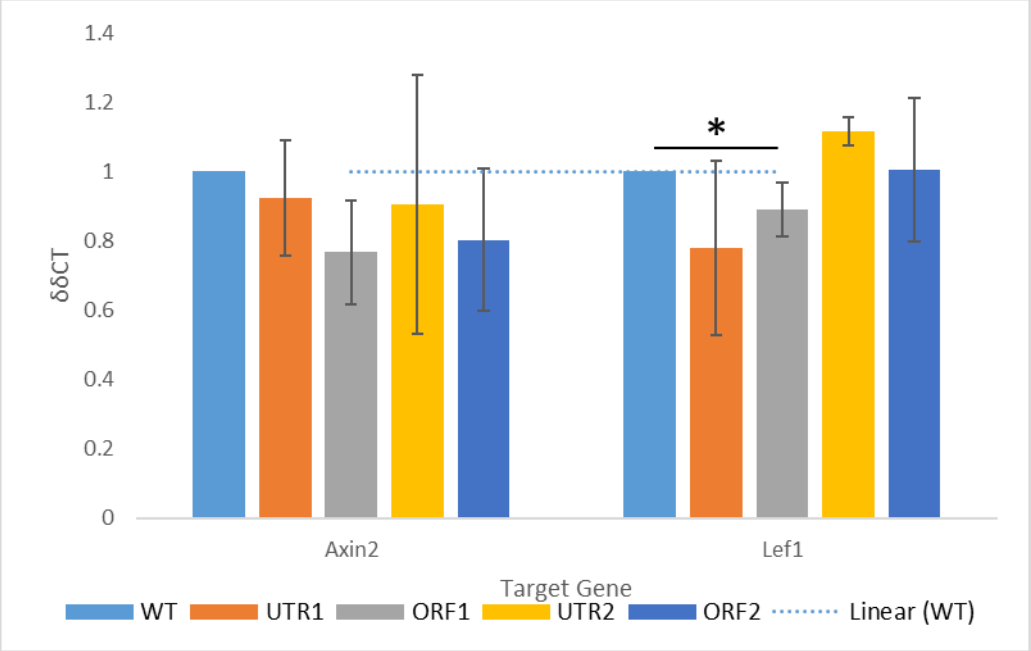

Figure 15: Expression of downstream Wnt target genes after targeting *wnt8a* with CRISPR or CRISPRi.
Signal variation demonstrated through error bars. *lef1* was significantly downregulated when targeting the first open reading frame (ORF1) of *wnt8a* using CRISPR. Error bars represent standard error, and asterisks indicate statistical significance (*P<0.05).

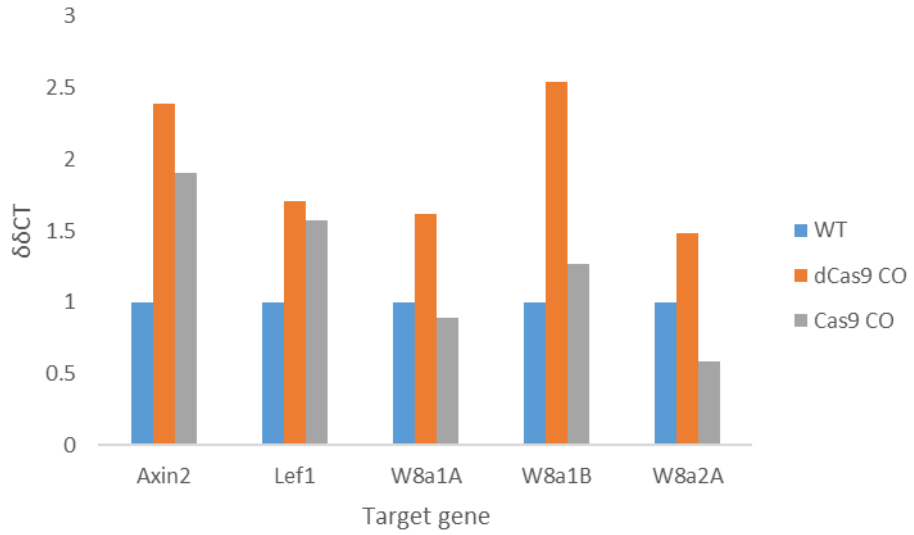

Figure 16: Impact of injection of endonuclease RNA without gRNA.
Expression of downstream Wnt target genes and both ORF1 and ORF2 of *wnt8a* in embryos injected with either dCas9 or Cas9 RNA without gRNA to guide the endonuclease.

3.6 Peroxisomes visualised in human AGS cells

Whilst preparing and testing the CRISPR/CRISPRi toolkit, a way to visualise peroxisomes, firstly in cell-culture, and secondly *in vivo* in zebrafish embryos was developed. Human AGS cells, chosen for their high levels of Wnt, and zebrafish PAC2 fibroblasts, chosen to act as a primer for moving on later to the study of peroxisomes within zebrafish embryos, were transfected with SKL-GFP, a peroxisomal targeting signal fused to the fluorescent marker. The marker is an endogenous targeting signal type 1 (PTS1) utilised to guide translated peroxisomal matrix proteins from the cytosol to the peroxisome import receptors situated on the single membrane of the organelle (Wolins & Donaldson, 1997). Therefore, it is proposed that the fluorescent signals detected by confocal microscopy were peroxisomes, or peroxisome-associated structures. Imaging of both PAC2 and AGS cells yielded images with high numbers of peroxisome-like structures, which was somewhat surprising given that cancerous cells are known to have low levels of oxidation activity – through the enhanced production of ROS, they are under consistent oxidative stress and this has indeed been manipulated to aid in their destruction (Hileman *et al.,* 2004) - yet high levels of ether lipids, major products of peroxisomes, have been detected in some cancer types (Lodhi & Semenkovich, 2014).

AGS cells were determined to be more amenable to imaging due to higher rates of proliferation than PAC2 cells and a higher number of SKL-positive structures per cell, represented in the images as green dots (Figure 17 A), and so AGS cells

were used for quantitative analysis. Once a baseline was established, the cells were treated with Wnt effectors; the inhibitor IWR1 and activator BIO, shown in Figure 17 B. After treatment, the number of peroxisome-like structures was quantified and both treatments caused the number of peroxisome-like structures to increase significantly per cell (Figure 18), with no significant difference between the two treatments, although a significant challenge was posed by the varied size and shapes of the cells in each sample. Reviewing all the cells in each image, there is no consistent change in the distribution of peroxisomes throughout the AGS cells, solely the number, although this upregulation does appear to make the peroxisomes seem clumped together. This could be verified by higher resolution imagery.

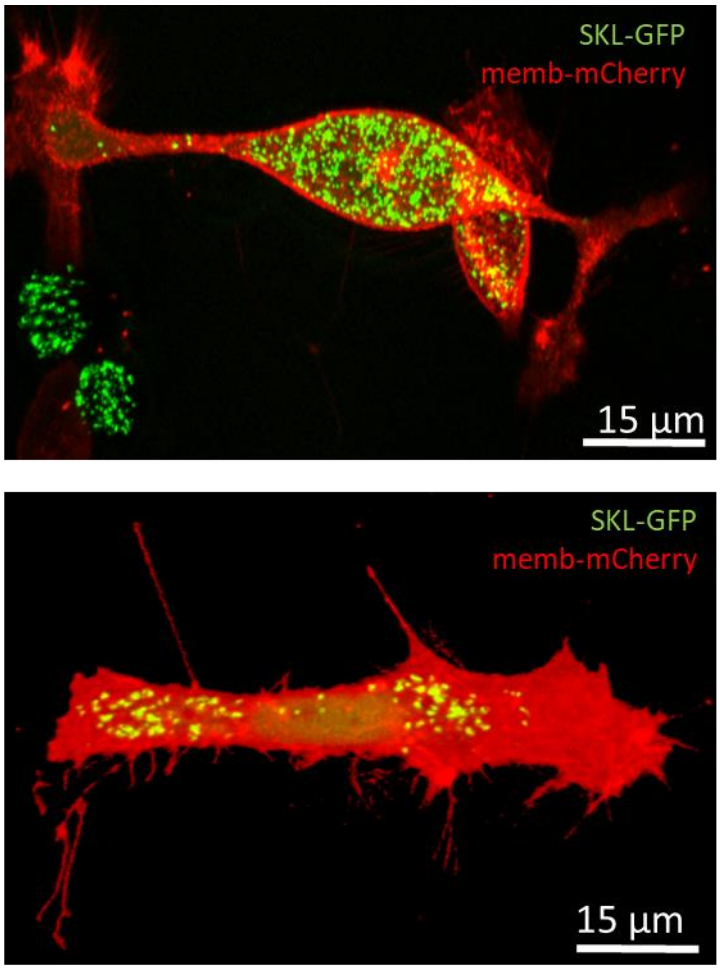

Figure 17 A: Human AGS cell (top) and zebrafish PAC2 cell (bottom) in culture transfected with SKL-GFP (green) and membrane-associated mCherry (red). Scale bar 15 µm. Image taken using the Leica SP8 Hyvolution II (Leica Microsystems, Germany).

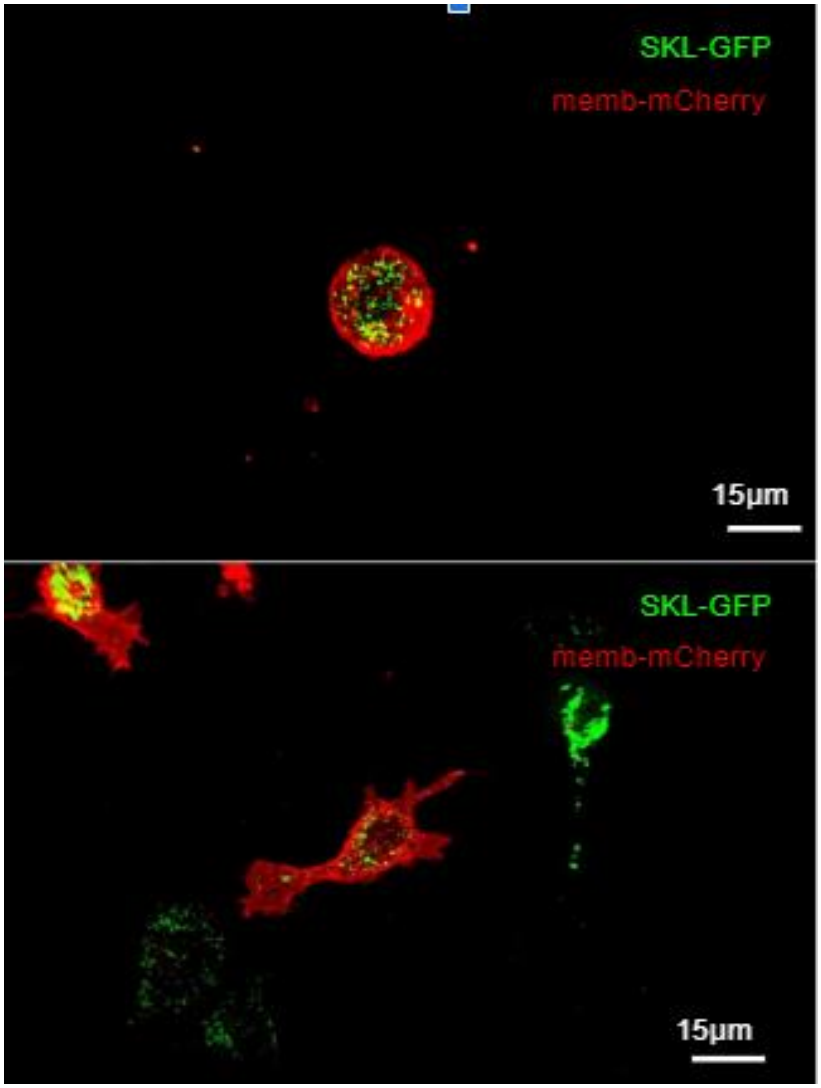

Figure 17 B: Human AGS cells transfected with SKL-GFP (green) and membrane-associated mCherry (red) and treated with BIO (2.5 µM, top) and IWR1 (25 µM, bottom)
Scale bar 15 µm. Image taken using the Leica SP8 Hyvolution II (Leica Microsystems, Germany).

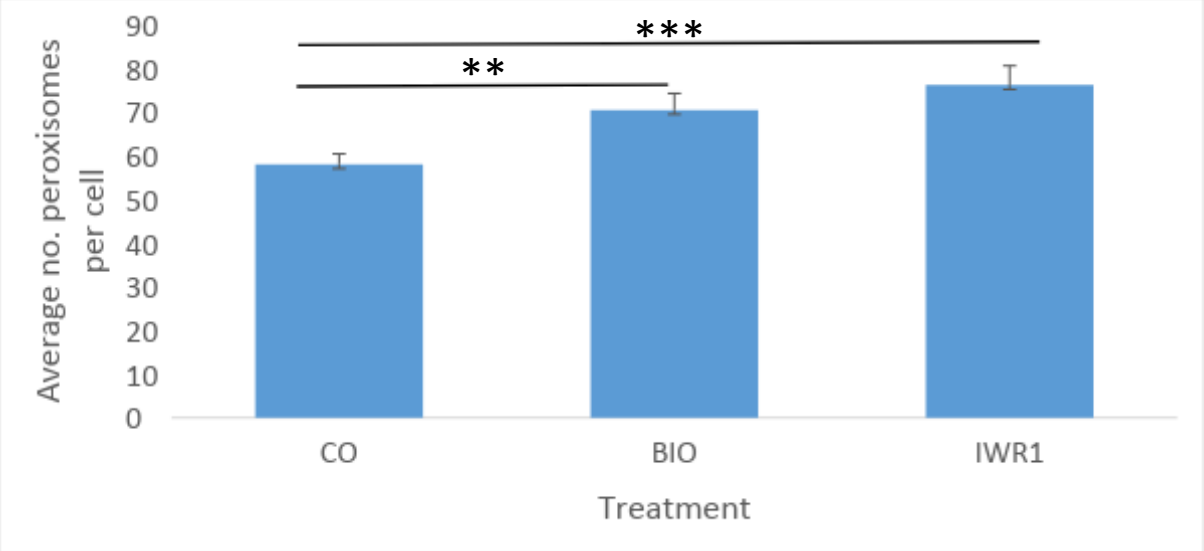

Figure 18: Quantification of the average number of peroxisomes per cell in human AGS cell culture.
Cells treated with either 25 µm IWR1 or 2.5 µm BIO. Control sample was treated with DMSO. Error bars represent standard error. Statistical significance calculated using a Student's t-Test (***P<0.0005, **P<0.005).

3.7 Peroxisomes visualised *in vivo* in zebrafish embryos

After successfully visualising peroxisome-like structures *in vitro* using SKL-GFP, peroxisomes were visualised in the more complex system of the living zebrafish embryo. SKL-GFP DNA was incorporated into injection mixes and injected in one-two cell stage embryos. Peroxisome-like structures represented as green dots similar to those seen in cell culture were visualised in large numbers in each cell (Figure 19). The peroxisome-like structures appeared to be distributed evenly throughout the cell as distinct puncta, with some small aggregations possibly attributable to peroxisomes in a proliferative state. The structures have a high density within each cell, the only part of the cell not emitting the GFP signal being the gap for the nucleus. The cell membranes are shown in red.

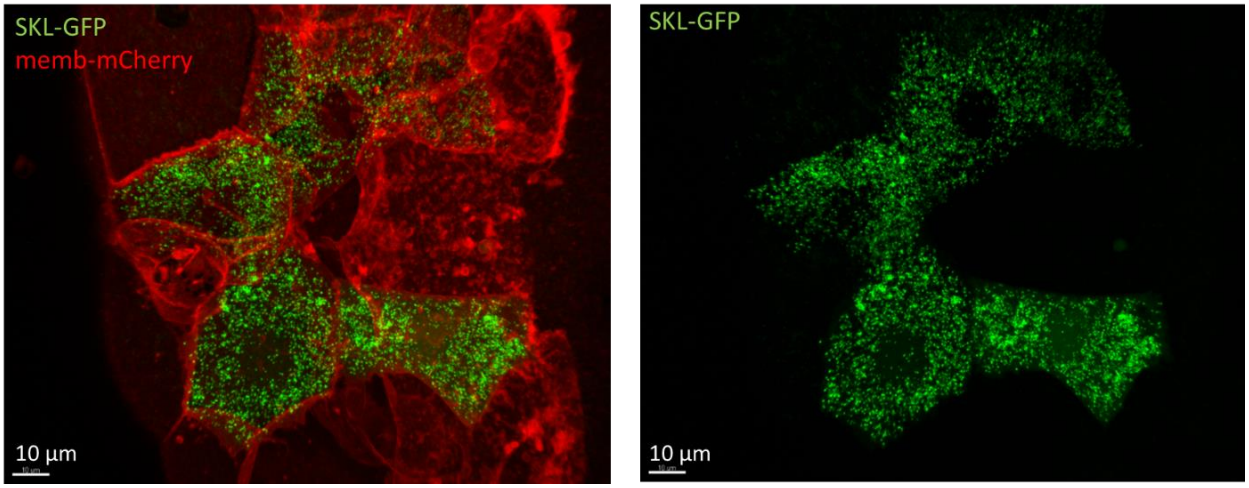

Figure 19: Peroxisome-like structures (green) in the live zebrafish embryo. Images taken using the Leica SP8 Hyvolution II confocal microscope (Leica Microsystems) at 63x magnification.

3.8 Peroxisomes in embryos injected with CRISPR/CRISPRi constructs

Injection with CRISPR/CRISPRi constructs targeted to *wnt8a* has induced quantifiable changes to both the phenotype (Figure 8) and transcriptome (Figure 16) of zebrafish embryos. To visualise the effect of changes in *wnt8a* expression on peroxisome dynamics, zebrafish embryos were injected with a combination of SKL-GFP DNA with CRISPR/CRISPRi constructs, Morpholino oligomer or *wnt8a* RNA (full details in Table 5).

In embryos injected with SKL-GFP only, the peroxisome-like structures detected have an even, dense distribution throughout the cell, itself delineated in red by membrane-bound mCherry. The structures appear mostly as individual round/spherical puncta, with some small exceptions where there is a clump/cluster of green fluorescent signal (Figure 20, row 1). In comparison, peroxisome-like structures in embryos injected with Morpholino oligomer targeted to both ORF1 and ORF2 of *wnt8a* have a distinctly different appearance (Figure 20, row 2). The prevalence of large spots of GFP signal is visibly greater, with

nearly every cell containing multiple large conglomerated green signals. The appearance of these clusters is not spherical, and therefore does not appear to resemble a single peroxisome of increased size. The clusters are oval, or tubular, and resemble more closely the 'beads on a string' phenotype of peroxisome proliferation. When quantified using image analysis (Figure 21), the proportion of the cell in which a green signal is found is less than controls; the peroxisome-like structures fill less of the cytosol in cells with Morpholino oligomer targeted to *wnt8a* than in control cells. The ability of Morpholino oligomers to knock out Wnt signalling has been previously established (Lekven *et al.,* 2001) and has been verified in this study by phenotypic analysis (Figure 8) and RTqPCR (Figure 16), and so it may be that the high level of knockdown of *wnt8a* in the embryonic cells is inducing phenotypic changes, more specifically clumping, in the peroxisomes of zebrafish embryos.

The phenotypic changes of the peroxisome-like structures in embryos injected with *wnt8a* Morpholino oligomers are the most visually apparent, when compared to the controls. This may be because Morpholino oligomers have a very strong ability to knock out their targets, with the caveat of a greater possibility of side effects than other methods (Schulte-Merker & Stainier, 2014). When observing morphological changes in embryos at 28 hpf that were injected with Morpholino oligomers targeted to *wnt8a* at the 2-4 cell stage, the phenotypes were consistently strong, with pronounced changes to the morphology of the nervous tissue ranging from the head to the tail along the dorsal axis. CRISPR Cas9 knockout of genes can induce high level mutagenesis of the target gene; for example, Cas9 systems have been developed in monocot and dicot plants with an 85.4% mutation rate (Ma *et al.,* 2015), a 60-100% deletion efficacy in

Streptomyces (Huang *et al.,* 2015) and a 75-99% mutagenesis rate in zebrafish (Jao *et a.,* 2013).

Following the example of Jao and colleagues (2013), for example with the transcription of Cas9 with nuclear localisation signals (nls) to enhance efficiency, despite the investigation at hand being in the primary stages of optimisation, we can expect a reasonable capacity of mutagenicity. The positioning of the embryo injected with CRISPR construct was suboptimal, with the upper two thirds of this image appearing to show the yolk syncytial layer (YSL), and the lower one third of the image showing cells from portions of the embryo equivalent to the cells seen in the other images. However, cells of embryos injected with CRISPR Cas9 and gRNAs directed to both ORF1 and ORF2 of *wnt8a* also appear to have more clustering than control cells (Figure 20, row 4), although the increase is less than in the samples injected with Morpholino oligomers targeted to *wnt8a*. When quantified using image analysis, cells in the lower third of the image were used for analysis only because these are more directly comparable to cells in the other images. There was a significantly lower amount of GFP fluorescence in these cells compared to the controls (Figure 21, $P<0.0005$).

In contrast, cells in embryos injected with *wnt8a* RNA as positive controls had significantly higher proportions of GFP fluorescence per cell ($P<0.005$). Phenotypically, there appears to be both a denser coverage of small puncta throughout the cells and contemporaneously clusters of signal which are larger than those seen in the control, Morpholino oligomer or CRISPR Cas9 samples.

In combination with the greatest level of knockout of *wnt8a* using Morpholino oligomer-mediated inhibition of translation, CRISPR Cas9-mediated knockout of *wnt8a*, the negative control with SKL-GFP and memb-mCherry injection only, and

the positive control using *wnt8a* RNA overexpression, a spectrum has been created. It is a dual spectrum; a spectrum of *wnt8a* expression, which is mirrored by a spectrum of changes to the shape/size and number of peroxisome-like structures/GFP fluorescence within the cells. There are tangible changes to the dynamics of peroxisome-like structures *in vivo* in zebrafish embryos under varying levels of manipulation of the expression of *wnt8a.*

The sizes of the peroxisome-like structures in each sample were bucketed into size bands or bins, from which the frequency in each bin could be calculated and compared to the total in each sample. A student's T-test, assuming unequal variances was calculated. None of the differences between the samples were statistically significant, but upon examination of the data a pattern can be seen, which may become more pronounced and significant by repeating the experiments with a larger sample size. The largest difference in the distribution of sizes of the peroxisome-like structures is between the sample which was injected with *wnt8a* RNA (Figure 22 C) and all other samples (Figure 22 A, B, D). Here, there is a noticeably larger frequency of peroxisome-like structures which fall into the smallest bin size, and much less that fit into the larger bins, than either the control (Figure 22 A) or the *wnt8a* Morpholino oligomer (Figure 22 B) or CRISPR samples (Figure 22 D). When considering the distribution patterns of the Morpholino oligomer and CRISPR samples, compared to the control there appears to be a greater frequency of peroxisome-like structures falling into bins 0.0005 and 0.001. The difference is small but noticeable. With future repeats, a greater difference may be established between the distribution of sizes of peroxisome-like structures within the control, Morpholino oligomer and CRISPR

samples, and confirm the shift in *wnt8a* overexpression sample to a much greater frequency of small (bin 0.00005) peroxisome-like structures.

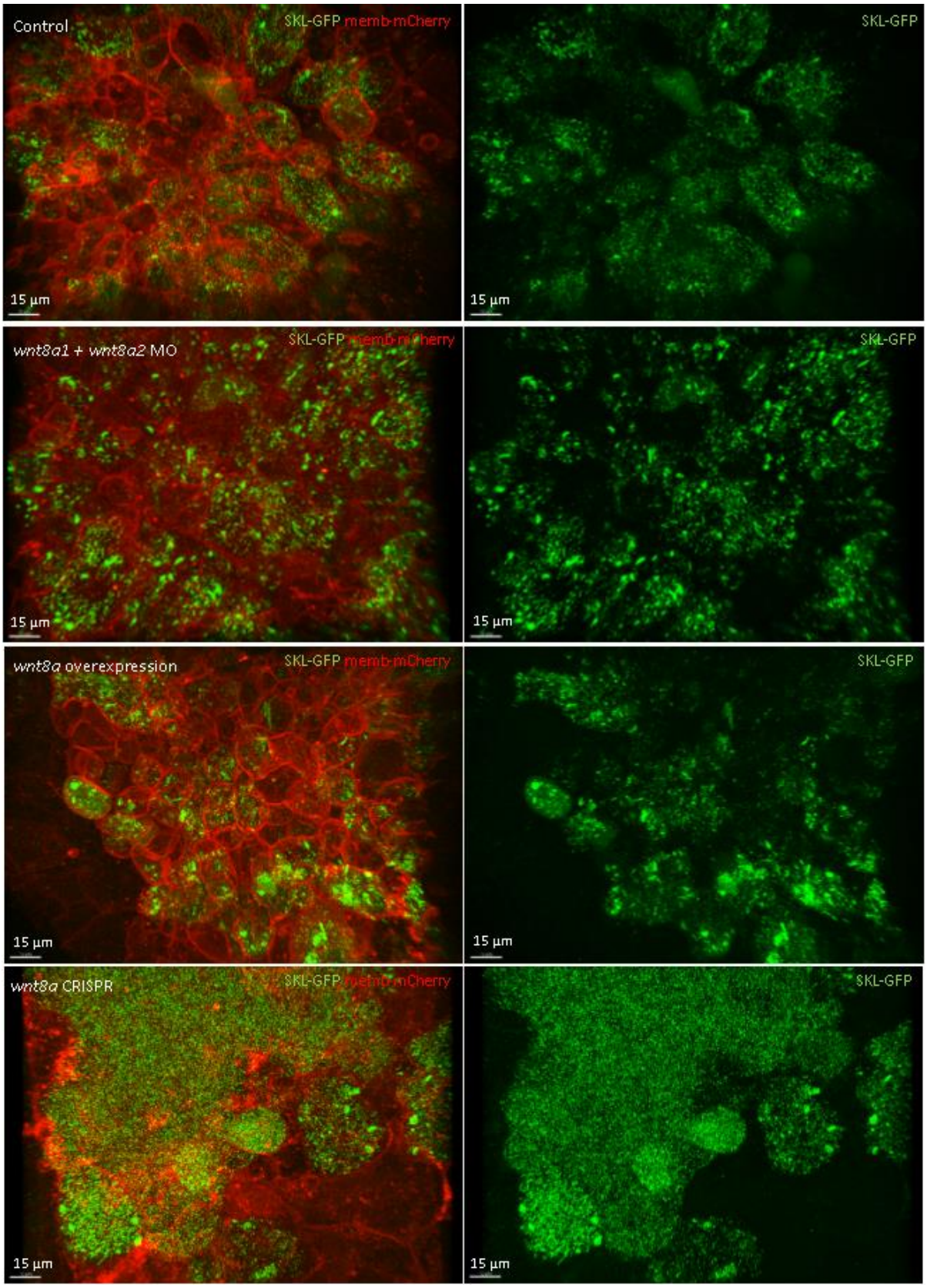

Figure 20: Peroxisomes (green) in zebrafish embryos with varying levels of *wnt8a* expression.
Construct injected is in white at the top left of each image. Scale bar represents 15 µm. Cell membranes are shown in red.

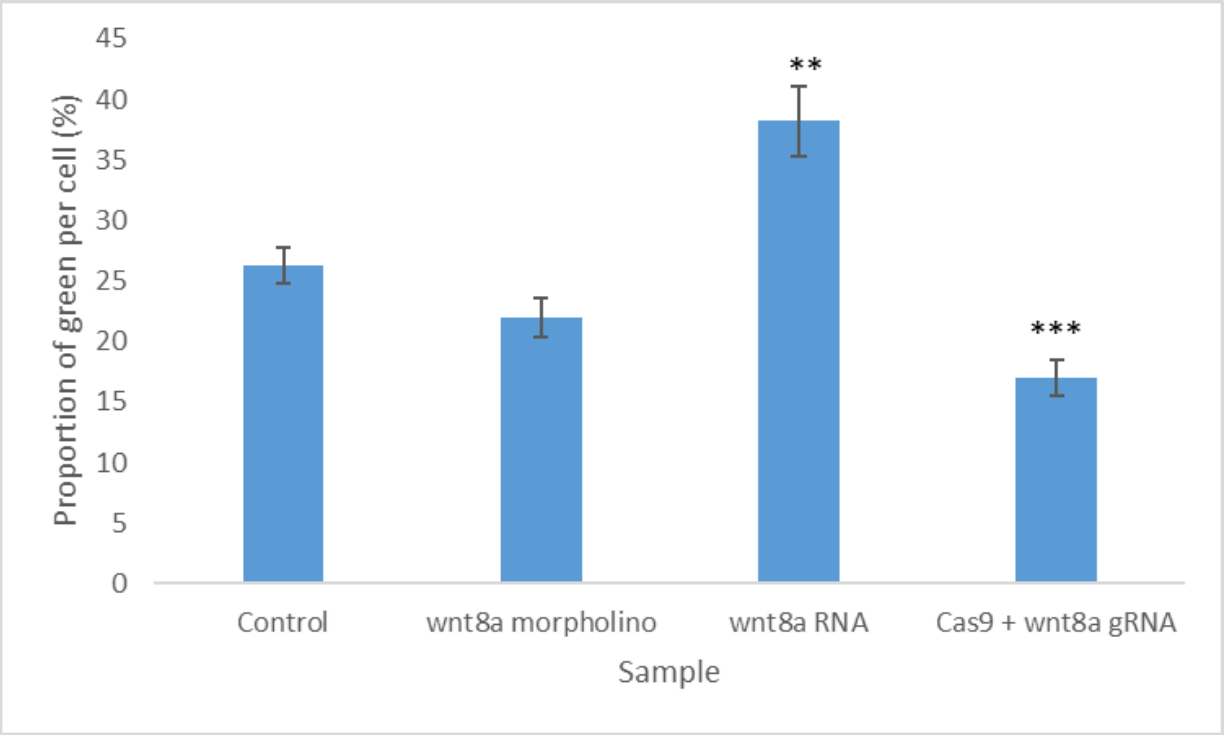

Figure 21: The proportion of peroxisome-like structures per cell in control, Morpholino, *wnt8a* RNA overexpression and Cas9 + *wnt8a* gRNA embryos. Error bars represent standard error. Significance calculated by student's t-Test, two sample assuming unequal variance (**P<0.005, ***P<0.0005).

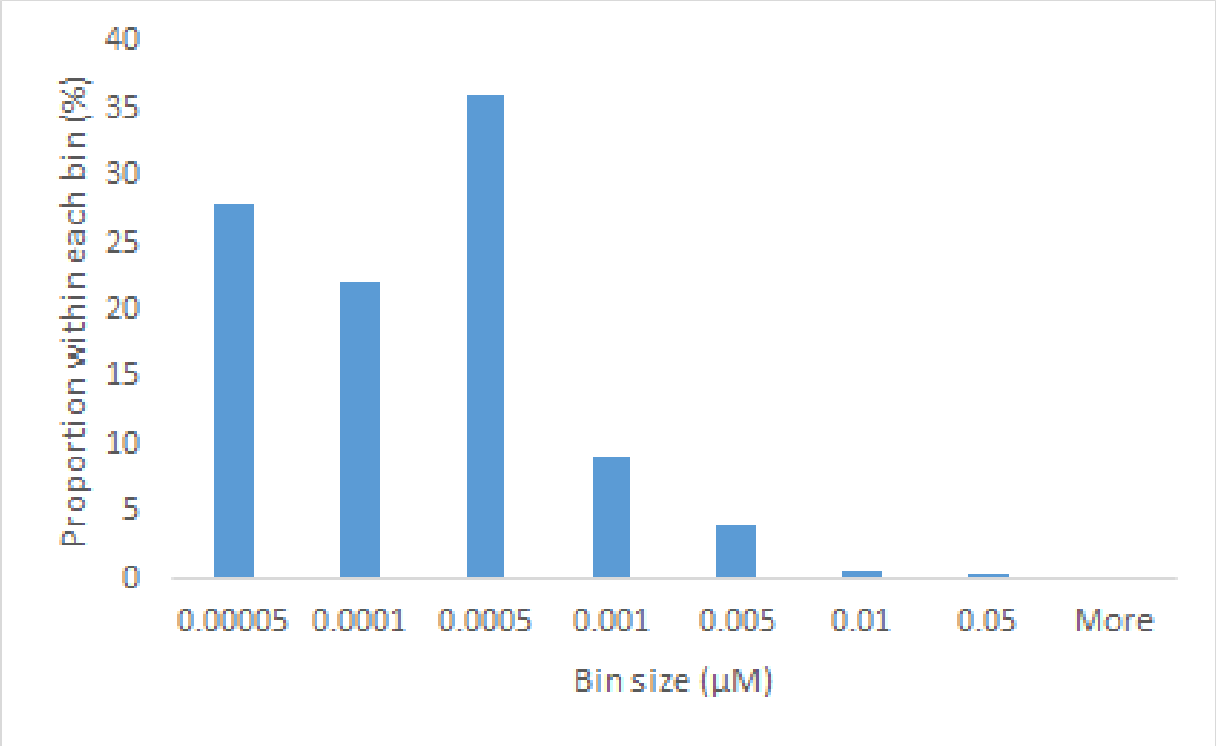

Figure 22 A: The distribution of sizes of peroxisome-like structures within live uninjected zebrafish embryos (control sample).
As visualised through confocal microscopy and analysed using ImageJ.

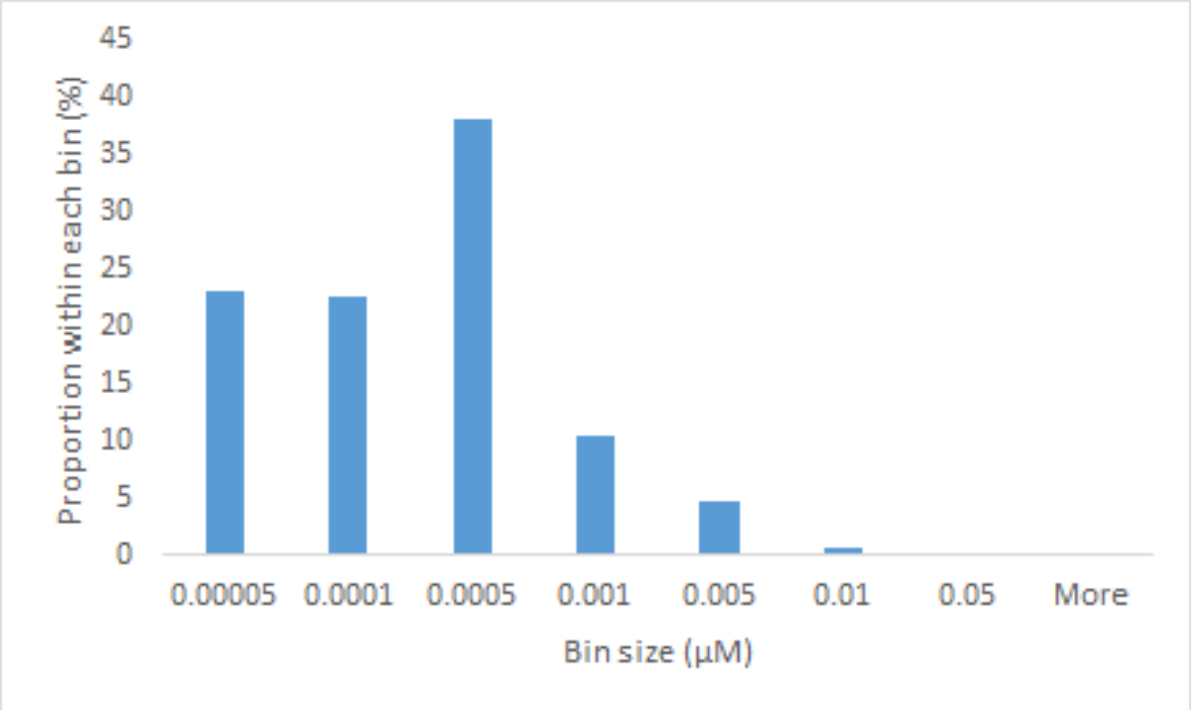

Figure 22 B: The distribution of sizes of peroxisome-like structures within live zebrafish embryos injected with Morpholino against *wnt8a* ORF1 and ORF2.
As visualised through confocal microscopy and analysed using ImageJ.

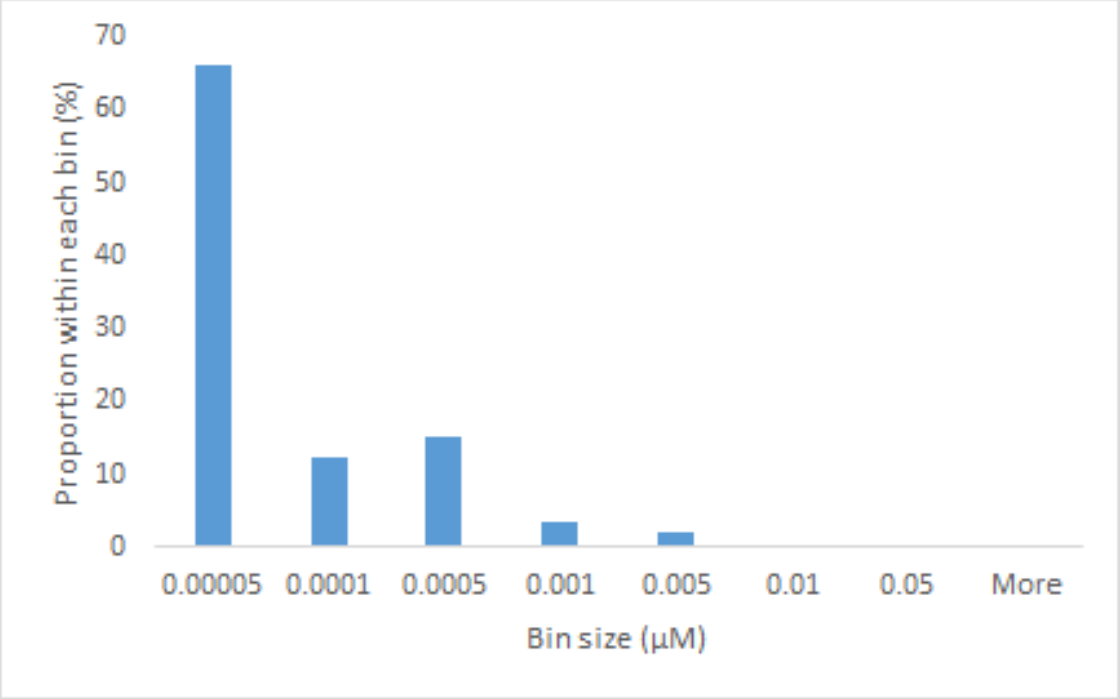

Figure 22 C: The distribution of sizes of peroxisome-like structures within live zebrafish embryos injected with *wnt8a* RNA.
As visualised through confocal microscopy and analysed using ImageJ.

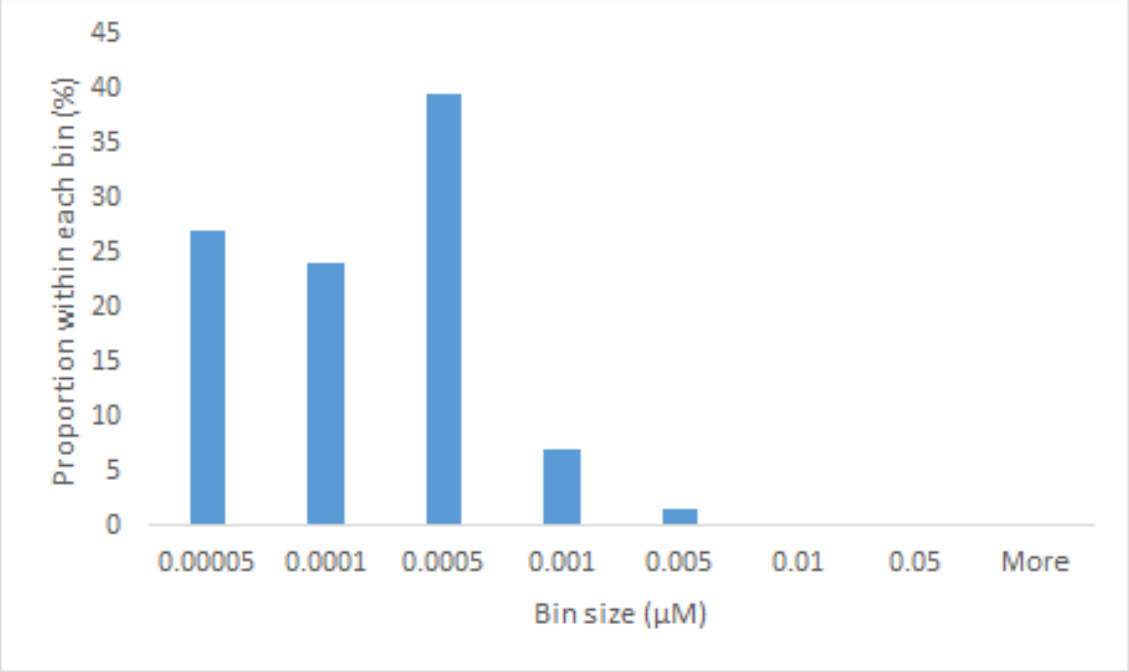

Figure 22 D: The distribution of sizes of peroxisome-like structures within live zebrafish embryos injected with CRISPR Cas9 and gRNA targeted to *wnt8a* ORF1 and ORF2.
As visualised through confocal microscopy and analysed using ImageJ.

4.0 Discussion

In this investigation I have demonstrated that it is possible to use CRISPR and CRISPR interference (CRISPRi) to reliably knock out and knock down the signalling of *wnt8a* in zebrafish. I demonstrate this by observing morphological changes to the wild type phenotype in embryos at 28 hpf on whole-organism in tissues impacted by *wnt8a* signalling; perturbations in wnt8a RNA patterning in embryos at 70-90% epiboly; and concurrent lowered expression levels of *wnt8a*, as determined by RTqPCR. Further, these genetically modified embryos can be used to observe peroxisome dynamics *in vivo*, and I observed that in embryos in which *wnt8a* had been knocked down, either by CRISPR/CRISPRi or by using Morpholino oligomers targeted to *wnt8a*, peroxisomes were more often found in large clusters as opposed to distinct puncta. This supports the hypothesis that *wnt8a*, in zebrafish at least, has an impact on the dynamics of peroxisomes.

4.1 Overview of the Wnt-peroxisome relationship

Wnt is a family of morphogens which form gradients across responsive tissues to induce cellular responses. These cellular responses are induced via a network of downstream proteins which form multiple interrelated signalling pathways. Of these, the canonical Wnt signalling pathway is perhaps the most well-studied and widely-known. The canonical pathway begins with the reception of a subset of Wnt ligands – the canonical Wnt proteins - at the cell membrane.

There are various schemes suggested to model the transport of Wnt proteins from the source cell to the receiving cell, the most recent of which is directional delivery on the tips of Ror2-mediated cytonemes. If we consider that Wnt proteins arrive at source cells via diffusion only, the question remains of how the complex

gradients of Wnt signalling are produced without fine-tuned control of delivery by the source cell (Stanganello *et al.,* 2015; Mattes *et al.,* 2018).

After reception of the canonical Wnt protein at the receiver cell membrane, a cascade of intracellular reactions is triggered which disables the β-catenin degradation complex, such that β-catenin persists in the cytosol. The pathway culminates in the translocation of stabilised cytosolic β-catenin into the nucleus. In the nucleus, β-catenin interacts with TCF/LEF transcription factors and facilitates the expression of multivariate target genes. The functions of these target genes are central to both the maintenance and commencement of life, and range from cell cycle maintenance (*cyclin*) to peroxisome proliferator-activated receptors *(PPAR)* (Huelsken & Behrens, 2000).

Dysregulation of the Wnt signalling network post-development has been implicated in several cancer types, most famously in breast cancer (Tsukamoto *et al.,* 1988) and intestinal tumours (Korinek *et al.,* 1998), underscoring its importance in influencing the cell cycle. Recently, Wnt has also been implicated in the cycling of organelles; Wnt signalling can increase or decrease mitochondrial biogenesis, depending on its subcellular localisation (Rauchenberger *et al.,* 2017; Bernkopf *et al.,* 2018), although the full implications of this are not yet known.

4.1.1 Wnt signalling and organelles

Last year (2018) Bernkopf and colleagues established that intrinsically-activated Wnt signalling can promote mitochondrial proliferation. Mitochondrial proliferation under the influence of Wnt signalling is mediated by the location of phosphoglycerate mutase Pgam5 which in normal, steady state conditions is

localised to the mitochondrial membrane, although debate remains as to whether this is the inner or outer membrane, or both (Chen *et al.,* 2014).

Whilst localised to the membrane, Pgam5 is instrumental in downregulating canonical Wnt signalling in the anterior portion of the embryo, which allows head formation to take place, because Wnt signalling induces posteriorisation. Pgam5 represses posteriorisation signals by promoting dephosphorylation of the dishevelled (Dvl) protein. In the dephosphorylated form, Dvl is part of the β-catenin-degradation complex. Through dephosphorylation of Dvl, Pgam5 promotes the instability of β-catenin in the cytosol that leads to its ubiquitination and targeting by proteosomes, preventing translocation to the nucleus and transcription of target genes, preventing the completion of the canonical Wnt signalling pathway and silencing the signal for posteriorisation of the embryo (Rauchenberger *et al.,* 2017).

In contrast, when mitochondrial membrane potential is lost, mitophagy is induced and Pgam5 has an important role in this process. Pgam5 is cleaved by presenilin-associated rhomboid-like protein (PARL), an intramembrane protease. Bernkopf and colleagues (2018) postulate that Pgam5 is a master regulator of mitochondrial abundance post-damage. Cleaved Pgam5 regulates mitochondrial abundance in two ways; by inducing mitophagy of damaged mitochondria, and by inducing biogenesis of novel mitochondria by activating canonical Wnt signalling.

When Pgam5 is localised to the mitochondrial membrane, it promotes the dephosphorylation of Dvl and therefore contributes to the destruction of β-catenin and blocking of the canonical Wnt signalling pathway. In contrast, through proteomics and immunoprecipitation, Bernkopf and colleagues found that the

cleaved form of Pgam5 generated by mitochondrial stress binds to amino acids 210-295 of axin, another key component of the β-catenin destruction complex which scaffolds the other constituents. Binding axin means that it is unable to function as a scaffold protein and therefore inactivates the destruction complex. This prevents the phosphorylation and ubiquitination of β-catenin such that it stabilises in the cytoplasm and can translocate to the nucleus to induce the transcription of target genes. This process is an example of cell-intrinsic activation of the Wnt signalling pathway without a requirement for an external ligand. The findings of Bernkopf and colleagues (2018) indicate that stimulation of mitochondrial biogenesis by Wnt signalling is a mechanism to replenish the cellular mitochondrial count, and are corroborated by other studies in C2C12 myocytes where Wnt signalling leads to enhanced mitochondrial biogenesis (Yoon *et al.,* 2010; Undi *et al.,* 2017).

Wnt signalling has a role in the proliferation of other cellular compartments such as late endosomes via the stabilisation of micropthalmia-associated transcription factor (MITF), the master melanocyte regulator involved in most melanomas. Stabilisation of MITF promotes the generation of late endosomes, which concentrate components of the canonical Wnt pathway such as axin 1, phospho-LRP6, GSK3 and phospho-β-catenin and amplifies Wnt signalling, thereby creating a strong feedback loop (Ploper *et al.,* 2015).

The ability of Wnt to stimulate the proliferation of cellular compartments is illustrated by these two examples. Interestingly, mitochondria and peroxisomes have both functional and proliferative similarities. For example, they share the burden of fatty acid oxidation, with mitochondria oxidising short, medium and long chain fatty acids, and peroxisomes oxidising very long chain fatty acids.

Mitochondria and peroxisomes also share roles in disease prevention and antiviral signalling (Camões *et al.,* 2009). Further, and perhaps of relevance to the relationship between Wnt and the organelles in question, mitochondria and peroxisomes share components of the division machinery, namely Fis1 and Mff (Schrader, 2006), strengthening the partnership between these two sister organelles. I propose that another factor which mitochondria and peroxisomes share is a positive signal for proliferation in the form of Wnt signalling.

4.2 Peroxisomes and peroxisomal diseases

The successful targeting and knock out/down of *wnt8a* is a means to observe the dynamics of peroxisomes under reduced Wnt signalling. The 'little sister' of the mitochondria, peroxisomes parallel Wnt signalling in that they are integral to both developing and maintaining life; defects in any of the PEX genes essential to their biogenesis result in a spectrum of peroxisomal biogenesis disorders which are highly debilitating and often neonatal-lethal. This is because of the roles of peroxisomes in producing plasmalogens for effective conduction of nervous impulses, ROS homeostasis and the β-oxidation of very long chain fatty acids, amongst others (Schrader *et al.,* 2012). Though their remit is narrower than Wnt signalling, peroxisomes are nevertheless crucial to both the development and maintenance of life, which is clearly demonstrated by the spectrum of diseases related to peroxisomal function such as the spectrum of Zellweger Syndrome, or cerebro-hepato-renal syndrome (Goldfischer *et al.,* 1973), X-Linked Adrenoleukodystrophy, Infantile Refsum's Disease, and others.

Zellweger Syndrome manifests on a macro level as the deficiency of plasmalogen (Heymans *et al.,* 1983), and at a cellular level as the presence of peroxisomal 'ghosts'; empty peroxisomes devoid of matrix proteins, which leads to the

hypothesis that the lethal syndrome is due to a defect of matrix protein import (Santos *et al.,* 1988). Studies have shown that the absence of functional peroxisomes has heterogeneous and multifaceted effects on mitochondrial morphology, ultrastructure, and respiratory chain complexes (Baumgart *et al.,* 2001). Tissues of infants affected by this hereditary disease can have less than 10% of normal levels of phosphatidylethanolamine plasmalogen, a component of phosphatidyl cell membranes and heart and muscle tissue (Heymans *et al.,* 1983).

In addition to defective protein import, other hereditary diseases of peroxisomes such as X-linked adrenoleukodystrophy arise from their subverted biochemical capacities. Defects in β-oxidative capacity, which is the process that breaks down very long chain fatty acids (VLCFAs) result in accumulation of intracellular VLCFAs, the root cause of which is a mutation in the *ABCD1* gene. In contrast to Zellweger Syndrome, where lethality occurs early in life, the symptoms of X-linked adrenoleukodystrophy, namely progressive paraparesis and other neurological implications, can have rapid onset in children, adolescents or adults (Moser, Mahmood & Raymond, 2007). Zellweger Syndrome and X-linked adrenoleukodystrophy are just two examples in a spectrum of diseases whose root cause is defective peroxisomes. I selected both because they contrast in their cause; at the root, either by total lack of biochemical capacity as empty shells, or by reduced biochemical function due to a mutation in a key gene. This difference also manifests further along the causative chain as differential symptoms and time of onset. Like Wnts, peroxisomes have multiple roles to play, and dysfunction can lead to varying and ultimately lethal diseases.

4.3 The function of peroxisome proliferator activated receptors - PPARs

Peroxisomes are acknowledged to be adaptive organelles, and the plasticity of peroxisomes is no better exemplified than by examining their genesis. Peroxisomes are exceedingly sensitive and dynamic organelles which change their characteristics in response to demands from the cellular environment. For example, peroxisomes are sensitive to the concentration of VLCFAs in the cell and proliferate in response to increased concentrations of this ligand (Hostetler *et al.,* 2006). This malleability allows peroxisomes to maximise their functions during the changing cellular environment.

The biogenesis of peroxisomes is governed by peroxisome proliferator activated receptors (PPARs), which have 3 isoforms – α, β, γ – with varying tissue distribution (Ibabe *et al.,* 2002). The receptors are targets of the Wnt canonical signalling pathway (Huelsken & Behrens, 2002). PPARα is found in mammals in tissues which catabolise fatty acids, PPARβ is expressed in a ubiquitous manner and PPARγ can be found in adipose tissue and the immune system. The distribution of the isoforms of PPAR in zebrafish was assessed using antibodies against the 3 isoforms. The analysis indicated that all three isoforms were present. PPARα was found in liver parenchymal cells, proximal tubes of the kidney, pancreas and enterocytes; PPARβ had a much more widespread distribution and was found in the same tissues as PPARα with multiple additions, such as lymphocytes and both male and female gonads. PPARγ signal was found in the liver and gonads but the signal was weak (Ibabe *et al.,* 2002).

The roles of PPARs during development include lipid homeostasis (Kersten *et al.,* 2000) and cellular differentiation, for example epidermal cell differentiation (Rivier *et al.,* 1998). PPARs bind environmental ligands – so-called peroxisome

proliferators – and increase the rate of proliferation of peroxisomes. Proliferation is required of all organelles in developing and growing tissues; thus the process of peroxisome proliferation is integral to the health of developing embryos, in maintaining processes such as the production of plasmalogens for the developing nervous system (Peters *et al.,* 2000) and perhaps in the zebrafish, for metabolising the fatty yolk. The yolk is a reserve of energy to fuel the consumptive morphological changes and growth required in early development. To unlock this energy source, the fats must be broken down. Mitochondria break down the short, medium and long-chain fatty acids which constitute the majority taken in via our diet, whilst peroxisomes oxidise VLCFAs (Reddy & Hashimoto, 2001). This stage of zebrafish development is termed lecithotrophic, that is, the utilisation of maternally deposited yolk in oviparous organisms. Developing zebrafish embryos contrast from *Xenopus* embryos in that they undergo discoidal meroblastic cleavage which results in the yolk being separate to the embryo, as opposed to the distribution of yolk granules throughout the cells of the embryo. The yolk is separated from the embryo by the yolk syncytial layer (YSL), which contains an abundance of nuclei and produces many genes required for fat and protein breakdown and utilisation (Miyares *et al.,* 2014). It would be interesting to investigate whether this is inclusive of any of the three isoforms of peroxisome proliferator activated receptors (PPARs); indeed, acyl-CoA oxidase 1 *(acox1)*, the first and rate limiting step in the PPAR pathway (Vluggens *et al.,* 2010), is expressed in the YSL alongside other members of the pathway including apoliporotein A1 (*apoa1)* and microsomal triglyceride transfer protein *(mtp)* (Raldúa *et al.,* 2008).

Not only does the yolk fuel the morphological changes required for the development of zebrafish through the embryonic and lecithotropic stages, it also directs some of the early processes by emitting signals for the development of the mesoderm, to which Wnt, particularly *wnt11,* is an early responder and goes on with *no tail (ntl)* to induce development of the zebrafish mesoderm; although these genes are not found within the YSL but rather are exogenous responders to emitted signals (Makita *et al.,* 1998).

Both Wnt signalling and peroxisome dynamics are integral to healthy development and life, and both are upregulated in early developmental stages. Additionally, the master regulators of peroxisome proliferation, the PPARs, are targets of the canonical Wnt signalling pathway. It is hypothesised that there is a relationship between Wnt signalling and peroxisome dynamics, perhaps similar to the relationship between Wnt signalling and mitochondrial biogenesis described in 2018 by Bernkopf and colleagues, where Wnt signalling promotes proliferation. To interrogate this hypothesised relationship, Wnt signalling was manipulated in zebrafish embryos by targeting with Morpholino oligomers and CRISPR. The dynamics of peroxisomes, inclusive of their subcellular localisation, number and morphology were observed under conditions of normal, reduced and enhanced Wnt signalling.

4.4 Wnt8a and its role in zebrafish

Investigating the relationship between Wnt signalling and peroxisome dynamics first required choosing a Wnt protein and a model organism. Canonical Wnt family member *wnt8a* is maternally-derived and essential for axis formation in zebrafish. In a study by Lu, Thisse and Thisse (2011), Wnt8a was found to be the only maternally-derived Wnt protein to accumulate at the vegetal pole, clearly

demonstrated by whole-mount *in situ* hybridisation of zebrafish embryos at the 2-cell stage using antisense RNA probes for various Wnt proteins. Only the embryo injected with a probe for *wnt8a* showed staining at the vegetal pole, despite the staining being performed for all Wnt probes used for 24 hours which was purportedly 10x longer than usual, to capture even very low levels of mRNA. In fact, ablation of the vegetal part of the yolk cell within the first 20 minutes post fertilisation resulted in complete radialisation of the developing embryo due to loss of the maternal axial determinants. Embryos treated with nocodazole – an agent which interferes with microtubule polymerisation - resulting in a spectrum of phenotypes ranging from missing notochord and head or complete radialisation, were able to be rescued by injection of 25 pg of *wnt8a* mRNA into a single blastomere at the 64-cell stage. Overexpression of *wnt8a* resulted in *chordin* activation, another indication of the relationship between *wnt8a* and the developing dorsal neural tissue in zebrafish embryos.

The role of Wnt8a in axis development in vertebrates is corroborated by multiple investigations (Baker et al., 2010; Christian & Moon, 1993; Erter *et al.,* 2001; Hoppler *et al*., 1996; Lekven *et al*., 2001; Ramel & Lekven, 2004; Martin & Kimelman, 2008, etc). One mechanism for axis establishment involves *wnt8a* assuming the role of a regulator, alongside Bone morphogenetic protein (BMP), of common target genes such as transcriptional repressors Vent, Vox and Ved (Ramel & Lekven, 2004) which repress dorsal genes (Imai *et al.,* 2001, Shimizu *et al.,* 2002).

Counterintuitively, loss of BMP does not produce the same phenotype as loss of Wnt8a, in that there is no expansion of the organiser (Ramel & Lekven, 2004) and therefore head region, nor loss of anteroposterior patterning in the

gastrulating embryo (Barth *et al.,* 1999), which led to the assumption that BMP regulates these transcriptional repressors in a different way to Wnt8a. However, a commonality between the phenotypes of Wnt8a and BMP mutants is the loss of posterior and ventral tissue (Ramel *et al.,* 2005).

The integrity of zebrafish body axis determination hinges on the efficacy of maternally-derived Wnt8a. Loss or repression of *wnt8a* produces recognisable phenotypes which have been thoroughly documented and reproduced at various stages of embryonic development, through RNA probes and microscopy. Thus, *wnt8a* is an ideal candidate for knock out and knock down via CRISPR or CRISPRi respectively because it will produce clear and recognisable phenotypes replicated throughout the literature.

Zebrafish embryos were selected as models in this investigation due to the clear understanding of the function of *wnt8a* elucidated above, in addition to the more widely applicable advantages as experimental models. Such advantages include a well-established staging system and optical clarity during development with clearly delineated brain boundaries, eye and ear, with the onset of pigmentation delayed until 24 hpf (Kimmel *et al.,* 1995), making them particularly amenable to physiological observation using light microscopy. In the zebrafish, canonical Wnt family member *wnt8a* is integral to the development of the anteroposterior axis, and previous studies using Morpholino oligomer inhibition of *wnt8a* translation demonstrated that reduced Wnt8a protein yielded phenotypes with twisted tails, developmental delay and changes to the neural tissue along the whole of the dorsal side of the embryo (Lekven *et al.,* 2001). This phenotype has been well documented and reproduced and can be seen as an initial marker to signify the efficacy of Morpholino oligomer- and CRISPR-mediated repression of zebrafish

wnt8a. Targeting a gene using Morpholino oligomers to inhibit translation is widely-accepted as an efficacious method, however, it is also associated with numerous side effects, such as off-target effects. The precision of modern tools such as CRISPR have circumvented some of these issues, including a large reduction in off-target effects.

4.5.0 Phenotypic changes in zebrafish embryos injected with CRISPR/CRISPRi constructs

Since CRISPR became available as a tool for the targeted modification of the sequences of genes, it has been successfully implemented to modify the genomes of multiple organisms. The system consists of a Cas9 endonuclease and a synthetic chimeric guide RNA targeted to a region of the gene of interest. Due to the short sequence of the gRNA, the targeting is inherently specific and lacks some of the lesser attributes of other methods used to modify gene expression, such as the high penetration of off-target effects associated with the use of Morpholino oligomers.

In CRISPR interference (CRISPRi), the Cas9 enzyme is rendered catalytically inactive, or dead, by mutations in the two endonuclease domains, and as such is termed dCas9. Effector molecules can be used in conjunction with dCas9 which can activate (VP64) or enhance the repression (KRAB) of the target gene (Boettcher & McManus, 2015). Future continuation of this study could implement the effectors to modify the action of dCas9-mediated knockdown of *wnt8a*; for example, one could compare the phenotypes, RNA patterning and RNA quantity in embryos injected with gRNA targeted to *tyrosinase* and either dCas9, dCas9-KRAB or dCas9-VP64 as a read-out for differences in efficiencies before moving to use the deactivated endonuclease and effectors with gRNA targeted to *wnt8a.*

4.5.1 Targeting tyrosinase with CRISPR and CRISPRi

To test the efficacy of dCas9 and Cas9 RNA transcribed during this investigation, the endonuclease RNAs were paired with gRNAs targeted the *tyrosinase* gene essential for the development of pigmentation. At 28 hpf, the eye and the dorsal line of the zebrafish are darkly pigmented, as demonstrated by the wild type embryo in Figure 5. Upon targeting tyrosinase with CRISPR, the area of the embryo which is pigmented is significantly reduced (Figure 6) as shown by the absence of pigmentation in the areas in which it occurs in the wild type (Figure 5) - the pigmentation was knocked out by targeting *tyrosinase* with CRISPR Cas9. The efficacy of the knockout was not 100%, which demonstrates the mosaicism typified by using CRISPR.

In contrast, when *tyrosinase* was targeted by CRISPRi, there was again significantly less pigmentation than in the wild type (Figure 6), but this in many places was shown by a mix of transparent tissue and tissue in shades of grey (Figure 5), which demonstrates where the transcription of *tyrosinase* has been reduced rather than prevented. Thus, this experiment clearly demonstrated that both of the endonucleases were functioning as expected when referring to published literature and highlighted the efficacy of zebrafish as experimental models due to the ease of observation through light microscopy.

4.5.2 Designing gRNA to target *wnt8a* with CRISPR and CRISPRi

To develop a stable method to manipulate the expression of *wnt8a* in the zebrafish, gRNAs were designed as synthetic 2-piece RNAs to target 20 nucleotide regions in the untranslated regions of both open reading frames, proximate to the ATG, and in exons 1 and 3 of each open reading frame, exon 2 being too short in both cases to likely generate enough possibilities for targeting.

Cas9 and dCas9 endonucleases were amplified from pCS2+ plasmids. Combined, the Cas9 endonuclease RNA and gRNA targeted to exon 1 and/or 3 of ORF1 or 2 cut *wnt8a in vitro* (Figure 7) with sufficient but incomplete efficiency indicated by the triple band pattern seen in all wells with the full complement of constituents, the triple bands indicating, in height order, the uncut template, and the two pieces of cut fragmented template DNA. The presence of three bands of DNA of differing sizes was taken to indicate that the combination of gRNA and Cas9 was appropriate for trialling *in vivo* in zebrafish embryos.

4.5.3 Measures taken for controls

A limitation of experimentation *in vivo* is the multitude of confounding factors which can influence the outcome. To mitigate these, several controls were put in place. Embryos which appeared to be less developed than the prim-6 stage were discarded, because any deviations from the phenotype set out by the staging system could be due to developmental delay rather than the impact of downregulated *wnt8a* signalling in the embryo.

Secondly, to control for any effects on the morphology of the embryos inflicted by Cas9 or dCas9 endonucleases, injections were performed with the two components in isolation at equal concentrations to those injected with gRNAs, replacing the gRNA component with nuclease-free water. In this case, it is expected that the endonucleases would not knock out or knock down *wnt8a* because they were injected in absence of the guiding RNA which directs them to the gene of interest.

Injection with the endonuclease only did not produce embryos that varied significantly (Figure 8 B, C) from the wild type (Figure 8 A) at 28 hpf. Image B has a slight kink to the tail, but not to a degree dissimilar to the intrinsic variation of

the wild types seen at this point in development, with reference to both the high volume of images captured of wild type zebrafish in this investigation and to images captured by other groups and published in the literature. Around 100 embryos were included in each injection batch (for example, 100 wild type embryos, 100 Cas9 control embryos were injected) and the images chosen for the figure represent the phenotype of the largest proportion of embryos within that batch.

Thirdly, bias was removed from the selection process for imagery by grouping the fixed embryos into categories based on the phenotypes first, and then counting the number of individuals within each group and selecting an embryo which represented the common phenotype of the group, be it ‘wild type’, ‘mild’ or ‘severe’.

4.5.4 Implementation of CRISPR and CRISPRi to target *wnt8a* and phenotypic observations

The morphological changes of the zebrafish embryo during development are well-documented and consistent, forming the basis of the staging series established by Kimmel and colleagues (1995) which has since been globally adopted for zebrafish studies. A staging system is more advantageous than using time after fertilisation, during which time variables such as temperature can affect how quickly the embryo develops. At 28 hpf, the wild type zebrafish is between stages prim-6 and prim-16. The somites have developed, the tail is straight or almost straight, and the eye, ear and MHB are all clearly visible through simple light microscopy. The nervous tissue has an organised appearance, with the brain divided clearly into forebrain/midbrain and hindbrain by the MHB (Kimmel *et al.,* 1995).

In contrast, zebrafish embryos injected with Cas9 or dCas9 RNA and gRNAs targeted to *wnt8a* did not retain the phenotype described by Kimmel and colleagues (1995) at 28 hpf. Zebrafish embryos were injected at the 1-4 cell stage with Cas9 or dCas9 RNA and a gRNA targeted to *wnt8a,* as previously described. Embryos were maintained in E3 medium at 28 °C until 60-90% epiboly for *in situ* hybridisation and until 28 hpf for morphological study.

The aberrant phenotypes generated included embryos with disorganisation of nervous tissue from the head along the dorsal line, including partial or entire loss of the MHB. The dorsal nervous tissue lost clear structural distinction which continued along the whole dorsal side of the embryo, resulting in highly crooked tails and trunks. Additionally, the aforementioned phenotypes also carried changes to eye and head shape (Figure 8 D-G). These phenotypes clearly differed from wild type embryos, and represent an effective knock out and knock down of *wnt8a.* The observed phenotypes distinctly resembled the phenotypes exhibited in the study by Lekven and colleagues (2001) using Morpholino oligomers targeted to *wnt8a*. Further mirroring Lekven and colleagues' findings, targeting the second open reading frame generated more severe phenotypes than targeting the first open reading frame of *wnt8a.* Consistent with expectations, targeting *wnt8a* with CRISPR yielded more severely defective phenotypes than targeting *wnt8a* with CRISPRi.

Knocking out or knocking down of posteriorisation factor *wnt8a* clearly affects the development of wild type morphology. On a protein level, part of the mechanism of posterior development involves a positive autoregulatory loop between zebrafish T box transcription factor *no tail* (*ntl*, also known as Brachyury, *Bra*, in the mouse) and *wnt8a* to maintain mesodermal progenitors which allow the

development of posterior somites (Martin & Kimelman, 2008). Loss of auto-regulation, which allows such maintenance and expansion, has been proposed to underlie the dorsalization of *wnt8a* knockout embryos such as those demonstrated by Lekven and colleagues (2001). An alternative hypothesis given by Baker, Ramel and Lekven (2010) is that mesodermal dorsalization results in a lower number of ventrolateral or mesoderm progenitors being specified, and that this is the root cause of the dorsalization rather than maintenance/expansion being the primary cause.

4.5.5 Comparison between targeting the first and second open reading frames of *wnt8a*

Targeting ORF2 with either Cas9 or dCas9 resulted in phenotypes with more severe defects than targeting ORF1. The most severe phenotype presented is Figure 8 F where there is severe truncation of the posterior end of the embryo, similar to the *no tail* (*ntl*) zebrafish mutant (Schulte-Merker *et al.,* 1994), enlargement of the forebrain and loss of visible MHB. Pigmentation is lost in Figure 8 D-G. Canonical Wnt activity produced by *wnt8a* is required after organiser formation is induced by ligand-independent β-catenin signalling to antagonise the action of β-catenin and to ensure ventralisation and posteriorisation of tissue. Hence, zebrafish *wnt8a* mutants or *Xenopus* double negative mutants show loss of ventral and posterior tissue alongside enlarged organiser (Hoppler *et al.,* 1996; Lekven *et al.,* 2001).

Due to the organiser releasing the proteins required for head formation, the phenotypes seen in these embryos also include enlarged heads (De Robertis *et al.,* 2000). Conversely, whilst an enlarged dorsal organiser is demonstrated in Figure 12, only a modest increase to the most anterior portion of the head is

visible in embryos at 28 hpf when targeting *wnt8a2* in Figure 8 F and G, which could perhaps be attributed to insufficient deletion of cells in this portion of the head or true expansion. In both Figures 12 and 8, the phenotypes are visible only when targeting *wnt8a2* rather than *wnt8a1*, the former of which has been demonstrated to be the open reading frame with the greatest impact seen on phenotypes when knocked out both in this investigation and in literature (Lekven *et al.,* 2001). Lack of significant increase to head size in the face of increased size of the dorsal organiser is indeed puzzling, and could be addressed by performing further iterations of the experiment to see whether this trend is consistent. If so, it would be interesting to gain a better understanding of the impact of *wnt8a* downregulation in this experiment on the downstream components of the canonical Wnt pathway and understand whether these could have an impact on head formation, and, more specifically, their interaction with the aforementioned components released from the organiser to induce head formation.

The same truncated phenotype as seen in Lekven (2001) and Hoppler's (1996) studies is found in embryos injected with Cas9 and gRNAs targeted to ORF1 of *wnt8a*, but to a lesser degree; reflecting the same pattern seen when targeting ORF1 with a Morpholino oligomer as opposed to ORF2 (Figure 10) and mirroring results found in the literature. When comparing embryos where ORF1 or UTR1 is targeted to embryos where ORF2 or UTR2 is targeted, a more enhanced defective phenotype was seen when targeting ORF2 or UTR2, which is consistent with both Morpholino oligomer-targeting experiments completed in this study and by Lekven and colleagues (2001), when they injected zebrafish embryos with Morpholino oligomers targeted to *wnt8a* and performed morphological analysis

at 24 hpf. Lekven and colleagues (2001) found milder defects presented in embryos injected with Morpholino oligomers targeted to ORF1 of *wnt8a* and heightened defects in embryos injected with Morpholino oligomers targeted to ORF2, including poor differentiation in the brain and a crooked notochord.

Injection of Morpholino oligomers targeted to both ORF1 and ORF2 simultaneously presented the most severe phenotype (Lekven *et al.,* 2001). These findings correspond to those presented here in Figure 10, with the mildest defective phenotype induced by injection with Morpholino oligomer targeted to ORF1, a stronger defective phenotype presented by embryos injected with ORF2 and the most severe defective phenotype in embryos injected with Morpholino oligomers targeted to both open reading frames. This pattern infers, as suggested by Lekven and colleagues (2001), that one ORF may be able to compensate for the loss of the other, a response which is disabled by blocking of both ORFs.

4.5.6 Comparison between targeting *wnt8a* with CRISPR or CRISPRi

In congruence with expectations for the efficacy of transcriptional downregulation by dCas9, embryos injected with gRNA - targeted to either untranslated region - and dCas9 RNA presented less severely defective phenotypes (Figure 8 E, G) than those injected with Cas9 RNA and gRNAs targeted to either open reading frame. While in Figure 8 E there is still some anterior extension of the forebrain, there is more distinction of form of the eye and the MHB is still visible, compared to image D, where the MHB is invisible and the tail is truncated. The same pattern can be observed in images G and F. This milder phenotype reflects the mode of action of dCas9 as a repressor of transcription as opposed to the action of Cas9, where the double stranded break, common mis-repair by non-homologous end joining and associated termination of transcription prevent the gene from being

transcribed from the point of the break. The action of dCas9 as a steric block to RNA polymerase may over time dissociate and allow the full gene to be once more transcribed. This highlights an advantage of CRISPRi in that effector molecules can be used to achieve an on/off switch for the deactivated endonuclease such that induced phenotypes are reversible and the DNA is not irreversibly damaged, as it is when a double stranded break is induced by Cas9 (Qi *et al.,* 2013).

The phenotypic changes observed subsequent to the injection of Cas9 or dCas9 with gRNA targeted to *wnt8a* are distinct to the phenotypes of either wild type zebrafish at the same stage or control embryos injected with the endonuclease only. The phenotypes are comparable with other investigations which also repress *wnt8a* signalling. These physiological phenotypes induced by manipulating the signalling of *wnt8a* can be corroborated by examining the expression patterns of *wnt8a* and downstream pathway components in embryos fixed earlier in development.

4.6 Changes in expression pattern of *wnt8a* at epiboly

Changes in levels or localisation of gene expression can be visualised by targeting fixed tissues with antisense RNA probes which are labelled with a marker, in this case digoxigenin, and complementary to the gene of interest using *in situ* hybridisation. A positive signal is detected using antibody staining targeted to the marker, digoxigenin (Thisse & Thisse, 2008). Antisense RNA probes against zebrafish *wnt8a1* and *wnt8a2* were transcribed from plasmids. To check that the probes would be effective against the *wnt8a* transcribed in the zebrafish used in this experiment, both open reading frames of *wnt8a* were amplified by PCR and sequenced by Eurofins from a wild type zebrafish. The first open

reading frame was successfully sequenced, and it had 100% congruence with the sequence data available in online databases within the introns of *wnt8a1.* Thus, it was considered likely that the same results would be seen for *wnt8a2* and therefore the pre-designed probes against *wnt8a1* and *wnt8a2* would be effective.

After *in situ* hybridisation was complete, wild type embryos at 70-90% epiboly showed a strong band of *wnt8a1* at the margin, with a gap for the organiser, this being directly comparable to established patterns of wild type *wnt8a* signalling. Embryos injected with *wnt8a*-targeted CRISPR or CRISPRi constructs exhibited RNA staining patterns incomparable with wild type embryos. Phenotypes observed include mosaicism and expansion of the dorsal organiser.

It could be argued that this loss of staining could be attributed to the embryo being fixed at a later stage; at 90-95% epiboly, *wnt8* is laterally downregulated and as such *in situ* mounts show a highly faded pattern (Kelly *et al.,* 2000). However, the embryos in Figures 11 and 12 were fixed earlier in epiboly – 70-80% - which is demonstrated by the positioning of the margin at the midline of the embryo and the strong signal of *wnt8a* in the wild type embryos, which were fixed contemporaneous to the injected samples.

The mosaic loss of *wnt8a* in certain cells adheres well to the principle of mosaic expression of CRISPR constructs in injected embryos; not all cells will express the construct, and therefore not all cells will have lost or downregulated *wnt8a* transcription, and it follows that staining, resulting in some deep purple stained cells, some lilac and some with only very light background staining, are seen throughout the literature and within this study. Mosaicism here is comparable to the mosaic pigmentation seen previously (Figure 5) when *tyrosinase* was

targeted by CRISPR Cas9 and CRISPRi dCas9, demonstrating consistency between the effects of the two methodologies.

Interestingly, *wnt8a1* and *wnt8a2* appear to have overlapping but distinct expression patterns in wild type zebrafish embryos, which one could consider to visually represent the two open reading frames' overlapping but distinct roles. In several studies, *wnt8a1* or *wnt8a2* loss has been shown to produce distinct phenotypes, with loss of *wnt8a2* inducing more severe defects (Lekven *et al.,* 2001), a pattern which has been reliably reproduced throughout this investigation when observing the phenotypes of injected embryos at 28 hpf (Figure 8). The *wnt8a2* expression pattern shows a band of signal around the margin, comparable to *wnt8a1,* with an additional band position towards the animal pole. This secondary band was lost in embryos injected with CRISPR and CRISPRi constructs targeted at *wnt8a2* (Figure 12). Topically and temporally differential expression of the two open reading frames is described elsewhere; in medaka, Mwafi and colleagues (2014) found that *wnt8a2* transcripts disappear from marginal cells by as early as 40% epiboly, which were taken to imply functional differences in Wnt signalling between the evolutionarily distant teleosts.

Other noticeable deviations from the wild type phenotype is a curious asymmetry in the images. This is particularly evident in embryos which were injected with CRISPR and CRISPRi constructs targeted to *wnt8a1.* Mosaicism and low levels of signalling – demonstrated by lower intensity, i.e. lighter purple, staining – is particularly apparent on the right side of the images. This is representative of a great number of the embryos staining during this experiment. The orange arrows in Figures 11 and 12 mark areas which are particularly affected by mosaic staining and therefore changes to RNA staining pattern. For example, in Figure

11 C, there is a mosaicism to the right of the dorsal organiser, marked with an asterisk. In Figure 11 F, the right side of the organiser is much depleted, compared to both the wild type and the left side of the organiser in the same image. This pattern is shown from the animal pole in images D and F, and reflects the same patterning.

Congruent with the more extreme phenotypes seen in embryos at 28 hpf both in this investigation and others, such as that by Lekven and colleagues in 2001, embryos at 70-80% epiboly targeted with CRISPR and CRISPRi constructs targeted to *wnt8a2* show a much stronger aberrant patterning phenotype than those where *wnt8a1* is targeted. A lesser degree of mosaicism was observed around the whole margin, however the secondary band of signalling, towards the animal pole, was greatly reduced or not visible. In addition, the width of the gap in marginal *wnt8a* signalling around the dorsal organiser noticeably increased while the entirety of the band adopted a misshapen appearance when compared to *wnt8a* patterning in wild type embryos. For example, in Figure 12 C, the right side of the margin is higher than the left, and in E there is a distinct curling to the ends of the band of Wnt signalling as they progress towards the dorsal organiser, which indicates possibly a misshapen embryo. One hypothesis to explain the changes in the shape of the band of *wnt8a* signalling is disturbance caused by the needle during injection. However, care was taken to inject as early as possible in the development of the embryo, at the 2-4 cell stage, to minimise the disturbance caused by needle insertion into the cells. Expansion of the dorsal organiser and concomitant increase of anteriorising signals causing increased head size in the developed embryo is a recognised hallmark of Wnt signalling

being knocked out. The organiser is induced by Wnt signalling, but also requires Wnt to prevent its excessive expansion (Ramel & Lekven, 2004).

In addition to distinct differences in patterning between the two open reading frames in both control and CRISPR Cas9 and CRISPRi dCas9 embryos, the application of either CRISPR Cas9 or CRISPRi dCas9 to knock *wnt8a* out or down resulted in embryos with consistently different expression patterns. For *wnt8a2,* this manifested as a generally higher level of signalling intensity being maintained in embryos injected with dCas9 and gRNA targeted to *wnt8a2* UTR2*,* which demonstrates the mode of action of dCas9 as a method to repress rather than prevent the transcription of the target gene in cells.

The phenotypic differences between embryos where *wnt8a* was knocked out by CRISPR Cas9, or knocked down by CRISPRi dCas9, are pronounced, which corroborates the phenotypic differences seen in embryos at 28 hpf that have been injected with CRISPR/CRISPRi.

4.7 Quantifying changes in expression levels of *wnt8a* downstream genes

In situ hybridisation using anti-sense probes for *wnt8a1* and *wnt8a2* revealed wild type embryos with *wnt8a* patterning which matched examples established in the literature. Embryos that had been injected with CRISPR and CRISPRi constructs targeted to one of the two open reading frames consistently deviated from the wild type phenotype, for example by showing staining mosaicism and fading in the strong band of *wnt8a* signalling displayed in wild type embryos.

For embryos where *wnt8a1* was knocked out or knocked down, the most noticeable phenotypic incongruence was mosaicism in the band of *wnt8a1* signalling at the marginal zone, where in wild types this was a strong and solid band. In embryos injected with CRISPR and CRISPRi constructs targeted to

wnt8a2, there was a degree of mosaicism, but more notably a disappearance of the second band of *wnt8a2* signalling which was apparent above the marginal region in the wild type embryos – and in embryos from other studies such as those by Mwafi and colleagues (2014) – in addition to a widening of the dorsal organiser.

A correlation between differences in RNA patterning and differences in the quantity of RNA transcribed can be established by RTqPCR. RNA was extracted from zebrafish embryos and the quantity of wnt8a RNA expressed by wild type embryos was established and compared to embryos injected with CRISPR Cas9 and CRISPRi dCas9 targeted to *wnt8a*. Additionally, the expression levels of downstream Wnt pathway components such as *axin* and *lef1* were measured to establish whether changes in *wnt8a* transcription had impacted on the transcription of the pathway constituents.

The results demonstrated that both open reading frames of *wnt8a* were significantly downregulated in embryos injected with CRISPR Cas9 or CRISPRi dCas9 targeted to *wnt8a*, compared to wild type embryos. This corroborates the results of morphological analysis and RNA patterning analysis and infers that the CRISPR Cas9 and CRISPRi dCas9 constructs targeted to *wnt8a* successfully downregulate the transcription of the target gene.

Curiously, despite targeting only one of the open reading frames in a sample, both open reading frames were downregulated. Lekven and colleagues (2001) suggest cross-talk between *wnt8a1* and *wnt8a2* in zebrafish. Such cross-talk may go some way to explain the unexpected pattern described above. To eliminate the possibility of primer binding infidelity, *wnt8a1* levels were artificially elevated by injection with *wnt8a1* RNA. The results showed a large upregulation of *wnt8a1,*

and a slight but much smaller uplift from *wnt8a2,* which inferred that the individual primers were not binding with both open reading frames and producing identical results. Interestingly, two primers were used for each open reading frame, and only one (*wnt8a1A*) underwent a large uplift, although why this occurred was not established. Overexpression of *wnt8a1* established primer fidelity, yet also raised the question that if only detection of *wnt8a1* is upregulated artificially by injection of *wnt8a1* RNA, then why if *wnt8a1* transcription is downregulated by injection with CRISPR/CRISPRi constructs, is *wnt8a2* downregulated in tandem? It is widely acknowledged that the *wnt8a* locus is complex, with two open reading frames, two untranslated regions and three transcription start sites (Lekven *et al.,* 2001), and my results do not deviate from this observation.

The consistency of downregulation of transcription of *wnt8a* contrasts to the results collected when quantifying the impact of *wnt8a* knockout and knockdown on Wnt downstream genes *axin2* and *lef1*. When *wnt8a1* RNA was injected in the overexpression experiment, there was no significant effect in the level of *axin2* and *lef1* RNA levels. This is somewhat surprising given the huge increase in *wnt8a1* RNA detected by *wnt8a1A* primer, and given that Axin2 and Lef1 are downstream components of the canonical Wnt pathway. A possibility may be that the samples were taken at a time point which was too early to see downstream effects, but this is doubtful because the cells were injected at the 2-cell stage, and harvested at 70-90% epiboly, which are distanced by around 9 hours of development within a 28°C incubator. If even a large increase in cellular *wnt8a1* levels did not have a significant effect on the translation of *axin2* or *lef1*, it is no surprise that a more nuanced decrease in the level of *wnt8a1* or *wnt8a2* transcribed did not produce significant changes in the transcription of the

downstream pathway components. The decrease in *wnt8a1* and *wnt8a2* cellular RNA levels is here described as more nuanced and a less precipitous decrease than the increase in *wnt8a1* RNA mediated by injection because the *wnt8a1* RNA injected was zebrafish RNA which then must undergo one step, translation, to form protein and participate in the network of Wnt pathways. In contrast, the method of action of CRISPR or CRISPRi constructs is multistep, and the uptake in cells is often mosaic; the constructs are injected as RNA and must be transcribed to form the Cas9/dCas9 proteins, which must then translocate to the nucleus, hybridise with the corresponding gene and induce a double stranded break or impair transcription. For the former, this must then be repaired incorrectly and produce a stop codon to prevent transcription. The multi-step process, coupled with the mosaic nature of uptake of CRISPR and CRISPRi constructs, lends itself to a process which both is temporally lengthy in comparison to simple injection of *wnt8a1* RNA and contemporaneously produces reduction in target DNA transcription in only some cells, and in the case of dCas9, only some of the transcript is prevented from transcription, hence the muted repression as opposed to knockout phenotypes associated with the catalytically active form of the enzyme. Thus, if no distinguishable effect is to be found in the amount of RNA of the downstream genes in the *wnt8a1* overexpression experiment, then it is concordant that in the CRISPR/CRISPRi samples, effects on downstream signalling components of the canonical Wnt pathway remain insignificant.

The results of the two experiments are therefore in agreement with each other, but are still unexpected. Axin2 is an established read-out for activity of the canonical Wnt pathway, for example in studying pathway activity in the developing zebrafish caudal fin (Wehner *et al.,* 2014), and in studying Wnt-

mediated control of scale formation in zebrafish (Aman, Fulbright & Parichy, 2018) Transcription of *axin2* is induced by canonical Wnt signalling via Tcf/LEF sites and acts as a negative regulator of the pathway, forming part of the degradosome which targets β-catenin for degradation within the cytoplasm. In mice, *Axin* is expressed constitutively, whereas *Axin2* is temporally limited to embryogenesis and organogenesis, underscoring the importance of controlling Wnt signalling during these formative processes. Jho & colleagues (2002) found that *Axin2* could be reliably and quickly induced by Wnt signalling, which is in contrast to the results of the overexpression experiment performed in this investigation. However, when *wnt8a1* ORF1 was targeted by Cas9, there was a significant decrease in the transcription of *lef1*, and a general pattern of decrease in *axin2* transcription, although this was too varied to be statistically significant. The results for both *axin2* and *lef1* were much more varied than for the *wnt8a1* and *wnt8a2* transcripts themselves. On the one hand, this could be considered intuitive as the proteins are distanced within the pathways and there are many confounding variables which could affect the translation of downstream proteins. At the same time, the interrelation of Wnt8a proteins and their downstream components is well-established and quickly reproducible in experiments such as those performed by Jho and colleagues (2002). *lef1* is a direct target of canonical Wnt signalling, an HMG box family member which acts as a positive transcription factor dependant on β-catenin, binding alongside Tcf and Lef binding sites which are found in upstream regulatory sequences. In the absence of β-catenin, Tcf is a transcriptional repressor, but upon binding of β-catenin, the repression mechanism is disabled, although how this is achieved remains unknown (Dorsky *et al.,* 2002).

Concurrent with the aberrant phenotypes documented in injected embryos at 28 hpf – including perturbations to the neural structure from the forebrain all the way along the dorsal axis, manifesting as nonspecific tissue, changes to head shape and developmental delay – and mosaicism in *wnt8a* expression demonstrated by aberrant staining patterns in *in situ* hybridisation samples at 70-80% epiboly, there is a consistent and highly statistically significant downregulation of *wnt8a1* and *wnt8a2* in samples injected with Cas9/dCas9 and gRNA targeted to either open reading frame. The consistency of the results, with all but one example falling within the 5% confidence levels, coupled with phenotypic and pattern data, infers that *wnt8a1* and *wnt8a2* were successfully downregulated in zebrafish embryos in this experiment via injection of Cas9 or dCas9 coupled with gRNA targeted to either the first or second open reading frame or untranslated region of *wnt8a.* Therefore, CRISPR and CRISPRi embryos could be used to study peroxisome dynamics compared to dynamics within wild type embryos.

4.8 Peroxisomes in human cell culture

Peroxisomes were studied both in human cell culture, where high rates of proliferation and adherence to the surface of the dish created samples highly amenable to rapid imaging and repeated experiment, and additionally in live zebrafish embryos, where the time investment to produce images is significantly greater. The purpose of beginning the studies with cell culture was to visualise peroxisomes and any changes generated by addition of Wnt-inhibiting or Wnt-activating chemicals in a simple isolated environment whilst developing my CRISPR toolkit. The distribution of the Wnt-inhibitor/activator chemical is more easily controlled over the surface of a plate than by application to embryo medium; the requirement of the former is adsorption across the flat surface of a

cell, as opposed to penetrance of a ball of many cells. Additionally, embryos are undergoing innate developmental processes mediated by many intermediary factors and chain reactions such as axes and tissue specification which may interfere with the effects of chemicals applied.

Human gastric adenocarcinoma (AGS) cells were chosen for imaging because they have higher rates of proliferation and greater cell sizes than zebrafish fibroblast (PAC2) cells, which were considered as an alternative. Both cell types are known to contain peroxisomes, a well-conserved organelle throughout evolution. Wnt signalling is known to be high in AGS cells, and I hypothesised that they would be a good candidate for manipulation of the pathway. Unbridled Wnt signalling in cancerous cells was first directly linked to colorectal cancer, where mutations in the adenomatous polyposis coli (APC) gene was found to be the underlying cause of hereditary colon cancer syndrome. APC was found to interact with β-catenin, and mutations in APC led to overactive β-catenin signalling (Zhan, Rindtorff & Boutros, 2017). High levels of Wnt signalling are established in AGS cells, and correlate with tumour progression and genesis in patients with gastric cancer, perhaps through maintenance of Cancer Stem Cells (CSCs). In particular, *Wnt1* has been found to be overexpressed, alongside CD44, in mouse gastric cancer cells (Mao *et al.,* 2014).

AGS cells were transfected with SKL-GFP. SKL is a type 1 peroxisomal targeting signal (PTS1), one of two such chaperones which guide proteins to receptors on the single peroxisomal membrane for import, a mechanism required to prevent the occurrence of peroxisomal ‘ghosts’, shell-like peroxisomes which do not contain any matrix proteins, because peroxisomes lack endogenous DNA, or transcriptional or translational machinery. SKL was fused to GFP, and therefore

marks peroxisomes, or peroxisome-like structures, in green. Here we use ‘peroxisome-like structures’ because the identity of the organelle was not confirmed via any method such as immunohistochemistry. However, SKL is used to illuminate peroxisomes throughout the literature, such as the work of Waterham and colleagues (2007), where pEGFP-SKL was used to examine the morphology and orientation of peroxisomes in control and patient fibroblasts. The analysis yielded images which showed mitochondria as long tangled chains and peroxisomes that were fewer in number, oft arranged in rows and of varying size within patient fibroblasts, as compared to controls. This was due to a defect in GTPase DLRP, and showed that the methodology was sufficient to gain an impression of changes in peroxisome morphology and dynamics.

In this investigation, numerous peroxisome-like structures were exposed by SKL-GFP transfection in AGS and PAC2 cells, with size, number and morphology comparable to examples seen in literature, such as control samples in Waterham and colleagues’ investigation in 2007.

A baseline number of peroxisomes per cell in similarly-sized cells was established. Following the setting of this wild type threshold, cells were divided into three groups which received either DMSO (volume equal to the largest volume applied to dilute either BIO or IWR1 to the required concentration in the test groups), which formed the control group, or Wnt activator BIO or Wnt inhibitor IWR1 for the test groups. The concentration chosen for measurement was the highest that could be withstood by the cells without inducing unacceptable side effects such as high mortality rates and serious malformation. However, in both experimental samples, peroxisome number increased. I hypothesise that the increase in number of the structures may have been an artefact of transfection,

and in fact that the high level of Wnt signalling in the cancer cells was so pronounced that the effectors could not reach the threshold required to upregulate or downregulate signalling without causing unacceptable side effects such as excessive cellular mortality or malformation. Therefore, AGS cells were actually disadvantageous to use for Wnt manipulation, contrary to my initial hypothesis. Nevertheless, future studies may consider implementing a more finely delineated scale of BIO and IWR1 in order to assess more accurately whether there are any changes in peroxisome dynamics, or alternatively persist using a non-cancerous cell line such as a fibroblast.

A secondary hypothesis can be postulated when examining the images presented in Figure 17 A. In the upper image, there is a large number of peroxisomes, whilst the lower image appears to have many less, despite both being untreated control cells. The upper image is a human AGS cell, and the lower a zebrafish PAC2 cell. On the one hand, this could represent intrinsic variation in peroxisome number between the two cell lines; on the other, it could be introduced by ineffective transfection, or differences in the orientation of the two cells when the images where taken. Therefore, a second reason that the lack of difference in the number of peroxisomes – apart from that in both cases, the number of peroxisomes in treated cells is greater than in untreated – could be that the intrinsic variation in peroxisome number, or differences in the efficacy of transfection, or orientation during imaging, led to too great a variation in peroxisome number to discern a pattern. It may be that it is more likely a combination of the first and second hypotheses. These same hypotheses apply to Figure 17 B, where you can see that the differing cell sizes, which intrinsically contain differing numbers of peroxisomes, and over-exposure present a difficulty

in determining whether peroxisome number in treated cells changed vs. untreated cells.

Therefore, it would be most effective to not only implement a more finely delineated scale of Wnt activator/inhibitor application, but also to test methods to induce more regularity in the number of peroxisomes revealed in control cells. For example, this may take the form of greater control over environmental conditions that the cells reside in, due to the plasticity of peroxisomes in response to the cellular environment.

4.9 Peroxisomes *in vivo* in zebrafish embryos with varying levels of *wnt8a* expression

In contrast with using Wnt-inhibiting and Wnt-activating chemicals in AGS cells *in vitro*, where we saw no significant difference in the number or morphology of peroxisomes in the various treatment groups, there was a distinct effect on peroxisomes in live zebrafish embryos where Wnt signalling was manipulated by microinjection of inhibiting/activating factors. Zebrafish embryos were injected with SKL-GFP and either Morpholino oligomer against *wnt8a1* and *wnt8a2*, *wnt8a* RNA or Cas9 directed to *wnt8a.* Therefore a spectrum of *wnt8a* repression – overexpression was synthesised. Targeting a gene with Morpholino oligomers is known to induce a strong knockout affect, which was consistent with morphological changes observed in 28 hpf embryos in this investigation, and Cas9 has strong repressive capabilities (Huang *et al.,* 2015; Jao *et al.,* 2013) but can be limited by mosaicism of uptake in cells. The control samples should retain normal levels of *wnt8a* for the developmental stage, and the embryos injected with *wnt8a* RNA should experience *wnt8a* overexpression. Control samples were injected only with SKL-GFP.

Similarly to my work in AGS cells, a baseline of peroxisome number and morphology was established by studying images of embryos injected with SKL-GFP only at epiboly. All non-control images of embryos were compared to this baseline. In addition to visual study of the images, the proportion of the cell that was fluorescing was analysed using ImageJ software. Both measures are presented because an increase in the proportion of the cell that was fluorescing could be due to an increase in the size of individual or clumped-together peroxisomes, or due to a greater number of individual puncta or clumps of peroxisomes of unchanged size. Conversely, a decrease in the proportion of the cell that is fluorescing could be due to clumping of peroxisomes without an increase in their number or due to a lesser number of individual puncta. Visual analysis of the images was therefore required to ensure that false assumptions were not made as a result of numerical data.

In embryos injected with SKL-GFP coupled with Morpholino oligomers targeting both open reading frames of *wnt8a* (*wnt8a1, wnt8a2*), there is severe clumping of the green signal, visible in Figure 20. The peroxisome-like structures have transitioned from the majority of singular puncta in control cells, with a low incidence of clumped signal, to the majority of the cell being occupied with clumped signal and a lower incidence of singular, distinct puncta, taken from the specificity of the marker SKL in its role as a targeting protein for peroxisomal proteins synthesised in the cytosol (Subramani, 1998), to be peroxisomes.

I hypothesise that these clumped structures may reflect a defect within the process of division of these organelles. Growth and division of peroxisomes, as discussed earlier within this thesis, occurs either *de novo* or from asymmetrical division of pre-existing peroxisomes, the latter of which forming the majority of

replenishment after cell division or a dynamic increase in response to cellular needs (Schrader *et al.,* 2012).

Growth and division of peroxisomes is a morphologically distinct process, commencing with extension of the peroxisomal membrane, constriction of the tubule into small 'beads', and scission of the membrane to produce several smaller peroxisomes which have asymmetrically budded off the originator (Grabenbauer *et al.,* 2000). A defect in peroxisome division produces a recognised 'beads on a string' phenotype where the final scission event, mediated by GTPase DLP1, does not occur. The extension and associated membrane bending does however, and the result is an asymmetric extension bent into spheres along the length of it with the resultant phenotype of a string of beads, which is commonly used as a marker for peroxisomal diseases of proliferation (Schrader *et al.,* 1996). If these structures fluoresce, it is reasonable to infer that at the relatively low resolutions offered by confocal microscopy, the resultant images would look like clumps of fluorescent signal. As this clump-like phenomenon is already recognised, it is not unreasonable to hypothesise that a similar effect may be taking place in the images in Figure 20. Further investigation must be performed to understand whether high level *wnt8a* repression does impact upon peroxisomal growth and division.

Wnt signalling is already associated with organelle proliferation; Wnt signalling can stimulate the proliferation of the 'sister organelle' of peroxisomes, mitochondria after reception of mitochondrial stress and concomitant loss of mitochondrial membrane potential, triggering mitophagy of damaged mitochondria and replenishment of the cellular quotient via Wnt signalling (Bernkopf *et al.,* 2018).

In embryos injected with SKL-GFP and *wnt8a* RNA in an overexpression treatment, the phenotype displayed is quite different. While there are also some areas of clumped signal, these appear to be larger than examples in the *wnt8a* Morpholino and *wnt8a* Cas9 samples. There is also a greater presence of small puncta in each cell. As a result, these cells had a significantly greater ($P<0.005$) proportion of cell that was fluorescent than the control cells. This infers that *wnt8a* may be a positive regulator of peroxisomal abundance; PPARβ is after all a target of the canonical Wnt pathway (Huelsken & Behrens, 2002). In this case, the clumping coupled with the greater volume of small puncta within the lumen of the cell could be due to enhanced multiplicative activity.

If there were greater numbers or larger clumps of fluorescent signal with an absence of high number of small puncta, one could surmise that a similar hypothesis to the one proposed for the Morpholino oligomer samples could be adopted; that overexpression of *wnt8a* interferes with replicative machinery and terminates the process in its intermediary stages. However, the large clumps of signal coupled with a high volume of small puncta could be taken to infer the opposite; that *wnt8a* overexpression increases the asymmetric growth and division of peroxisomes. In this scenario, the incidence of clumped areas of signal are replicating peroxisomes caught in an intermediary stage at the time of imaging, rather than replicating peroxisomes in stasis at an intermediary stage due to a defect in replication.

Embryos injected with SKL-GFP and Cas9 RNA targeted to *wnt8a* appear differently to controls (Figure 20) and fit into the pattern displayed by the spectrum of Wnt pathway signalling developed here by microinjection of various factors. Single puncta within the lumen of the cell appear to be less numerous, and some

areas of conglomerated fluorescent signal can be observed, both in the bottom third of the image. The clumps of signal are not as numerous as comparable cells in the images of the embryos injected with Morpholino oligomers directed to *wnt8a* open reading frames 1 and 2, but the appearance of the cells is more consistent within the sample, excepting the cells in the top two thirds of the image, which are consistent within themselves but look to be clearly a contrasting cell type, and I propose that they are part of the yolk syncytial layer. They do not look to have taken up Cas9, demonstrating the mosaicism which can sometimes limit this technique. Only cells in the bottom third of the image were used for calculating the proportion of each cell that is fluorescing, to make the images more comparable to the remaining samples. In this case, injection of Cas9 RNA guided by gRNA targeted to *wnt8a1* and *wnt8a2* resulted in cells with significantly lower proportion of fluorescence per cell ($P<0.0005$, Figure 21). This result infers that there may be a relationship between *wnt8a* signalling and peroxisome dynamics, particularly their replication.

4.10 Future Studies

The establishment of a relationship between *wnt8a* signalling and peroxisome dynamics has opened a new series of questions. Is this relationship consistent between peroxisome dynamics and other Wnt proteins - both canonical and non-canonical? One of the benefits of using the CRISPR/CRISPRi system is that to answer this question, only the gRNA must be redesigned. Multiple constructs can be injected contemporaneously within a single collection of eggs which further enhances the efficiency of using CRISPR/CRISPRi systems, and allows direct comparison of the effects of targeting the different Wnts throughout the establishment of the targeting systems.

Secondly, is the relationship between Wnt signalling and peroxisome dynamics exclusive to the zebrafish, or is the same seen in other model organisms, or cell lines? Examples may include *Xenopus, Drosophila* and murine disease models. An advantage of the CRISPR system is that it can be modified to be tissue-specific - for example by using a tissue specific promoter (Xu *et al.,* 2016) - and thus the specificity of the relationship between Wnt signalling and peroxisome dynamics can be examined in terms of species and tissue type.

Zebrafish have a 70% similarity to the human genome (Howe *et al.,* 2013), but it would be interesting to see if the same relationship observed in this investigation is conserved in humans. In this investigation, manipulating Wnt signalling in AGS cells by application of Wnt inhibitors and activators was not effective, possibly due to being unable to surpass the threshold of chemical required to impact upon the endemically high Wnt levels of cancerous cells (Mao *et al.,* 2014). Alternative cell lines could be used to investigate whether Wnt signalling impacts upon peroxisome dynamics in humans and further whether this is limited to particular cell types. Cell type specificity could be related to the distribution of the isoforms of PPARs - the master regulators of peroxisome proliferation - in different tissues, however this hypothesis assumes that the proliferative dynamics of peroxisomes observed in this investigation are dependent on PPARs, and that the isoforms may be acted upon unequally by Wnts. Investigation could include culturing multiple cell lines and transfecting with CRISPR/CRISPRi constructs targeting multiple Wnts with custom gRNAs. Initial indications of the efficacy of knockdown could be given using the TOP-flash reporter (Molenaar *et al.,* 1996). The impact of the knockdown/knockout could be investigated by transfecting SKL-GFP and visualising the dynamics via confocal microscopy.

It would also be interesting to establish which components of the Wnt pathway are depended upon to induce peroxisome proliferation; is it β-catenin, or is the proliferative signal reliant on the Wnt receptor? Is Wnt reception at the membrane required, or is intrinsic activation of the pathway sufficient? The tractable CRISPR system could be used to sequentially knockout components of the signalling pathway and observe the effects on peroxisome dynamics, complemented with rescue experiments.

The above experiments assume that the relationship between Wnt signalling on peroxisome dynamics is dependent on the physical characteristics of a protein, tissue type or species. The question remains whether the relationship is temporally limited; is it true throughout the lifespan of the organism, or limited? During development the zebrafish embryo expresses high levels of Wnt signalling, demonstrated by the strong band of wnt8a RNA observed at the margin during epiboly (Figure 11). To assess whether the observed relationship between Wnt signalling and peroxisome dynamics is continued into adulthood, lines of transgenic zebrafish could be produced, each deficient of a Wnt protein, for example Wnt8a. A possible limitation to this method is that embryos showing a strong Wnt8a-deficient phenotype may not reach breeding maturity; embryos in this investigation were terminated post 28 hpf and thus longevity was not required, so this remains an open question.

Prior to investigating the above questions, it would be prudent to test the efficacy of CRISPR Cas9 directed to *wnt8a* in zebrafish by sequencing the locus of injected embryos for insertions and deletions induced by inaccurate repair of DSBs by the rapid yet inaccurate repair method of non-homologous end joining. Additionally, successful sequencing of the second open reading frame of *wnt8a*

in the zebrafish line used in this investigation would lend greater confidence to the fidelity of the primers used to target the same for RTqPCR. Unfortunately sequencing data is not informative of the action of dCas9, but visual report via experiments such as targeting *tyrosinase* does engender confidence in the action of the endonuclease. The aforementioned advantages of CRISPRi dCas9 include the use of effector molecules, in the form of enhanced repressive activity (dCas9KRAB) and activating activity (dCas9VP64), and it would be interesting to implement these forms of interference in targeting Wnts. The positive control of Wnt8a overexpression by injection of wnt8a RNA would form an interesting comparison to activation of transcription of the endogenous *wnt8a* gene by dCas9VP64.

Clearly the investigation performed here can be expanded and with a greater time resource, can be replicated. Deeper study of the morphology of peroxisomes under conditions of varying Wnt signalling may be illuminating because morphology seems to be a revealing metric of this organelle. For example, the ‘beads on a string’ morphology seen in some peroxisomal disorders is archetypal of a defect in asymmetrical growth and division. To gain a more granular view of the peroxisome ‘clumps’ that were visualised through confocal microscopy in this investigation, techniques such as scanning electron microscopy (SEM) or correlative light-electron microscopy (CLEM) could be utilised. CLEM has been successfully employed to identify a novel interaction of peroxisomes, melanosomes and phagosomes in the retinal pigment epithelium of retinal tissue, and additionally Burgoyne and colleagues (2018) found that using cryostat sections greatly improved the ability to identify subcellular compartments.

Alternatively, there are benefits to using transmission electron microscopy (TEM), in that it combines the ability of confocal microscopy to scan a large area before focussing in on an area of interest, with high resolution. Here SKL was used to illuminate peroxisomes within the cell using GFP, whereas a study by Cajaraville and colleagues (2003) used antibodies for SKL coupled with the protein A gold technique and TEM which produced much clearer images than the use of DAB staining of peroxisomes using catalase, another method used within the literature. All of the above - SEM, CLEM, TEM - should generate a higher-resolution image than confocal microscopy was able to and therefore facilitate counting of peroxisomes without the noise caused by fluorescence which was a limitation of using SKL tagged with GFP.

An indirect method of measuring peroxisome abundance could be by measuring biochemical activity; that is, by measuring the activity of an enzyme endemic to peroxisomes and indicative of their activity. However, this should be addressed with caution because it would assume that varied levels of *wnt8a* signalling affect the morphology and number of peroxisomes but not their biochemical activity. An example would be to measure acyl-CoA oxidase which is part of the β-oxidation pathway activated by peroxisome proliferation. The activity of the enzyme could be compared to a positive control in the form of embryos exposed to a known peroxisome proliferator of which there are numerous examples of both endogenous and exogenous candidates, many of the latter of which include pollutants and cause peroxisomal proliferation in aquatic animals the matter of which is of concern within the research community (Cajaraville *et al.,* 2003).

A similar method could be used to assess mitochondrial number, using an endemic mitochondrial enzyme. Bernkopf and colleagues (2018) highlighted the

relationship between mitochondrial proliferation and Wnt signalling, which has been discussed previously in this text. It would be interesting to use a similar method as followed in this investigation, with the improvements suggested above, to observe whether the manipulation of *wnt8a* expression specifically induces changes in mitochondrial morphology and number. Further, to deduce whether the morphological and proliferative changes mirror the pattern displayed by peroxisomes, or whether mitochondria respond in a different way to *wnt8a* manipulation.

Thus far, focus has been directed solely on the impact of manipulating *wnt8a* expression on peroxisomes. If indeed the relationship between *wnt8a* expression and peroxisome dynamics holds true during further investigation, perhaps using some of the ideas listed above, it would be useful to understand how much, if any, impact the change in peroxisome number and morphology has on the phenotypes demonstrated in both imaging 28 hpf embryo morphology and *in situ* hybridisation experiments; that is, how much of the *wnt8a*-deficient phenotype is due to the changes in peroxisome dynamics observed in this investigation?

One hypothesis is that the lower number of peroxisomes and the clumped nature of their appearance observed in *wnt8a*-deficient embryos is due to a defect in their proliferation. Therefore, a simple test could be performed to understand whether peroxisome number contributes to the morphologies observed *in situ* hybridisation and imaging of 28 hpf embryos. Components of the peroxisome proliferative machinery could be targeted using CRISPR; for example, to isolate the impact on peroxisomes, *pex11β* could be targeted. To manipulate the proliferation of both peroxisomes and mitochondria, one of their shared components of the division machinery could be targeted such as *fis1* or *mff.* Once

knockouts have been established, a cohort of injected embryos could be raised until 70-80% epiboly and fixed for *in situ* hybridisation, using the same probes for *wnt8a1* and *wnt8a2*, to determine whether any of the hallmarks of *wnt8a* deficiency observed, such as asymmetry of the signalling band around the margin, or widening of the dorsal organiser, are seen. These changes may bely changes to morphology which may be observed in a second cohort of embryos raised to 28 hpf and fixed for morphological analysis through imaging.

5.0 Conclusion

Paracrine or cell-cell signalling locally controls the behaviour of a group of cells by reducing heterogeneity in the transcription of genetic content. This is important so that the cells can coordinate and acquire a collective cell fate (Handly *et al.,* 2015). An important example of a paracrine signal is Wnt, which forms a concentration gradient throughout responsive tissues and determines tissue and axes patterning (Nusse & Clevers, 2017) which underscores the importance of Wnt signalling during development.

Paracrine Wnt signalling operates via a collection of pathways, the most renowned of which is the canonical signalling pathway. The reception of the canonical Wnt ligand at the receiver cell membrane triggers a cascade of intracellular reactions which lead to the preservation of β-catenin, which translocates to the nucleus and mediates the expression of multivariate target genes. These target genes include *PPARs* (Huelsken & Behrens, 2002), the master regulators of peroxisome proliferation (Ziouzenkova *et al.,* 2002), and *cyclin* (Huelsken & Behrens, 2002). Wnt signalling is therefore important for managing the proliferation of cells, and its repertoire has been expanded recently

to managing the cellular abundance of mitochondria (Bernkopf *et al.,* 2018), the 'sister organelle' to the peroxisome.

Peroxisomes are single membrane bound organelles with multiple biochemical functions such as the breakdown of VLCFAs. Peroxisomes are also key components during development and life; the organelle produces plasmalogens, which facilitate nervous conduction, and perturbation of any of the PEX proteins which manage the function and biogenesis of the organelles results in a spectrum of severe diseases (Schrader *et al.*, 2012).

The relationship between Wnt signalling and peroxisome dynamics is undetermined. To investigate this relationship, I knocked out and knocked down the canonical Wnt family member *wnt8a* in zebrafish embryos using the genomic engineering tools CRISPR and CRISPRi. In Wnt8a-deficient embryos I observed the morphology and number of peroxisomes and found them to be more aggregated and less numerate than in control samples. In embryos with *wnt8a* overexpression, I found peroxisomes to be more numerate and appear more often as distinct and singular puncta.

Based on the results from this investigation, I hypothesise that in addition to other roles including axes determination of tissue specification, Wnt signalling has a novel and stimulating relationship with peroxisome proliferation.

Future studies may wish to use other model organisms such as *Xenopus* and murine models, human non-cancerous cell lines such as fibroblasts, and tissue-specific promoters to understand whether the relationship between Wnt signalling and peroxisome dynamics is consistent in different species and tissue types. Further, a line Wnt-deficient transgenic zebrafish could be produced to investigate the relationship between Wnt signalling and peroxisomes throughout

key life stages of the zebrafish to better understand whether the relationship observed in this investigation is dependent on a physical variable such as the species, tissue or pathway component, or whether the time at which the relationship is tested is key to understanding the novel relationship between Wnt signalling and peroxisome dynamics.

Acknowledgements

I would like to thank my supervisors, Prof Steffen Scholpp and Prof Michael Schrader, for their guidance and support during my Masters. I would also like to thank my colleagues in the Scholpp lab, where I performed all of the experiments, especially Dr Benjamin Mattes for his daily support and good humour, Dr Lucy Brunt, Simone Schindler and Dr Jenna Concoran.

References

Ablain, J. *et al.,* 2015. A CRISPR/Cas9 Vector System for Tissue-Specific Gene Disruption in Zebrafish. *Developmental Cell,* 23 3, 32(6), pp. 756-764.

Albrecht, L. V., Ploper, D., Tejeda-Muñoz, N. & De Robertis, E. M., 2018. Arginine methylation is required for canonical Wnt signaling and endolysosomal trafficking. *Proceedings of the National Academy of Sciences of the United States of America,* 5 6, 115(23), pp. E5317-E5325.

Aman, A. J., Fulbright, A. N. & Parichy, D. M., 2018. Wnt/b-catenin regulates an ancient signaling network during zebrafish scale development.

Baker, A., Lanyon-Hogg, T. & Warriner, S. L., 2016. Peroxisome protein import: a complex journey. *Biochemical Society transactions,* 44(3), pp. 783-9.

Baker, K. D., Ramel, M.-C. & Lekven, A. C., 2010. A direct role for Wnt8 in ventrolateral mesoderm patterning. *Developmental Dynamics,* 1 11, 239(11), pp. 2828-2836.

Barth, K. A., Kishimoto, Y. A., Rohr, K. B., Seydler, C., Schulte-Marker, S., Wilson, S. W., 1999. Bmp gradient in the neural plate. *Development,* 126, pp. 4977-4987.

Baumgart, E. *et al*., 2001. Mitochondrial Alterations Caused by Defective Peroxisomal Biogenesis in a Mouse Model for Zellweger Syndrome (PEX5 Knockout Mouse). *The American Journal of Pathology,* 1 10, 159(4), pp. 1477-1494.

ten Berge, D. *et al.,* 2008. Wnt Signaling Mediates Self-Organization and Axis Formation in Embryoid Bodies. Cell Stem Cell, 6 11, 3(5), pp. 508-518.

Bernkopf, D. B. *et al.,* 2018. Pgam5 released from damaged mitochondria induces mitochondrial biogenesis via Wnt signaling. *The Journal of cell biology,* 8 2.p. jcb.201708191.

Boettcher, M. & McManus, M. T., 2015. Choosing the Right Tool for the Job: RNAi, TALEN, or CRISPR. *Molecular cell,* 21;58(4), pp. 575-585.

Bolotin, A., Quinquis, B., Sorokin, A., Ehrlich., 2005. Clustered regularly interspaced short palindrome repeats (CRISPRs) have spacers of extrachromosomal origin. *Microbiology,* 1 8, 151(8), pp. 2551-2561.

Braverman, N. *et al*., 1997. Human PEX7 encodes the peroxisomal PTS2 receptor and is responsible for rhizomelic chondrodysplasia punctata. *Nature Genetics,* 1 4, 15(4), pp. 369-376.

Brunt, L. & Scholpp, S., 2018. The function of endocytosis in Wnt signaling. *Cellular and Molecular Life Sciences,* 14 3, 75(5), pp. 785-795.

Burgoyne, T. *et al.,* 2018. Correlative light and immuno-electron microscopy of retinal tissue cryostat sections. *PLoS ONE,* 1 1.13(1).

Cajaraville, M. P., Cancio, I., Ibabe, A. & Orbea, A., 2003. Peroxisome proliferation as a biomarker in environmental pollution assessment. *Microscopy research and technique,* 61(2), pp. 191-202.

Camões, F., Bonekamp, N. A., Delille, H. K., Schrader, M., 2009. Organelle dynamics and dysfunction: A closer link between peroxisomes and mitochondria. *Journal of Inherited Metabolic Disease*, 32, pp. 163-180.

Camp, E. & Lardelli, M., 2001. Tyrosinase gene expression in zebrafish embryos. *Development Genes and Evolution,* 2 4, 211(3), pp. 150-153.

Chen, B., *et al.,* 2009. Small molecule-mediated disruption of Wnt-dependent signaling in tissue regeneration and cancer. *Nature chemical biology,* 2, 5(2), pp. 100-7.

Chen, G. *et al*., 2014. A regulatory signaling loop comprising the PGAM5 phosphatase and CK2 controls receptor-mediated mitophagy. *Molecular Cell,* 8 5, 54(3), pp. 362-377.

Christian, J. L. & Moon, R. T., 1993. Interactions between Xwnt-8 and Spemann organizer signaling pathways generate dorsoventral pattern in the embryonic mesoderm of Xenopus.. *Genes & development,* 1 1, 7(1), pp. 13-28.

Chung, H. M. & Malacinski, G. M., 1980. Establishment of the dorsal/ventral polarity of the amphibian embryo: use of ultraviolet irradiation and egg rotation as probes.. *Developmental biology,* 11, 80(1), pp. 120-33.

Cimini, A. *et al*., 2005. Expression of peroxisome proliferator-activated receptors (PPARs) and retinoic acid receptors (RXRs) in rat cortical neurons. *Neuroscience,* 1, 130(2), pp. 325-337.

Cimini, A. & Cerù, M. P., 2008. Emerging Roles of Peroxisome Proliferator-Activated Receptors (PPARs) in the Regulation of Neural Stem Cells Proliferation and Differentiation. *Stem Cell Reviews,* 17 12, 4(4), pp. 293-303.

De Robertis, E. M., Larraín, J., Oelgeschläger, M. & Wessely, O., 2000. The establishment of spemann's organizer and patterning of the vertebrate embryo. *Nature Reviews Genetics,* 1 12, 1(3), pp. 171-181.

Den Broeder, M. J., Kopylova, V. A., Kamminga, L. M. & Legler, J., 2015. Zebrafish as a Model to Study the Role of Peroxisome Proliferating-Activated Receptors in Adipogenesis and Obesity. *PPAR Research,* Volume 2015.

Deveau H., Garneau J. E., M. S., 2010. CRISPR/Cas System and Its Role in Phage-Bacteria Interactions. Annual Review of Microbiology, Volume 64, pp. 475-493.

Ding, Q. *et al*., 2013. Enhanced efficiency of human pluripotent stem cell genome editing through replacing TALENs with CRISPRs. *Cell stem cell,* 4 4, 12(4), pp. 393-4.

Dorsky, R. I., Sheldahl, L. C. & Moon, R. T., 2002. A Transgenic Lef1/β-Catenin-Dependent Reporter Is Expressed in Spatially Restricted Domains throughout Zebrafish Development. *Developmental Biology,* 15 1, 241(2), pp. 229-237.

Draper, B. W., Morcos, P. A. & Kimmel, C. B., 2001. Inhibition of zebrafishfgf8 pre-mRNA splicing with Morpholino oligos: A quantifiable method for gene knockdown. *genesis,* 1 7, 30(3), pp. 154-156.

Dougan, S. T., Warga, R. M., Kane, D. A., Schier A. F., Talbot, W., S., 2003. The role of the zebrafish nodal-related genes squint and cyclops in patterning of mesendoderm. *Development*, 130(9), pp. 1837-1851.

Erter, C. E., Wilm, T. P., Basler, N., Wright, C. V. E., Solnica-Krezel, L., 2001. Wnt8 is required in lateral mesendodermal precursors for neural posteriorization in vivo. *Development,* 128, pp. 3571-3583.

Fagotto F., Guger K., Gumbiner. B., 1997. Induction of the primary dorsalizing center in Xenopusby the Wnt/GSK/β -catenin signaling pathway, but not by Vg1, Activin or Noggin. *Development*, 124, pp. 453-460.

Farrell, J. A. *et al.,* 2018. Single-cell reconstruction of developmental trajectories during zebrafish embryogenesis. *Science (New York, N.Y.),* 1 6, 360(6392), p. eaar3131.

Filipovich, A., Gehrke, I., Poll-Wolbeck, S. J. & Kreuzer, K.-A., 2011. Physiological inhibitors of Wnt signaling. *European Journal of Haematology,* 1 6, 86(6), pp. 453-465.

Galceran, J., Farinas, I., Depew, M. J., Clevers, H., Grosschedl, R., 1999. Wnt3a −/−-like phenotype and limb deficiency in Lef1 −/− Tcf1 −/− mice. *Genes & Development,* 13(6), pp. 709-717.

Geisbrecht, B. V., Collins, C. S., Reuber, B. E. & Gould, S. J., 1998. Disruption of a PEX1-PEX6 interaction is the most common cause of the neurologic disorders Zellweger syndrome, neonatal adrenoleukodystrophy, and infantile Refsum disease.. *Proceedings of the National Academy of Sciences of the United States of America,* 21 7, 95(15), pp. 8630-5.

Gilbert, L. *et al.,* 2013. CRISPR-Mediated Modular RNA-Guided Regulation of Transcription in Eukaryotes. *Cell,* 18 7, 154(2), pp. 442-451.

Goldfischer, S. *et al*., 1973. Peroxisomal and mitochondrial defects in the cerebro-hepato-renal syndrome. *Science (New York, N.Y.),* 5 10, 182(4107), pp. 62-4.

Gonzalez, F. J., Peters, J. M. & Cattley, R. C., 1998. Mechanism of action of the nongenotoxic peroxisome proliferators: role of the peroxisome proliferator-activator receptor alpha. *Journal of the National Cancer Institute,* 18 11, 90(22), pp. 1702-9.

Grabenbauer, M., Sätzler, K., Baumgart, E. & Fahimi, H. D., 2000. Three-dimensional ultrastructural analysis of peroxisomes in HepG2 cells. Absence of peroxisomal reticulum but evidence of close spatial association with the endoplasmic reticulum. *Cell biochemistry and biophysics,* 32, pp. 37-49.

Groden, J. *et al*., 1991. Identification and characterization of the familial adenomatous polyposis coli gene. *Cell,* 9 8, 66(3), pp. 589-600.

Gross, J. C., Chaudhary, V., Bartscherer, K. & Boutros, M., 2012. Active Wnt proteins are secreted on exosomes. *Nature Cell Biology,* 16 10, 14(10), pp. 1036-1045.

Handly, L. N., Pilko, A., & Wollman, R., 2015. Paracrine communication maximizes cellular response fidelity in wound signaling. *eLife,* 4:e09652

Harland, R. & Gerhart, J., 1997. Formation and function of Spemann's organiser. *Annual Review of Cell and Developmental Biology,* 11, 13(1), pp. 611-667.

Hegazy, W. A. H. & Youns, M., 2016. TALENs Construction: Slowly but Surely. *Asian Pacific journal of cancer prevention,* 17(7), pp. 3329-34.

He, X., Semenov, M., Tamai, K. & Zeng, X., 2004. LDL receptor-related proteins 5 and 6 in Wnt/β-catenin signaling: Arrows point the way. *Development,* 131(8), pp. 1663-1677

Heymans H. S. A., Schutgens R. B. H., Tan R. & van den Bosch H., B. P., 1983. Severe plasmalogen deficiency in tissues of infants without peroxisomes (Zellweger syndrome). Nature Letters, 306, pp. 69-70.

Hileman, E. O. *et al*., 2004. Intrinsic oxidative stress in cancer cells: a biochemical basis for therapeutic selectivity. *Cancer Chemotherapy and Pharmacology,* 1 3, 53(3), pp. 209-219.

Hobmayer, B., Rentzsch, F., Kuhn, K. *et al.,* 2000. WNT signalling molecules act in axis formation in the diploblastic metazoan Hydra. *Nature* 407, pp. 186–189.

Holstein, T. W., 2012. The Evolution of the Wnt Pathway. *Cold Spring Harbor Perspectives in Biology,* 1 7, 4(7), pp. a007922-a007922.

Hoppler, S., Brown, J. D. & Moon, R. T., 1996. Expression of a dominant-negative Wnt blocks induction of MyoD in Xenopus embryos. *Genes & development,* 1 11, 10(21), pp. 2805-17.

Hostetler, H. A., Kier, A. B. & Schroeder, F., 2006. Very-long-chain and branched-chain fatty Acyl-CoAs are high affinity ligands for the peroxisome proliferator-activated receptor α (PPARα). *Biochemistry,* 20 6, 45(24), pp. 7669-7681.

Howe, K. *et al*., 2013. The zebrafish reference genome sequence and its relationship to the human genome. *Nature,* 17 4, 496(7446), pp. 498-503.

Huang, H. *et al*., 2015. One-step high-efficiency CRISPR/Cas9-mediated genome editing in Streptomyces. *Acta Biochimica et Biophysica Sinica,* 1 4, 47(4), pp. 231-243.

Huelsken, J. & Behrens, J., 2002. The Wnt signalling pathway. *Journal of cell science,* 1 11, 115(Pt 21), pp. 3977-8.

Hwang, W. Y. *et al*., 2013. Efficient genome editing in zebrafish using a CRISPR-Cas system. *Nature Biotechnology,* 29 3, 31(3), pp. 227-229.

Ibabe, A. et al., 2005. Expression of peroxisome proliferator-activated receptors in zebrafish (Danio rerio). *Histochemistry and Cell Biology,* 118(3), pp. 231-239.

Imai, Y., Gates, M. A., Melby A. E., Kimelman, D., Schier A. F. & Talbot, W. S., 2001. The homeobox genes vox and vent are redundant repressors of dorsal fates in zebrafish. *Development,* 128(12), pp. 2407-2420.

Jao, L.-E., Wente, S. R. & Chen, W., 2013. Efficient multiplex biallelic zebrafish genome editing using a CRISPR nuclease system. *Proceedings of the National Academy of Science USA,* 110(34), pp. 13904-13909.

Jho, E-H. *et al*., 2002. Wnt/beta-catenin/Tcf signaling induces the transcription of Axin2, a negative regulator of the signaling pathway. *Molecular and cellular biology,* 15 2, 22(4), pp. 1172-83.

Jinek, M. *et al*., 2012. A programmable dual RNA-guided DNA endonuclease in adaptive bacterial immunity, *Science,* 337(6096), pp. 816-821.

Jung, C. J. *et al*., 2016. Comparative Analysis of piggyBac, CRISPR/Cas9 and TALEN Mediated BAC Transgenesis in the Zygote for the Generation of Humanized SIRPA Rats. *Scientific Reports,* 17 11, 6(1), p. 31455.

Kelly, C., Alvin, J. C., Leatehrman, J. L., Kozlowaki, D. J., Weinberg, E. S., 2000. Maternal control of the zebrafish organizer*. Development*, 127, pp. 3899-3911.

Kersten, S., Desvergne, B. & Wahli, W., 2000. Roles of PPARs in health and disease. *Nature,* 25 5, 405(6785), pp. 421-424.

Kim, C. H. *et al*., 2000. Repressor activity of Headless/Tcf3 is essential for vertebrate head formation. *Nature,* 19 10, 407(6806), pp. 913-6.

Kimmel, C. B. *et al*., 1995. Stages of embryonic development of the zebrafish. *Developmental Dynamics,* 1 7, 203(3), pp. 253-310.

Kitajewski, J., Mason, J. O. & Varmus, H. E., 1992. Interaction of Wnt-1 proteins with the binding protein BiP. *Molecular and cellular biology,* 2, 12(2), pp. 784-90.

Korinek, V. *et al*., 1998. Depletion of epithelial stem-cell compartments in the small intestine of mice lacking Tcf-4. *Nature Genetics,* 1 8, 19(4), pp. 379-383.

Krysko, O. *et al*., 2010. Peroxisomes in zebrafish: distribution pattern and knockdown studies. *Histochemistry and cell biology,* 7, 134(1), pp. 39-51.

Kühl, M., Sheldahl, L. C., Park, M., Miller, J. R., Moon, R. T., 2000. The Wnt/Ca2+ pathway A new vertebrate Wnt signaling pathway takes shape. *Trends in genetics, 16(7), pp. 279-283.*

Kusserow, A*. et al.,* 2005. Unexpected complexity of the Wnt gene family in a sea anemone. *Nature,* 13 1, 433(7022), pp. 156-160.

Lai, D. Y., 2004. Rodent Carcinogenicity of Peroxisome Proliferators and Issues on Human Relevance. *Journal of Environmental Science and Health, Part C,* 26 12, 22(1), pp. 37-55.

Larson, M. H. *et al*., 2013. CRISPR interference (CRISPRi) for sequence-specific control of gene expression. *Nature Protocols,* 17 10, 8(11), pp. 2180-2196.

Lecarpentier, Y., Claes, V., Duthoit, G. & Hébert, J.-L., 2014. Circadian rhythms, Wnt/beta-catenin pathway and PPAR alpha/gamma profiles in diseases with primary or secondary cardiac dysfunction. *Frontiers in Physiology,* 4 11, Volume 5, p. 429.

Lekven, A. C., Thorpe, C. J., Waxman, J. S. & Moon, R. T., 2001. Zebrafish wnt8 Encodes Two Wnt8 Proteins on a Bicistronic Transcript and Is Required for Mesoderm and Neurectoderm Patterning. *Developmental Cell,* 1 7, 1(1), pp. 103-114.

Lian, X. *et al*., 2012. Robust cardiomyocyte differentiation from human pluripotent stem cells via temporal modulation of canonical Wnt signaling. Proceedings of the National Academy of Sciences of the United States of America, 3 7.109(27).

Lodhi, I. J. & Semenkovich, C. F., 2014. Peroxisomes: A nexus for lipid metabolism and cellular signaling. *Cell metabolism,* 19(3), pp. 380-392.

Lu, F.-I., Thisse, C. & Thisse, B., 2011. Identification and mechanism of regulation of the zebrafish dorsal determinant. *Proceedings of the National Academy of Sciences of the United States of America,* 20 9, 108(38), pp. 15876-80.

Luz, M. *et al*., 2014. Dynamic Association with Donor Cell Filopodia and Lipid-Modification Are Essential Features of Wnt8a during Patterning of the Zebrafish Neuroectoderm. *PLoS ONE,* 10 1, 9(1), p. e84922.

Lyman Gingerich, J., Westfall, T. A., Slusarski, D. C. & Pelegri, F., 2005. Hecate, a zebrafish maternal effect gene, affects dorsal organizer induction and intracellular calcium transient frequency. *Developmental Biology,* 15 10, 286(2), pp. 427-439.

Makita, R. *et al*., 1998. Zebrafish wnt11: Pattern and regulation of the expression by the yolk cell and No tail activity. *Mechanisms of Development,* 2, 71(1-2), pp. 165-176.

Mao, J. *et al.,* 2014. Roles of Wnt/β-catenin signaling in the gastric cancer stem cells proliferation and salinomycin treatment. *Cell Death & Disease,* 30 1, 5(1), pp. e1039-e1039.

Martin, B. L. & Kimelman, D., 2008. Regulation of Canonical Wnt Signaling by Brachyury Is Essential for Posterior Mesoderm Formation. *Developmental Cell,* 8 7, 15(1), pp. 121-133.

Mattes, B. *et al.,* 2018. Wnt/PCP controls spreading of Wnt/β-catenin signals by cytonemes in vertebrates. *eLife,* 31 7. Volume 7.

Maxwell, M. *et al.,* 2003. Pex13 inactivation in the mouse disrupts peroxisome biogenesis and leads to a Zellweger syndrome phenotype. *Molecular and cellular biology,* 15 8, 23(16), pp. 5947-57.

Ma, X. *et al.,* 2015. A Robust CRISPR/Cas9 System for Convenient, High-Efficiency Multiplex Genome Editing in Monocot and Dicot Plants. *Molecular Plant,* 3 8, 8(8), pp. 1274-1284.

Miyares, R. L., De Rezende, V. B. & Farber, S. A., 2014. Zebrafish yolk lipid processing: A tractable tool for the study of vertebrate lipid transport and metabolism. *DMM Disease Models and Mechanisms,* 7(7), pp. 915-927.

Mojica, F. J., Díez-Villaseíor, C., García-Martínez, J. & Soria, E., 2005. Intervening Sequences of Regularly Spaced Prokaryotic Repeats Derive from Foreign Genetic Elements. *Journal of Molecular Evolution,* 2, 60(2), pp. 174-182.

Mojica, F. J. M., Díez-Villaseñor, C., Soria, E. & Juez, G., 2000. *Biological significance of a family of regularly spaced repeats in the genomes of Archaea, Bacteria and mitochondria.* s.l.:s.n.

Molenaar, M., Van De Wetering, M., Oosterwegel, M., Peterson-Maduro, J., Godsave, S., Korinek, V., Roose, J., Destrée, O., Clevers, H., 1996. XTcf-3 transcription factor mediates β-catenin-induced axis formation in xenopus embryos. *Cell, 86*(3), 391-399.

Moser, H. W., Mahmood, A. & Raymond, G. V., 2007. X-linked adrenoleukodystrophy. *Nature Clinical Practice Neurology,* 1 3, 3(3), pp. 140-151.

Mwafi, N., Beretta, C. A., Paolini, A. & Carl, M., 2014. Divergent Wnt8a Gene Expression in Teleosts. *PLoS ONE,* 20 1, 9(1), p. e85303.

Nissim, L. *et al.,* 2014. Multiplexed and Programmable Regulation of Gene Networks with an Integrated RNA and CRISPR/Cas Toolkit in Human Cells. *Molecular Cell,* 22 5, 54(4), pp. 698-710.

Nusse, R. *et al.,* 1991. A new nomenclature for int-1 and related genes: the Wnt gene family. *Cell,* 25 1, 64(2), p. 231.

Nusse, R. & Clevers, H., 2017. Wnt/β-Catenin Signaling, Disease, and Emerging Therapeutic Modalities. s.l.:Cell Press.

Nusse, R. & Varmus, H. E., 1982. Many tumors induced by the mouse mammary tumor virus contain a provirus integrated in the same region of the host genome. *Cell,* 11, 31(1), pp. 99-109.

Nüsslein-Volhard, C. & Wieschaus, E., 1980. Mutations affecting segment number and polarity in *Drosophila. Nature,* 30 10, 287(5785), pp. 795-801.

Peifer, M., Orsulic, S., Pai, L. M. & Loureiro, J., 1993. A model system for cell adhesion and signal transduction in *Drosophila. Development (Cambridge, England). Supplement,* pp. 163-76.

Peifer, M. & Wieschaus, E., 1990. The segment polarity gene armadillo encodes a functionally modular protein that is the *Drosophila* homolog of human plakoglobin. *Cell,* 21 12, 63(6), pp. 1167-76.

Pelegri, F., 2003. Maternal Factors in Zebrafish Development. *Developmental dynamics: an official publication of the American Association of Anatomists,* 228(3), pp. 535-554.

Perez-Pinera, P. *et al*., 2013. RNA-guided gene activation by CRISPR-Cas9–based transcription factors. *Nature Methods,* 25 10, 10(10), pp. 973-976.

Peters, J. M., Cheung, C. & Gonzalez, F. J., 2005. Peroxisome proliferator-activated receptor-α and liver cancer: where do we stand? *Journal of Molecular Medicine,* 23 10, 83(10), pp. 774-785.

Peters, J. M. *et al.,* 2000. Growth, adipose, brain, and skin alterations resulting from targeted disruption of the mouse peroxisome proliferator-activated receptor beta(delta). *Molecular and cellular biology,* 15 7, 20(14), pp. 5119-28.

Ploper, D. *et al.,* 2015. MITF drives endolysosomal biogenesis and potentiates Wnt signaling in melanoma cells. *Proceedings of the National Academy of Sciences of the United States of America,* 3 2, 112(5), pp. E420-E429.

Qi, L. *et al.,* 2013. Repurposing CRISPR as an RNA-Guided Platform for Sequence-Specific Control of Gene Expression. *Cell,* 28 2, 152(5), pp. 1173-1183.

Raldúa, D., André, M. & Babin, P. J., 2008. Clofibrate and gemfibrozil induce an embryonic malabsorption syndrome in zebrafish. *Toxicology and Applied Pharmacology,* 1 5, 228(3), pp. 301-314.

Ramel, M.-C. & Lekven, A. C., 2004. Repression of the vertebrate organizer by Wnt8 is mediated by Vent and Vox. *Development (Cambridge, England),* 15 8, 131(16), pp. 3991-4000.

Ramel, M. C., Buckles, G. R., Baker, K. D. & Lekven, A. C., 2005. WNT8 and BMP2B co-regulate non-axial mesoderm patterning during zebrafish gastrulation. Developmental Biology, 15 11, 287(2), pp. 237-248.

Rauchenberger, V. et al., 2017. The phosphatase Pgam5 antagonizes Wnt/β-Catenin signaling in embryonic anterior-posterior axis patterning. *Development (Cambridge, England),* 15 6, 144(12), pp. 2234-2247.

Reddy, J. K., Azarnoff, D. L. & Hignite, C. E., 1980. Hypolipidaemic hepatic peroxisome proliferators form a novel class of chemical carcinogens. *Nature,* 24 1, 283(5745), pp. 397-8.

Reddy, J. K. & Hashimoto, T., 2001. Peroxisomal β-oxidation of Peroxisome Proliferator-activated Receptor α: An Adaptive Metabolic System. *Annual Review of Nutrition,* 7, 21(1), pp. 193-230.

Reddy, J. K., Lalwai, N. D. & Farber, E., 1983. Carcinogenesis by Hepatic Peroxisome Proliferators: Evaluation of the Risk of Hypolipidemic Drugs and Industrial Plasticizers to Humans. *CRC Critical Reviews in Toxicology,* 26 1, 12(1), pp. 1-58.

Reya, T. & Clevers, H., 2005. Wnt signalling in stem cells and cancer. *Nature,* 14 4, 434(7035), pp. 843-850.

Rhinn, M. et al., 2005. Positioning of the midbrain-hindbrain boundary organizer through global posteriorization of the neuroectoderm mediated by Wnt8 signaling. Development, 3, 132(6), pp. 1261-1272.

Rijsewijk, F., Schuermann, M., Wagenaar, E., Parren, P., Weigel, D. & Nusse, R., 1987. The *Drosophila* homology of the mouse mammary oncogene int-1 is identical to the segment polarity gene wingless. Cell, 50(4), pp. 649-657.

Rivier, M. et al., 1998. Differential Expression of Peroxisome Proliferator-Activated Receptor Subtypes During the Differentiation of Human Keratinocytes. *Journal of Investigative Dermatology,* 1 12, 111(6), pp. 1116-1121.

Sanchez, A., & Golding, I. (2013). Genetic determinants and cellular constraints in noisy gene expression. Science, 342(6163), 1188-1193.

Sander, J. D. & Joung, J. K., 2014. CRISPR-Cas systems for editing, regulating and targeting genomes. *Nature biotechnology,* 4, 32(4), pp. 347-55.

Santos, M. J. *et al.,* 1988. Peroxisomal membrane ghosts in Zellweger syndrome--aberrant organelle assembly. *Science (New York, N.Y.),* 25 3, 239(4847), pp. 1536-8.

Scharf, S. R. & Gerhart, J. C., 1980. Determination of the dorsal-ventral axis in eggs of Xenopus laevis: complete rescue of uv-impaired eggs by oblique orientation before first cleavage. *Developmental biology,* 9, 79(1), pp. 181-98.

Schier, A. F. & Talbot, W. S., 2005. Molecular Genetics of Axis Formation in Zebrafish. *Annual Review of Genetics,* 12, 39(1), pp. 561-613.

Schlange, T. *et al*., 2007. Autocrine WNT signaling contributes to breast cancer cell proliferation via the canonical WNT pathway and EGFR transactivation. *Breast Cancer Research,* 26 10, 9(5), p. R63.

Schneider, C. A., Rasband, W. S. & Eliceiri, K. W., 2012. NIH Image to ImageJ: 25 years of image analysis. *Nature Methods,* 1 7, 9(7), pp. 671-675.

Schohl, A. & Fagotto, F., 2002. Two novel nodal-related genes initiate early inductive events in Xenopus Nieuwkoop center. *Development,* 1 1, 127(24), pp. 5319-5329.

Schrader, M., 2006. Shared components of mitochondrial and peroxisomal division. *Biochimica et Biophysica Acta (BBA) - Molecular Cell Research,* 1 5, 1763(5-6), pp. 531-541.

Schrader, M. *et al.,* 1996. Interaction of microtubules with peroxisomes. Tubular and spherical peroxisomes in HepG2 cells and their alterations induced by microtubule-active drugs. *European journal of cell biology,* 1, 69(1), pp. 24-35.

Schrader, M. *et al*., 2016. Proliferation and fission of peroxisomes — An update. *Biochimica et Biophysica Acta (BBA) - Molecular Cell Research,* 1 5, 1863(5), pp. 971-983.

Schrader, M. *et al*., 1998. Expression of PEX11beta mediates peroxisome proliferation in the absence of extracellular stimuli. *The Journal of biological chemistry,* 6 11, 273(45), pp. 29607-14.

Schrader, M., Bonekamp, N. & Islinger, M., 2012. Fission and proliferation of peroxisomes. *Biochimica et Biophysica Acta (BBA) - Molecular Basis of Disease,* 1 9, 1822(9), pp. 1343-1357.

Schrader, M. & Fahimi, H. D., 2008. The peroxisome: Still a mysterious organelle. *Histochemistry and cell biology,* 129(4), pp. 421-440.

Schulte-Merker S., van Eeden F. J. M., Halpern M. E., Kimmel C. B., Nüsslein-Volhard, C., 1994. no tail(ntl) is the zebrafish homologue of the mouse T (Brachyury) gene. *Development*, 120, pp. 1009-1015.

Schulte-Merker, S. & Stainier, D. Y., 2014. Out with the old, in with the new: Reassessing Morpholino knockdowns in light of genome editing technology. *Development (Cambridge),* 141(16), pp. 3103-3104.

Seiliez, I., Thisse, B. & Thisse, C., 2006. FoxA3 and goosecoid promote anterior neural fate through inhibition of Wnt8a activity before the onset of gastrulation. *Developmental Biology,* 1 2, 290(1), pp. 152-163.

Selleck, M. & Stern, C., 1991. Fate mapping and cell lineage analysis of Hensen's node in the chick embryo. *Development,* 112(2).

Semenova, E. et al., 2011. Interference by clustered regularly interspaced short palindromic repeat (CRISPR) RNA is governed by a seed sequence. *Proceedings of the National Academy of Sciences of the United States of America,* 108(25), pp. 10098-10103.

Shimizu, T. *et al*., 2002. A novel repressor-type homeobox gene, ved, is involved in dharma/bozozok-mediated dorsal organizer formation in zebrafish. *Mechanisms of Development,* 1 10, 118(1-2), pp. 125-138.

Shimozawa, N. *et al.,* 1999. Defective PEX gene products correlate with the protein import, biochemical abnormalities, and phenotypic heterogeneity in peroxisome biogenesis disorders. *Journal of medical genetics,* 1 10, 36(10), pp. 779-81.

Shimozawa, N. *et al.,* 2004. Identification of a new complementation group of the peroxisome biogenesis disorders andPEX14 as the mutated gene. *Human Mutation,* 1 6, 23(6), pp. 552-558.

Siegfried, E., Chou, T. B. & Perrimon, N., 1992. wingless signaling acts through zeste-white 3, the *Drosophila* homolog of glycogen synthase kinase-3, to regulate engrailed and establish cell fate. *Cell,* 24 12, 71(7), pp. 1167-79.

Spemann, H. & Mangold, H., 1924. über Induktion von Embryonalanlagen durch Implantation artfremder Organisatoren. *Archiv für Mikroskopische Anatomie und Entwicklungsmechanik,* 9, 100(3-4), pp. 599-638.

Stanganello, E. *et al.,* 2015. Filopodia-based Wnt transport during vertebrate tissue patterning. *Nature Communications,* 5 12, 6(1), p. 5846.

Steinberg, S. *et al*., 2004. The PEX Gene Screen: molecular diagnosis of peroxisome biogenesis disorders in the Zellweger syndrome spectrum. *Molecular Genetics and Metabolism,* 1 11, 83(3), pp. 252-263.

Stemmer, M. *et al.,* 2015. CCTop: An Intuitive, Flexible and Reliable CRISPR/Cas9 Target Prediction Tool. *PLOS ONE,* 24 4, 10(4), p. e0124633.

Strutt, D., 2003. Frizzled signalling and cell polarisation in Drosophila and vertebrates*. Development,* 130(19), pp. 4501-4513.

Subramani, S., 1998. Components Involved in Peroxisome Import, Biogenesis, Proliferation, Turnover, and Movement. *Physiological Reviews,* 1, 78(1), pp. 171-188.

Summerton, J. E., 2007. Morpholino, siRNA, and S-DNA Compared: Impact of Structure and Mechanism of Action on Off-Target Effects and Sequence Specificity.

Summerton, J. & Weller, D., 1997. Morpholino Antisense Oligomers: Design, Preparation, and Properties. *Antisense and Nucleic Acid Drug Development,* 30 6, 7(3), pp. 187-195.

Takada, R. *et al.,* 2006. Monounsaturated Fatty Acid Modification of Wnt Protein: Its Role in Wnt Secretion. *Developmental Cell,* 1 12, 11(6), pp. 791-801.

Tao, Q. *et al.,* 2005. Maternal Wnt11 Activates the Canonical Wnt Signaling Pathway Required for Axis Formation in Xenopus Embryos. *Cell,* 25 3, 120(6), pp. 857-871.

Thisse, C. & Thisse, B., 2008. High-resolution in situ hybridization to whole-mount zebrafish embryos. *Nature Protocols,* 1 1, 3(1), pp. 59-69.

Tseng, A.-S., Engel, F. B. & Keating, M., 2006. The GSK-3 Inhibitor BIO Promotes Proliferation in Mammalian Cardiomyocytes. *Chemistry & Biology,* 1 9, 13(9), pp. 957-963.

Tsukamoto, A. S. *et al*., 1988. Expression of the int-1 gene in transgenic mice is associated with mammary gland hyperplasia and adenocarcinomas in male and female mice. *Cell,* 18 11, 55(4), pp. 619-625.

Undi, R. B., Gutti, U. & Gutti, R. K., 2017. LiCl regulates mitochondrial biogenesis during megakaryocyte development. *Journal of Trace Elements in Medicine and Biology,* 1 1, Volume 39, pp. 193-201.

Veeman, M. T., Axelrod, J. D. & Moon, R. T., 2003. A second canon: Functions and mechanisms of β-catenin-independent Wnt signalling. *Developmental cell,* 5(3), pp. 367-377.

Vermeulen, L. *et al*., 2010. Wnt activity defines colon cancer stem cells and is regulated by the microenvironment. *Nature Cell Biology,* 25 5, 12(5), pp. 468-476.

Vluggens, A. *et al.,* 2010. Functional significance of the two ACOX1 isoforms and their crosstalks with PPARα and RXRα. *Laboratory Investigation,* 90(5), pp. 696-708.

Walker, C. L., Pomatto, L. C. D., Tripathi, D. N. & Davies, K. J. A., 2018. Redox Regulation of Homeostasis and Proteostasis in Peroxisomes. *Physiological Reviews,* 1, 98(1), pp. 89-115.

Wang, J. *et al.,* 2006. Dishevelled genes mediate a conserved mammalian PCP pathway to regulate convergent extension during neurulation. *Development,* 5, 133(9), pp. 1767-1778.

Waterham H. R., Koster J., van Roermund C. W. T., Mooyer P. A. W., Wanders R. J. A. & Leonard, J. V., 2007. A Lethal Defect of Mitochondrial and Peroxisomal Fission. *The New England Journal of Medicine*, 356, pp. 1736 - 1741.

Wehner, D. *et al.,* 2014. Wnt/β-catenin signaling defines organizing centers that orchestrate growth and differentiation of the regenerating zebrafish caudal fin. Cell Reports, 13 2, 6(3), pp. 467-481.

Wiese, K. E., Nusse, R. & van Amerongen, R., 2018. Wnt signalling: conquering complexity. *Development (Cambridge, England),* 26 6, 145(12), p. dev165902.

Wolins, N. E. & Donaldson, R. P., 1997. Binding of the peroxisomal targeting sequence SKL is specified by a low-affinity site in castor bean glyoxysomal membranes. A domain next to the SKL binds to a high-affinity site. *Plant physiology,* 3, 113(3), pp. 943-9.

Wylie, A. D., Fleming, J.-A. G., Whitener, A. E. & Lekven, A. C., 2014. Post-transcriptional regulation of wnt8a is essential to zebrafish axis development. *Developmental Biology,* 1 2, 386(1), pp. 53-63.

Xu, L. *et al*., 2016. Empower multiplex cell and tissue-specific CRISPR-mediated gene manipulation with self-cleaving ribozymes and tRNA. *Nucleic Acids Research,* 30 10, 45(5), p. gkw1048.

Yoon, J. C. *et al*., 2010. Wnt signaling regulates mitochondrial physiology and insulin sensitivity. *Genes and Development,* 15 7, 24(14), pp. 1507-1518.

Yoon, J. C. *et al.,* 2010. Wnt signaling regulates mitochondrial physiology and insulin sensitivity. *Genes & development,* 15 7, 24(14), pp. 1507-18.

Zeng, L. *et al.,* 1997. The Mouse FusedLocus Encodes Axin, an Inhibitor of the Wnt Signaling Pathway That Regulates Embryonic Axis Formation. *Cell,* 11 7, 90(1), pp. 181-192.

Zhan, T., Rindtorff, N. & Boutros, M., 2017. Wnt signaling in cancer. *Oncogene,* 36, pp. 1461-1473.

Zhang, J. *et al.,* 1998. The Role of Maternal VegT in Establishing the Primary Germ Layers in Xenopus Embryos. *Cell,* 21 8, 94(4), pp. 515-524.

Ziouzenkova, O. *et al.,* 2002. Peroxisome proliferator-activated receptors. *Current Atherosclerosis Reports,* 1, 4(1), pp. 59-64.